Energy

FOSSIL

12
9/27/91
M.I.T. (2)

DOE/PC/90008-T8(Vol.2)
(DE91016811)

HEAT TRANSFER INVESTIGATIONS IN A SLURRY BUBBLE COLUMN

Final Report

Volume II of II

February 1991

Work Performed Under Contract No. AC22-82PC90008

For
U.S. Department of Energy
Pittsburgh Energy Technology Center
Pittsburgh, Pennsylvania

By
The University of Illinois at Chicago
Chicago, Illinois

DISCLAIMER

DOE/PC/90008--T8-Vol.2

DE91 016811

HEAT TRANSFER INVESTIGATIONS IN A SLURRY BUBBLE COLUMN

FINAL REPORT
Volume II of II

S.C. SAXENA ET AL.

Department of Chemical Engineering
The University of Illinois at Chicago
Box 4348, Chicago, IL 60680, U.S.A.

FEBRUARY 1991

Prepared for the United States Department of
Energy Under Contract No. DE-AC-22-86-PC90008

Project Manager: Mr. GEORGE CINQUEGRANE
Pittsburgh Energy Technology Center

LIST OF CONTENTS

5. DISCUSSION OF EXPERIMENT AND THEORY: GAS HOLDUP

5.1 Available Data and Correlations for Two-Phase Systems

Akita and Yoshida [53] measured gas holdup (air, helium,oxygen and carbon dioxide) in liquids (water, glycol, methanol, carbon tetrachloride and sodium chloride and sodium sulfate solutions) in the temperature range 283-303 K for gas velocities of 0.007-0.15 m/s in a column 0.152 m in diameter equipped with a single nozzle (5 mm diameter) gas distributor plate. They also report limited data in a 0.60 m column. They found negligible influence of gas density on gas holdup. The effect of liquid velocities up to 0.044 m/s was found to be negligible on gas holdup. On the basis of their data, they [53] proposed the following correlation:

$$\epsilon_g = C_1 (1 - \epsilon_g)^4 \, Bo^{1/8} \, Ga^{1/12} \, Fr \qquad 5.1$$

where C_1 is 0.20 for nonelectrolytes and is 0.25 for electrolytes.

Hughmark [54] measured the air holdup in a 2.54 cm column for water, sodium sulfate solution, kerosine, and a light oil in the bubbling regime. Air velocities ranged up to 0.305 m/s, and liquid velocities up to 0.09 m/s. His correlation is :

$$\epsilon_g = \frac{1}{2 + (0.35/U_g)\left[(\rho_L/\rho_w)(\sigma_L/\sigma_w)\right]^{1/3}} \qquad 5.2$$

for semibatch operation and zero liquid flow velocity. For continuous operation when the gas and liquid are in co-current flow, he found

$$U_g = \epsilon_g \left[(U_g/\epsilon''_g) - (V_L/1 - \epsilon''_g)\right] \qquad 5.3$$

On the basis of other workers data, he concluded that the column diameter has an effect on gas holdup as long as its value is less than 7.62 cm and is independent of its value for values greater than 10.2 cm.

Hikita et al. [55] measured gas holdup in a 10 cm diameter column with single-nozzle gas sparger at temperatures in the range 283-304 K. They used seven gases (air, hydrogen, carbon dioxide, methane, propane and the mixtures of hydrogen and nitrogen) and six liquids (water, sucrose solutions, methanol, n-butanol, aniline and i-butanol). They also employed nine electrolyte solutions with air. They determined gas holdup for three sections of the column and found it to be constant throughout the column height except for the lowest section (15 cm) where its value was lower due to larger gas bubbles and jetting gas stream. They found ϵ_g to be dependent on gas density but assumed it to be independent of nozzle opening, column diameter and ungassed liquid column height. Their correlation is:

$$\epsilon_g = 0.672 \left(U_g \mu_L/\sigma_L\right)^{0.578} \left(\mu_L^4 g/\rho_L \sigma_L^3\right)^{-0.131} \left(\rho_g/\rho_L\right)^{0.062} \left(\mu_g/\mu_L\right)^{0.107} \qquad 5.4$$

Reilly et al. [56] measured gas holdup in a 0.3 m diameter column for three different gas spargers at temperatures in the range 288-313 K. Three different gases (air, helium and argon) and three different liquids (deionized water, Esso Solvent Varsol DX 3641 with and without the addition of an antifoam agent, and a technical grade trichloro-ethylene) were used. They proposed a correlation which could represent their data as well as the literature data within ± 20 percent. The correlation is:

$$\epsilon_g = 0.009 + 296\, U_g^{0.44}\, \rho_L^{-0.98}\, \sigma_L^{-0.16}\, \rho_g^{0.19} \qquad 5.5$$

Zahradnik and Kastanek [48] reported air holdup data for air-water system as obtained in two columns for diameters 0.152 and 0.292 m equipped with perforated plate air spargers with hole diameters ranging from 0.0005 to 0.003 m with corresponding open plate area ranging between 0.1 to 1.0 percent. The air flow rate ranged form 0.031 to 0.276 m/s. Their results were correlated by:

$$\epsilon_g = U_g/\left(0.3 + 2.0\, U_g\right) \qquad 5.6$$

For a two-phase, gas-liquid, system Smith et al. [57] proposed the following

correlation:

$$\epsilon_g = \left[2.25 + \frac{0.379}{U_g} \left(\frac{\rho_L \sigma_L}{72} \right)^{0.31} \mu_L^{0.016} \right]^{-1} \qquad 5.7$$

Kumar et al. [59] generated air holdup data in columns of diameters 5.0, 7.5, and 10.0 cm and orifice plate distributors having 21-49 holes of diameters in the range 0.087 - 0.309 cm. As liquids, they employed water, kerosene and 40 percent glycerol, and air velocities in the range 0.2 - 13.83 cm/s. Their correlation is:

$$\epsilon_g = 0.728\, U_g' - 0.485\, U_g'^2 + 0.0975\, U_g'^3 \qquad 5.8$$

where

$$U'_g = U_g \left[\rho_L^2 / \{ \sigma_L (\rho_L - \rho_g) g \} \right]^{1/4} \qquad 5.9$$

Sada et al. [60] introduced the effect of gas density on holdup by modifying the correlation of Akita and Yoshida [53] on the basis of their data as

$$\epsilon_g = 0.32 \left(1 - \epsilon_g\right)^4 Bo^{0.121}\, Ga^{0.086}\, Fr \left(\rho_g / \rho_L\right)^{0.068} \qquad 5.10$$

The data were obtained in a 7.3 cm diameter column provided with a single nozzle gas sparger of diameters 1.5, 2.7 and 5.7 mm. Helium and nitrogen were used as gases; and water, sodium nitrate, methanol, and a mixture of lithium chloride and potassium chloride as liquid media. The experiments were conducted in the temperature range 298-723 K for gas velocities in the range 0.005-0.11 m/s.

Hills [61] measured air holdup for air-water system in a 150 mm diameter column equipped with either a single 51 mm diameter orifice of a cylindrical sparger cap with 60 holes 3.1 mm diameter arranged in five rows with twelve holes in each row. The air velocity was varied in the range 0.07-3.5 m.s and that of the liquid in the range 0-2.7 m/s. For liquid velocities less than or equal to 0.3 m/s, he found that

$$\left(U_g/\epsilon''_g\right) - \left(V_L/\left(1 - \epsilon''_g\right)\right) = 0.24 + 4.0\ \epsilon_g^{1.72} \qquad 5.11$$

and

$$\epsilon_g = U_g \left[0.24 + 4.0\ \epsilon_g^{1.72}\right]^{-1} \qquad 5.12$$

Correlations of Grover et al. [62] and Zou et al. [63] were developed to correlate the gas holdup data at elevated temperatures for the two-phase systems. Both these groups of workers [62, 63] realized that the temperature dependence of the gas holdup cannot be simulated only through the dependence on temperature of thermodynamic and transport properties of the phases involved. Grover et al. [52] correlation is a modification of Hikita et al. [55] correlation and has the same dimensionless groups and an additional term containing vapor pressure of the liquid at that temperature. Grover et al. [62] measured the gas holdup for the air-water, and air-aqueous solution of NaCl (or $CuCl_2$) in the temperature range 303-353 K. A 10 cm diameter bubble column, 1.5 m in height, was used in the semi-batch mode for air velocities up to 0.045 m/s. A sintered glass disc with a mean pore size of 100-120 μm was used as an air distributor plate. They [62] found the air holdup to decrease substantially with increase in temperature up to 323 K and the influence was only marginal beyond this temperature. They determined the six constants of the correlation on the basis of their experimental data. The correlation is:

$$\epsilon_g = \left(\frac{1 + a\,P_v}{b\,P_v}\right)\left(\frac{U_g\,\mu_L}{\sigma_L}\right)^{0.76}\left(\frac{\mu_L^4\,g}{\rho_L\,\sigma_L^3}\right)^{-0.27}\left(\frac{\rho_g}{\rho_L}\right)^{0.09}\left(\frac{\mu_g}{\mu_L}\right)^{0.35} \qquad 5.13$$

where

$a = 1.1 \times 10^{-4}$, and $b = 5 \times 10^{-4}$

Zou et al. [63] also developed their correlation on the basis of the Hikata et al. [55] correlation after dropping the density and viscosity ratio terms of the two phases involved and adding a term containing vapor pressure of the liquid

and the total system pressure. They [63] represented their data by such a correlation by adjusting four parameters. Zou et al. [63] have employed a stainless steel bubble column, 0.1 m in diameter and 1.05 m in height. The gas and liquid were introduced in the column by a single nozzle of 10 mm inside diameter. Data were generated in the continuous mode with gas and liquid flowing in concurrent streams. The gas and liquid velocities ranged up to 0.16 m/s and 0.007 m/s respectively. Air-water, air-alcohol and air-50% NaCl systems were studied and the maximum temperature range was 298.2-369.7 K. They [63] found the air holdup to increase with increase in temperature at all air velocities. Their form is:

$$\epsilon_g = 0.17283 \left(\frac{\mu_L^4 g}{\rho_L \sigma_L^3} \right)^{-0.1544} \left(\frac{U_g \mu_L}{\sigma_L} \right)^{0.5897} \left(\frac{P + P_v}{P} \right)^{1.6105} \qquad 5.14$$

The temperature dependence of air holdup given by the correlation of Eq. (5.14) is opposite to that of the relation of Grover et al. [62], Eq. (5.13).

5.2 Available Data and Correlations for Three-Phase Systems

Some of the important gas holdup correlations developed for three-phase systems are due to Reilly et al. [56], Smith et al. [57], and Roy et al. [64]. All these correlations have been developed by considering the data for two and three-phase systems. It is clear from these expressions that the correlations of Reilly et al. [56], and Smith et al. [57] predict negligible dependence of gas-phase holdup on temperature, and their predictions at best can be regarded as only in approximate agreement with the experimental data.

Roy et al. [64] on the basis of their fractional gas holdup data for three-phase systems (air-water-quartz, air-compressor oil-quartz, air-light diesel oil-quartz, and air-water-coal) proposed two-regions of gas holdup characterized by Reynolds number based on the column diameter, $Re_c = D_c G / H_g$ as

$$\epsilon_g = 3.88 \times 10^{-3} \left[Re_C \, (\sigma_w / \sigma_L)^{1/3} (1 - v_s)^3 \right]^{0.69} \text{ for } Re_C < 350 \qquad 5.15$$

and

$$\epsilon_g = 1.72 \times 10^{-2}\left[Re_C\,(\sigma_w / \sigma_L)^{1/3}(1 - v_s)^3\right]^{0.44} \text{ for } Re_C > 500 \qquad 5.16$$

where

$$v_s = \frac{(W_s / \rho_s)}{(W_s / \rho_s) + (W_L / \rho_L)}$$

These authors [64] found that the fractional gas holdup values decreased with increasing concentration of the solids in the system. However, for coal the ϵ_g values were considerably higher than those for the systems containing quartz. This was attributed to the very different solid-liquid interface behavior for coal than for quartz. Ying et al. [65] found that the reduction in ϵ_g values because of the presence of solids in the column was dependent on the column diameter. The effect was negligible for a 2-in. diameter column, but for a 5-in. diameter column, ϵ_g values decreased in the presence of solids.

On the basis of works by Hughmark [54] and by Smith and Ruether [66], Smith et al. [57] have proposed for three-phase bubble columns:

$$\epsilon_g = \left[2.25 + \left(\frac{33.9}{U_g}\right)\left(\frac{\sqrt{\rho_L}\,\sigma_L}{72}\right)^{0.31}\mu_{SL}^{0.16}\right]^{-1} \qquad 5.17$$

Barnea and Mizrahi [58] correlation was used to estimate the slurry viscosity from liquid viscosity, μ_L, according to the following relation:

$$\mu_{sL} = \mu_L \exp\left[\frac{(5 / 3)\, v_s}{(1 - v_s)}\right] \qquad 5.18$$

μ_{sL} and μ_L are in centipoise.

Roy et al. [56] correlation given in the previous section will also be employed here for the analysis of three-phase systems. This is in view of their [56] recommendation that solid particles have only negligible influence on gas holdup. They also felt similarly for gas and liquid viscosities and hence did not

include them in their correlation.

5.3 Comparison of Present Two-Phase Data with Theory

The effect of initial liquid column height on ϵ_g is presented in Fig. 4.2 and for five H_s values in the range 70-99 cm. A weak dependence of ϵ_g on H_s is found mostly within an average deviation of ±5%. The ϵ_g increases with increase in H_s. Holdup is also measured for increasing and decreasing air velocities in the range 3.2 to 33.2 cm/s [67-69]. In most cases, a pronounced maximum and minimum is observed for increasing air velocity, and a monotonic variation of increasing ϵ_g with increasing U_g is found for decreasing air velocity. This hysteresis effect has been observed by other workers [48, 70-72], and as discussed earlier by Saxena [67] this is primarily due to the formation and accumulation of foam at the top of air-water dispersion, and secondarily due to the foam accumulation in the column.

Saxena and Verma [69] have found that for semi-batch mode operation ($V_L = 0$), the influence of heat transfer probe internal on ϵ_g is negligible. This is not surprising as the internal occupied only four percent of the column cross-section. Saxena and Vadivel [73] on the other hand with a five-tube bundle in the column found the gas holdup to be larger than for an unbaffled column under otherwise identical conditions. This is explained on the basis that the bubble size is smaller in a baffled column in comparison to that in an unbaffled column. Consequently, the holdup is larger in the former than in the latter for the same conditions of operation.

For co-current flow of air and water (velocities in the range up to 12.2 mm/s) it is found [67, 69] that the effect of liquid flow rate on gas holdup is small. The averages of four sets of experimental values differ on the average by about 8 percent from the individual values. Saxena et al. [68] have found that the ϵ_g values do not exhibit any systematic variation with changes in liquid flow velocity in the range 3.73 to 8.92 mm/s. The air holdup values with liquid flow are smaller than the corresponding values with no liquid circulation for air velocities greater than 7 cm/s. For air velocities smaller than 7 cm/s, the effect is

negligibly small. For runs in the continuous mode, no foam formation is visible and the hysteresis effect is absent. The gas holdup variation with gas velocity is found to be monotonic.

The local air holdup, ϵ'_g, at a particular gas velocity, U_g, and and at a particular height above the air distributor plate, h, is obtained by measuring the pressure drop, ΔP, across a section of known height, H, of the air-water dispersion and the relationship given by Eq. (4.5).

Saxena [67] has found the gas holdup to be similar along the column height with and without the single probe for various decreasing air velocities. Saxena and Verma [69] have found similar result for increasing gas velocity. This result which is in agreement with the result for total gas holdup is indeed not surprising and the two sets of observations for local and total holdup are consistent with each other as expected.

These workers [67, 69] have observed certain qualitative trends of variation in ϵ'_g values and the same are explained on the basis of prevailing bubble dynamics in the column. In the lower section of the column, $h < 50$ cm, the bubble coalescence becomes increasingly pronounced as the air velocity is increased. This behavior causes the air holdup to decrease with increasing U_g in this region of $h < 50$ cm. For $50 < h < 120$ cm, the air holdup is relatively constant over the entire air velocity range. For the column region $120 < h < 150$ cm, the air holdup increases with h, the increase is relatively more pronounced for higher air velocities. This was attributed to the foam formation in the column. It is emphasized that the formation and breakup of foam takes place in the major portion of the column, $h > 50$ cm, and more so for higher gas velocities.

The uncertainties in the measurements of total and local holdups are estimated as follows. In the ϵ'_g values, it is about 4% at the highest gas velocity and decreases with decrease in gas velocity, being about 0.5% at the lowest gas velocity. The uncertainty in ϵ'_g is dependent on the air velocity as well as on the value of air holdup. At the top end of the column, the air holdup is large due to foam formation and the pressure difference uncertainty was relatively large because of the small magnitude of the pressure difference. The uncertainty is estimated to be ±5% at the top section at the lowest air velocity and ±50% percent

at the highest air velocity. In the remaining portion of the column the uncertainties are ±5 and ±35 percent for the lowest and highest air velocities respectively.

Additional new data on air-water system are taken and these are displayed in Fig. 5.1. Two different procedures are adopted for measuring the air holdup. In one procedure, an initial unaerated water column of 1.10 m in height (H_s) is employed and the holdup is determined as a function of decreasing air velocity. In this case the expanded height (H_e) of the air-water dispersion is different at each air velocity. In the procedure, the air holdup was measured for an expanded aerated water column height of 1.70 m and again for decreasing air velocity. Typical results of these two procedures are shown in Fig. 5.1 as set A and set B respectively. The two sets of air holdup values agree with each other for air velocities up to about 0.08 m/s and thereafter set B is consistently greater than set A for the entire air velocity range.

Uniform bubbles, spherical in shape, moving almost vertically up in the column are observed up to air velocity of 0.05 m/s. At the air velocity of about 0.05 m/s, air bubbles are observed to move downwards near the column wall in small sections of upper column region (h > 0.5 m). This establishes a cellular flow pattern in the column. The overall region of liquid circulation in the column descends further down with increase in the air velocity, and it extends up to 0.3 m at the air velocity of 0.08 m/s. For air velocities greater than 0.08 m/s, the bubble coalescence is observed and at column heights of greater than 1 m, the coalesced bubbles escape from the middle of the column. The region of coalescence in the column increases with air velocity and more bubbles are observed to be swept down in the local circulating water eddies. The opposite influence of coalescence and circulating eddies on air holdup almost balance for the range of air velocities between 0.10 to 0.17 m/s, and a somewhat constant holdup is observed for set A. The degree of coalescence increases with an increase in air velocity , and the coalesced bubbles almost slug the top portion of the column for air velocities greater than 0.3 m/s. However, the number of bubbles and their residence time in the column due to water circulation is such that the increased holdups are consistently observed with increase in air velocity over the entire range. The higher holdup values of set B data than that of set A

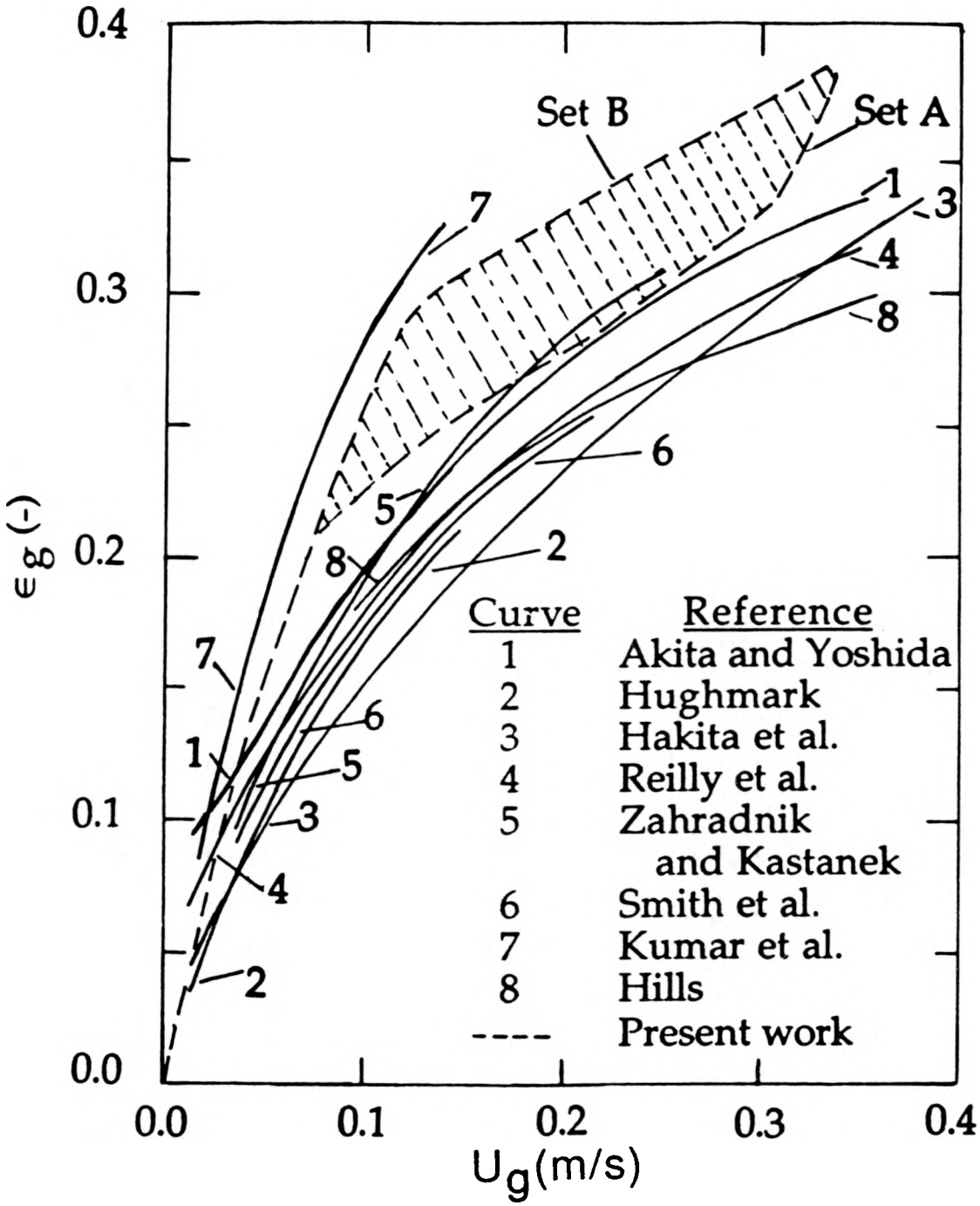

Fig. 5.1. Comparison of experimental and computed air holdup values for the air-water system as a function of superficial air velocity at 309K.

are partly due to a larger water column height and associated bubble dynamics. Our systematic measurements of air holdup for unaerated water column heights between 70 to 110 cm reveal that air holdup increases with increase of the water column height. Repeated measurements corresponding to sets A and B did represent some scatter and the dashed curve represents only the extreme values. The degree of foaming observed in the column has also varied in these runs and this also has partly been responsible for variation of the air holdup at the same air velocity. Our present holdup data are compared with the predictions of the air holdup values based on different correlations listed in section 5.1.

The computed values based on Akita and Yoshida's [53] correlation, Eq. (5.1), are shown in Fig. 5.1 as curve 1. Except for the very low air velocities (< 0.04 m/s), the computed values are generally smaller than our measured values. Hughmark's [54] correlation of Eq. (5.2) leads to values shown as curve 2 in Fig. 5.1, and these are systematically smaller than our measured values. The differences are significant and this correlation is not considered adequate for predicting the present air holdup values. Predictions based on Hikita et al.'s [55] correlation, Eq. (5.4), are shown as curve 3 in Fig. 5.1. This correlation like that of Hughmark's [54], underestimates the measured values of air-water system, and are systematically smaller than the computed values based on Akita and Yoshida's [53] correlation. For electrolytes, the air holdup is found to be greater than given by the above correlation and a multiplicative factor is introduced to represent the experimental data. Computed values from Reilly et al.'s [56] correlation, Eq. (5.5) are graphed in Fig. 5.1 as curve 4. These predictions are in better agreement with our data than those based on correlations of Hughmark [54], and Hakita et al. [55]. However, Akita and Yoshida's [53] correlation is relatively better in reproducing our data than that of Reilly et al.'s [56]. Zahraknik and Kastanek's correlation [48] based values are shown as curve 5 in Fig. 5.1 and these represent our data nearly as well as that of Eq. (5.1) by Akita and Yoshida [53]. Calculated values from Eq. (5.7) of Smith et al. [57] are shown as curve 6 in Fig. 5.1. These values are also lower than our measured values. Smith et al. [57] have examined the relation of Eq. (5.7) on the basis of data taken in a 0.108 cm diameter column for nitrogen and four liquids (water, silicone oil, glycol and aqueous ethanol). Calculated values from the correlation

of Kumar et al. [59] are shown as curve 7 in Fig. 5.1 and set B is reproduced well by this correlation. Predictions based on Sada et al.'s [60] correlation, Eq. (5.10), are almost identical with those obtained from Eq. (5.9). Hills's [61] correlation based values, Eq. (5.12), are shown as curve 8 in Fig. 5.1, and these consistently underestimate our data.

Lastly, we examine the approach of Nicklin [73] for correlating the gas holdup data in two-phase systems using the concept of drift velocity, Wallis [75]. This approach in the absence of liquid flow yields [74]:

$$\epsilon_g = U_g \left[U_g + U_o\right]^{-1} \qquad 5.19$$

Here, U_o is the drift velocity and in the churn turbulent regime, O'Dowd et al. [75] have proposed to express it as

$$U_o = U_g + U'_{b\infty} \qquad 5.20$$

$U_{b\infty}$ may be identified with the terminal rise velocity of bubbles and we have treated it as an adjustable parameter in correlating the gas holdup data. Equation (5.19) may then be written as

$$\epsilon_g = U_g \left[2U_g + U'_{b\infty}\right]^{-1} \qquad 5.21$$

The extreme sets A and B of experimental gas holdup data are examined in Fig. 5.2 on the basis of Eq. (5.21) and a constant value of 0.241 m/s for $U_{b\infty}$. This parity plot of gas holdup well substantiates the approach for correlating the data outlined here and the implicit assumption in Eq. (5.20).

In summary, we find that most of the correlations predict values of air holdup which are generally smaller than those obtained in our repeated measurements. We think that the column hydrodynamics plays a significant role and in particular the presence of a 19 mm axial probe in the column and the air sparger plate design has increased the residence time of bubbles, and hence the larger air holdup. Unaerated water column height and the mode of

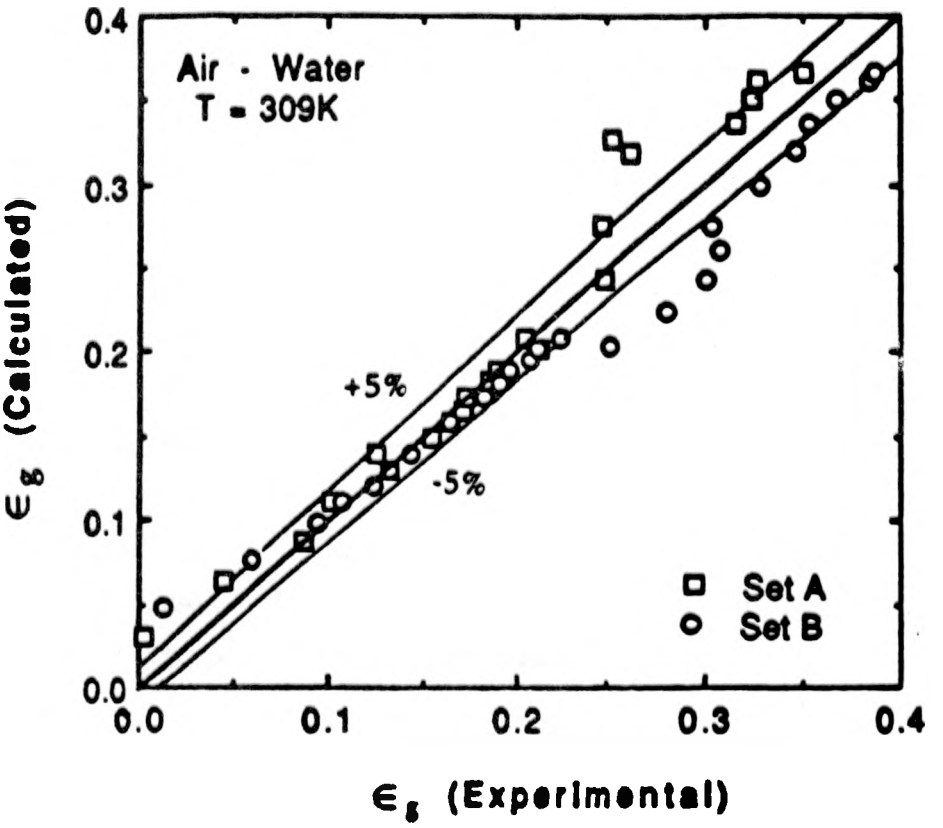

Fig. 5.2. Parity plot for gas holdup.

measurement (sets A and B) also influence the data significantly as the air velocity is increased. The air holdup knowledge is important for characterizing the column and in this perspective we attach special significance to such measurements. Heat transfer data reported later are taken for such a column operation as discussed above.

The knowledge of bubble size and bubble size distribution is particularly useful not only in interpreting the gas holdup data but also in establishing the magnitude of interfacial area. This parameter is essential for computing the mass transfer from bubble to the liquid phase. We [77] have taken limited data using high speed photographic and an image carrying fiber optic probe techniques. Saxena et al. [78] have reviewed the different techniques employed to obtain bubble size distributions in multiphase reactors. Patel et al. [79] have recently discussed the dynamic gas disengagement technique used to obtain these parameters. Obviously considerable research and development work needs to be done in this area to assist the development of a variety of chemical and biochemical processes performed in such bubble column reactors. Some relevant results obtained in our preliminary effort [77] are quoted here. In Figs. 5.3 through 5.8 are given the various measured bubble size frequency distributions and histograms. Based on these data, following conclusions may be drawn.

(a) The bubble size does not vary much with gas flow rate, at least in the air velocity range of 3.6 to 9.2 cm/s. A mean value of 6.1 ± 0.3 mm for air bubble diameter in water at ambient temperatures seems appropriate. This conclusion is based on the measurements made on the larger 30.5 cm diameter column.

(b) The bubble size is found to be dependent on the column diameter as judged from the data on the two columns at one gas velocity, 3.2-3.6 cm/s. The bubble diameter is smaller in the smaller baffled column than in the larger column where the baffles are relatively much less congested. O'Dowd et al. [76] have reported smaller bubbles in a baffled column than in the unbaffled column at lower gas velocities.

(c) The bubbles at the column wall are relatively smaller in size as recorded by the fiber optic probe than those farther away from the wall as observed in the photographic film. This is in agreement with detailed measurements made using a conductivity probe (O'Dowd et al. [76]), though in this technique bubble

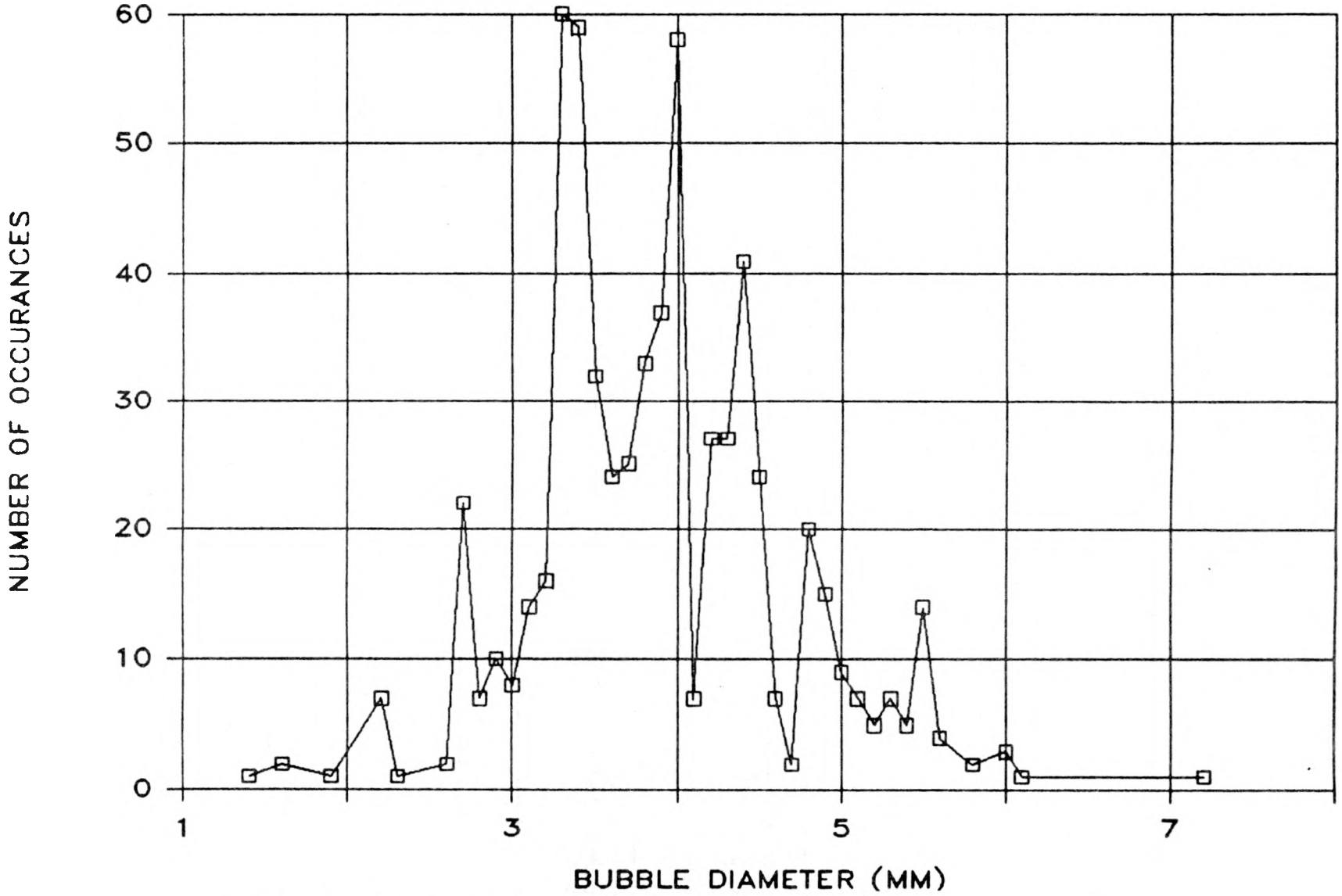

Fig. 5.3. Bubble size frequency distribution in the 10.8 cm diameter bubble column for the air-water system. Air velocity = 3.2 cm/s.

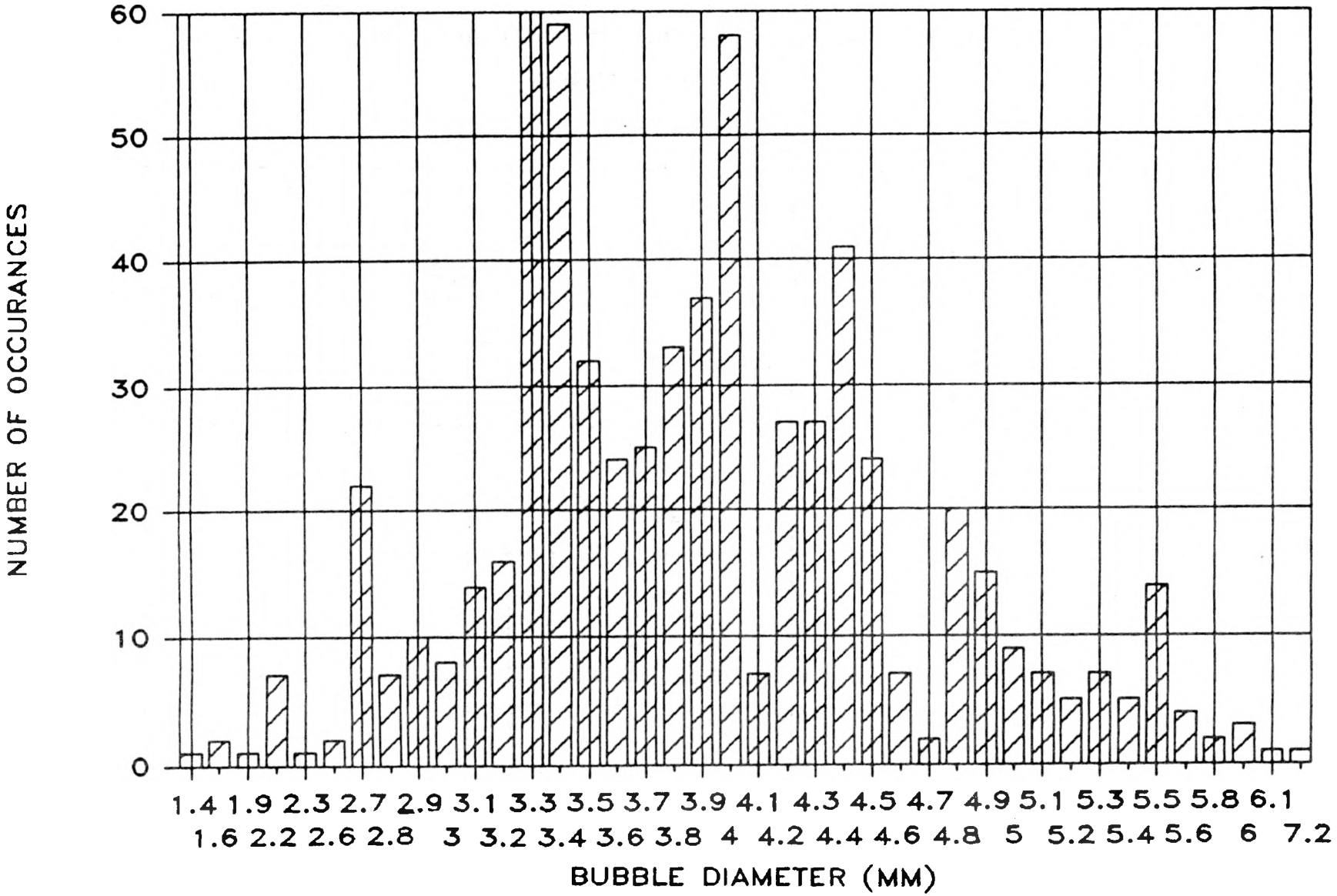

Fig. 5.4. Histogram of bubble-size distribution in the 10.8 cm diameter bubble column for the air-water system. Air velocity = 3.2 cm/s.

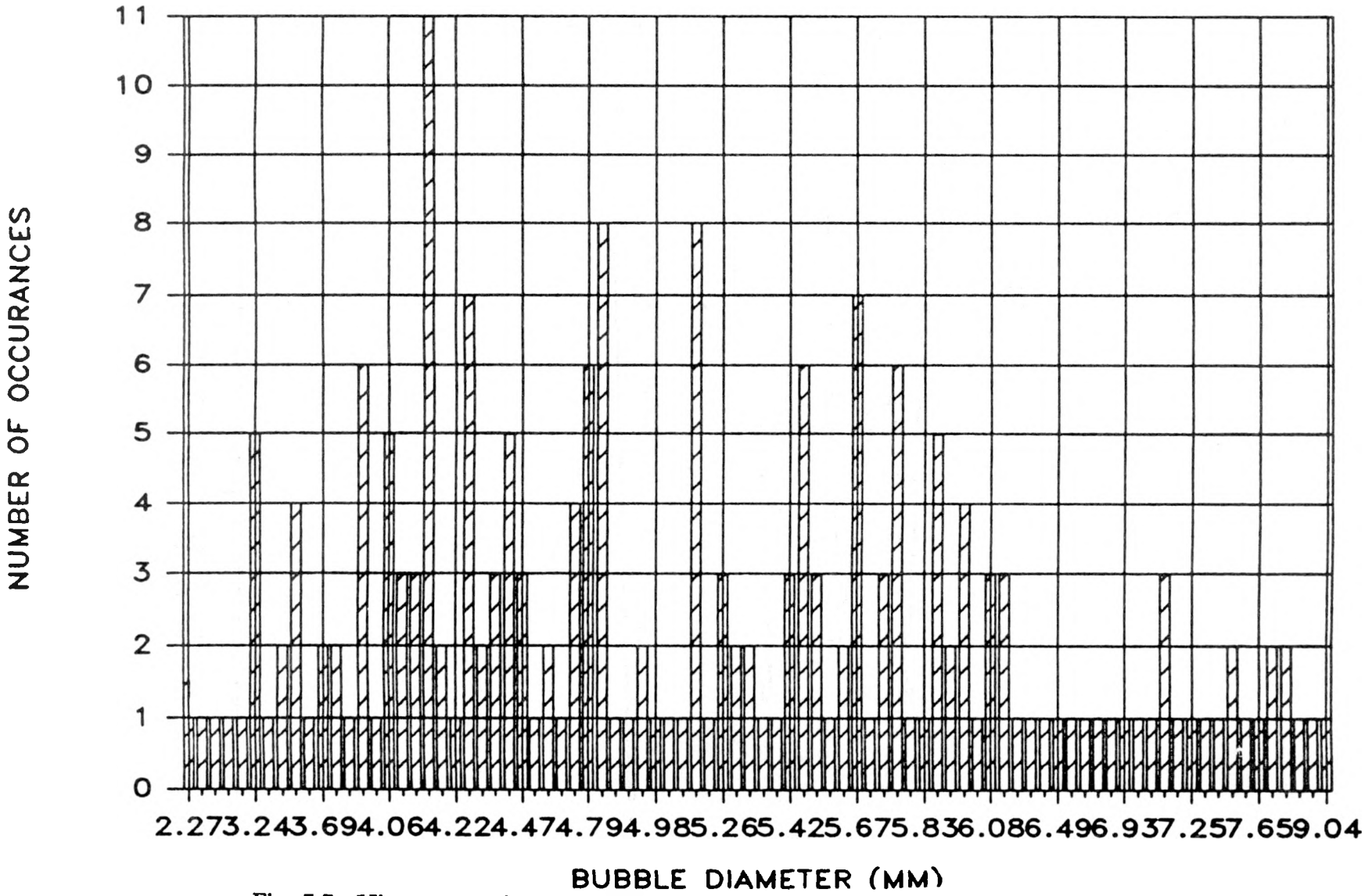

Fig. 5.5. Histogram of the bubble-size distribution in the 30.5 cm diameter bubble column for the air-water system. Air velocity = 3.2 cm/s.

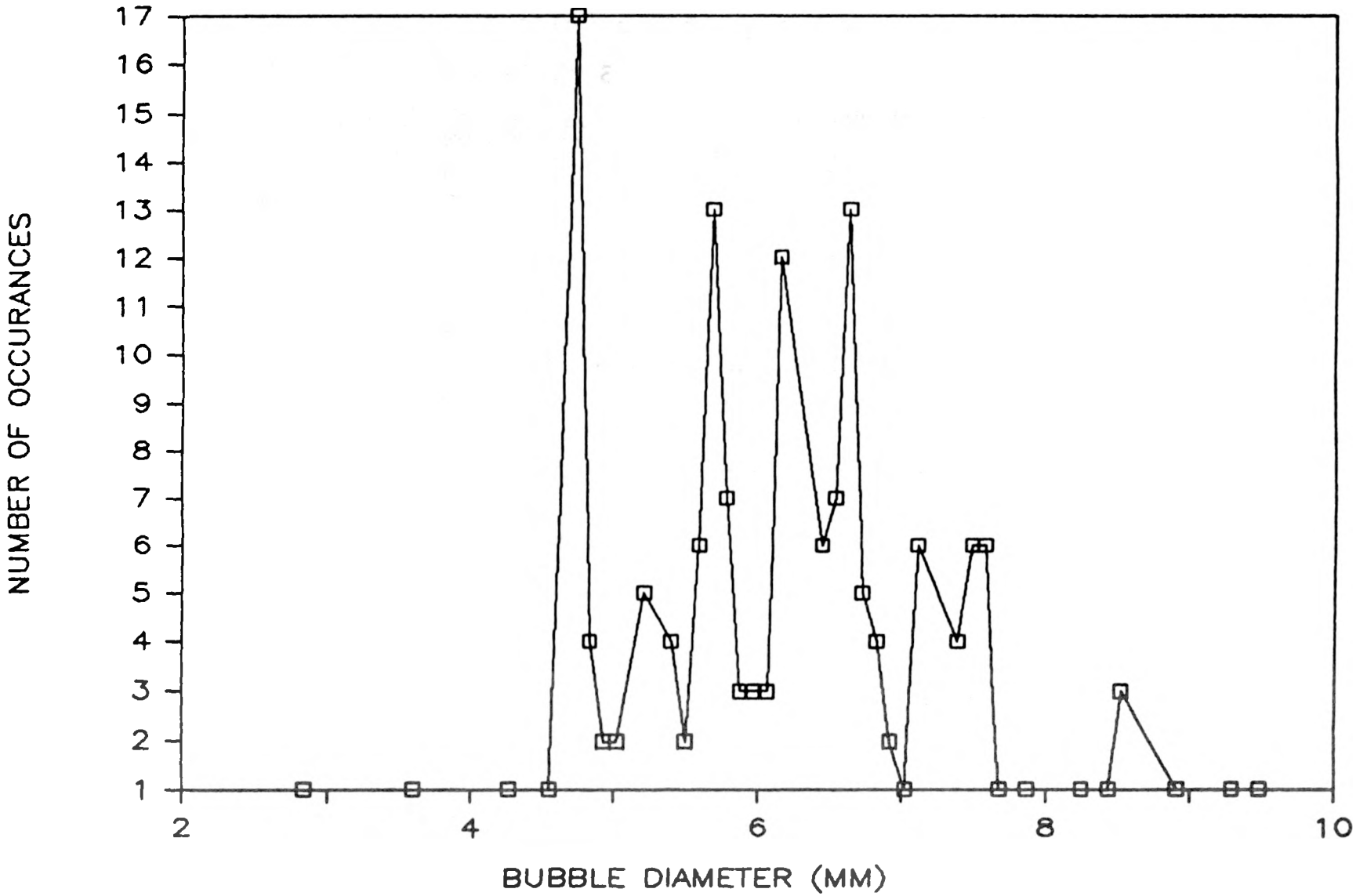

Fig. 5.6. Bubble size frequency distribution in the 30.5 cm diameter bubble column for the air-water system. Air-velocity = 3.6 cm/s.

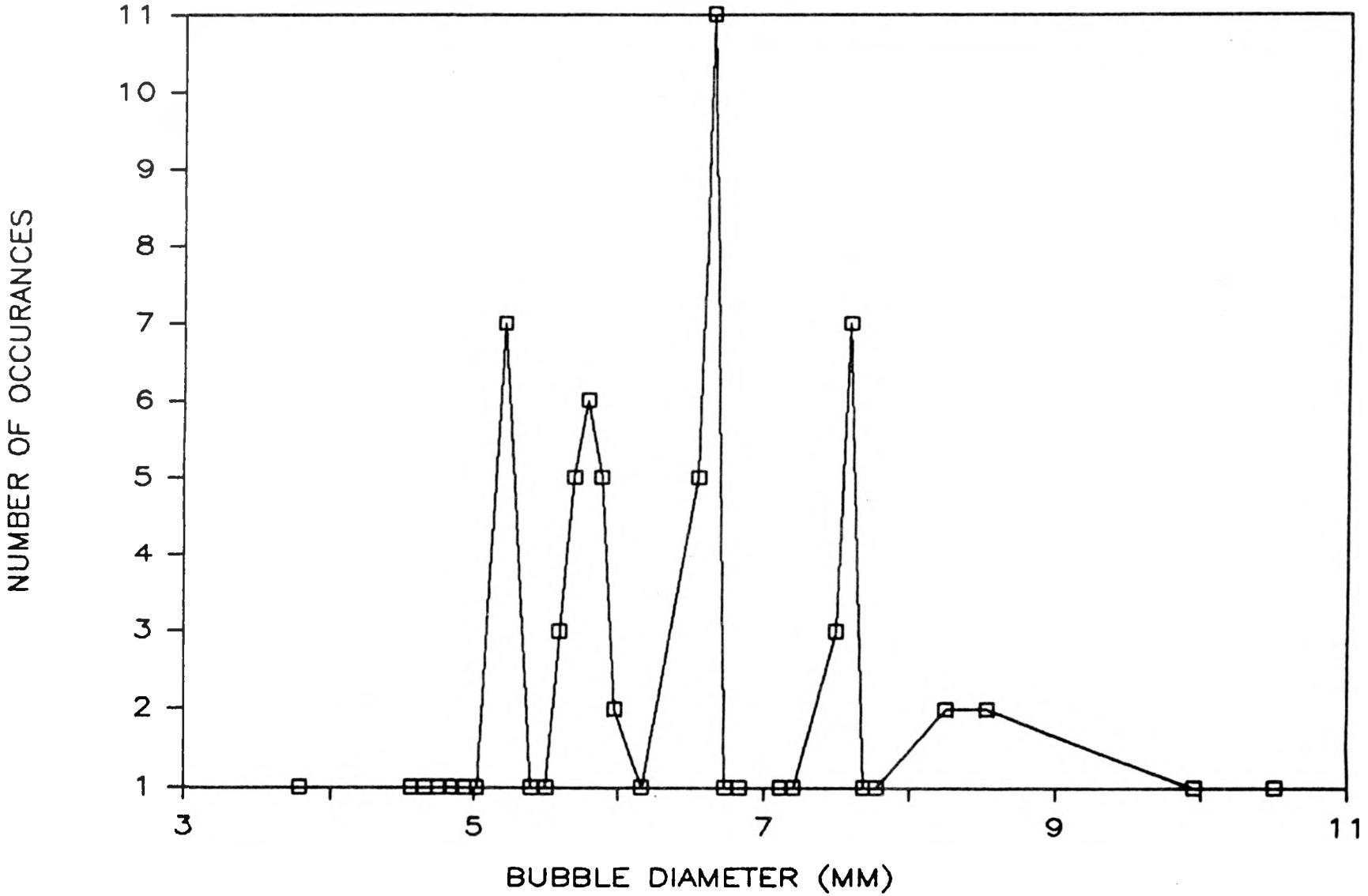

Fig. 5.7. Bubble size frequency distribution in the 30.5 cm diameter bubble column for the air-water system. Air velocity = 5.8 cm/s.

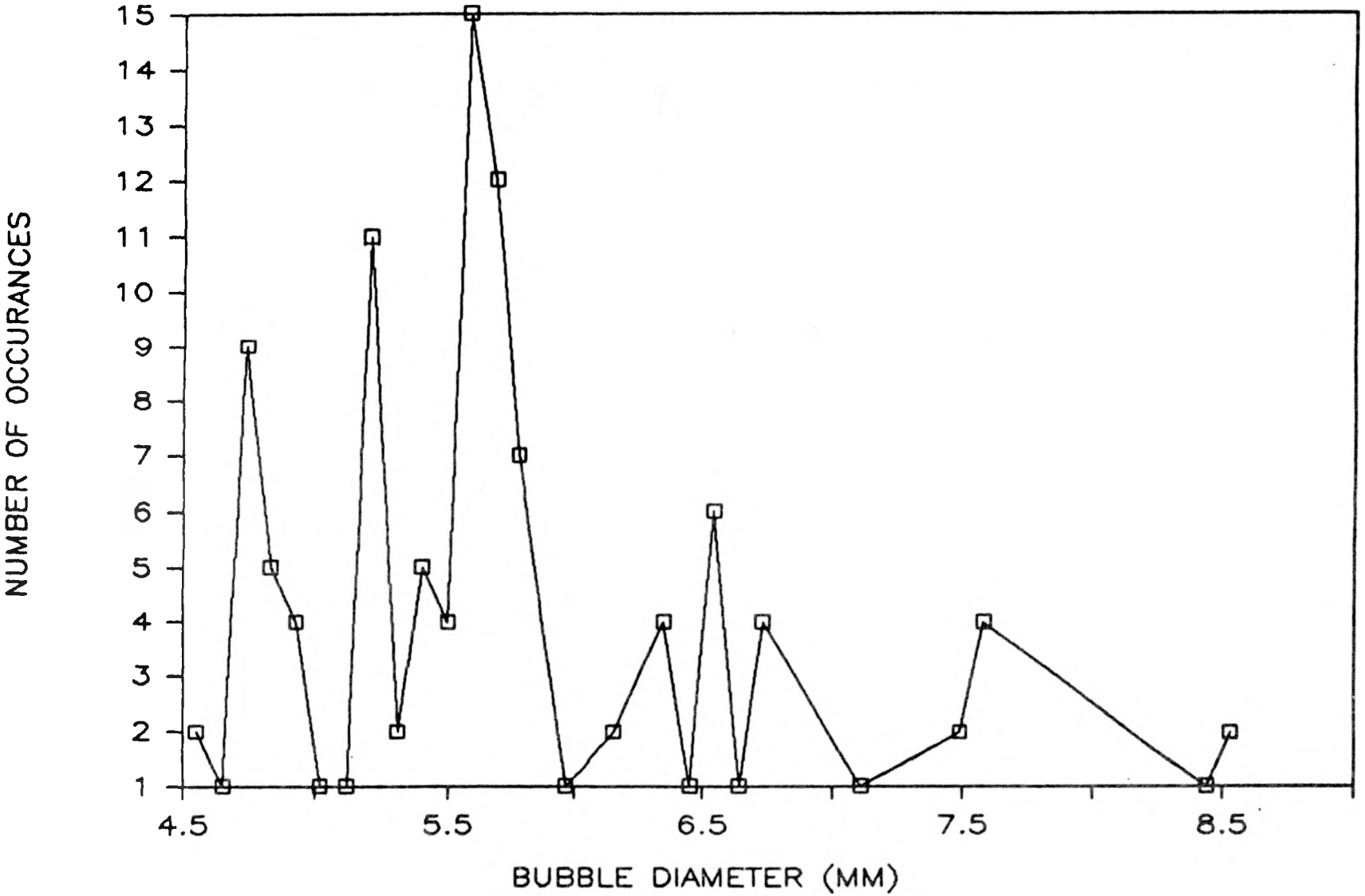

Fig. 5.8. Bubble size frequency distribution in the 30.5 cm diameter bubble column for the air-water system. Air velocity = 9.2 cm/s.

size distribution is measured at a point.

In Fig. 4.4, we have presented the data of holdup for the small column equipped with a single probe and a seven-tube bundle. The presence of a tube bundle inhibits to some extent bubble coalescence and therefore the holdup is larger and is independent of the initial column height. The models and correlations developed for unbaffled column operations will not be appropriate to represent these data. Additional data for air-water system are taken by Saxena and Patel [80] in this smaller bubble column equipped with a single 19 mm probe, and with a seven-tube bundle, and these have been correlated following the drift-flux theory of Wallis [75] as discussed by Zuber and Findlay [81] and detailed earlier in this section. This leads to $U_{b\infty}$ values listed in Table 5.1, and experimental gas holdup values are shown compared with the calculated values in Fig. 5.9. The agreement of theory and experiment is considered reasonable.

The experimental air holdup data taken at various temperatures in the larger column are compared with the predictions of available correlations in Fig. 5.10. In view of our experimental results, only those correlations which exhibit temperature dependence are considered. The correlations of Reilly et al. [56], Sada et al. [60], Hikita et al. [55], Smith et al. [57] and Kumar et al. [59] reproduce the present data rather poorly. All these correlations predict a dependence of gas holdup of less than 5 percent for the temperature range of our data. However, the experimental data suggest a more pronounced dependence, particularly for the range of air velocities where liquid circulation sets in, in the bubble coalescing regime at lower temperatures. It follows from this comparison of experiment and theory that the temperature dependence of gas holdup cannot be predicted only through the temperature dependence of the thermodynamic and transport properties used in the development of these correlations. This is not suprising as these correlations have been developed and tested mostly on data around 300 K or for a narrow band of temperatures around this value.

Grover et al. [62], and Zou et al. [63] have developed correlations to predict gas holdup for temperatures up to 370 K. Zou et al. [63] have reported the air holdup to increase with an increase in temperautre at all air velocities. This temperature dependence of air holdup is opposite to that found by Grover et al. [62], and also to that observed in the present experimental work. The predictions

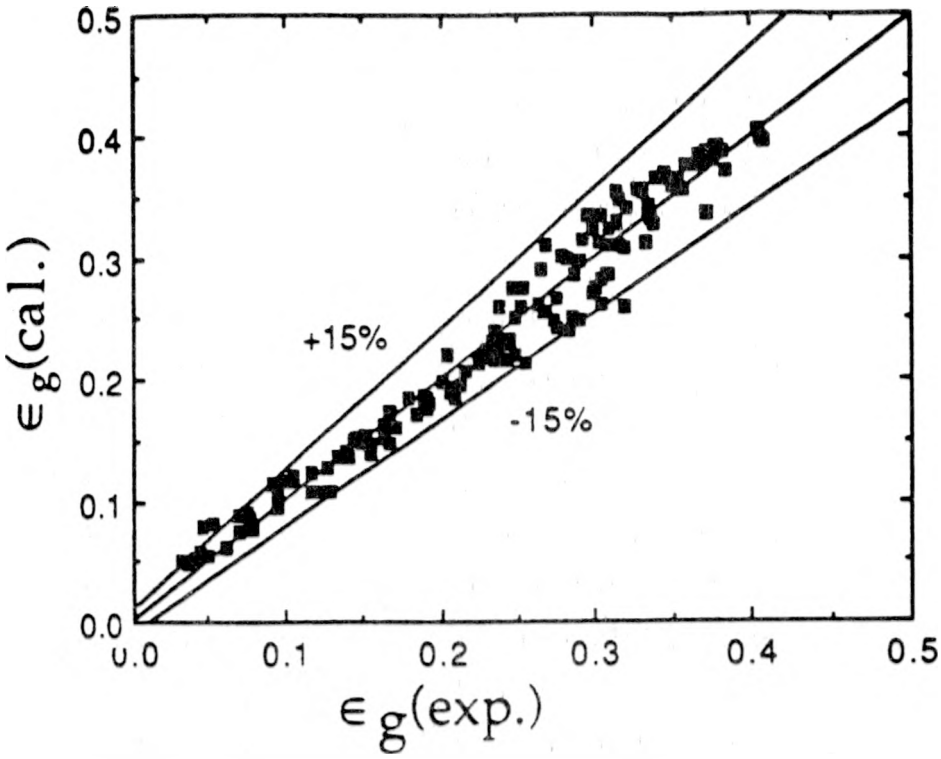

Fig. 5.9. Comparison of experimental and calculated gas holdup values.

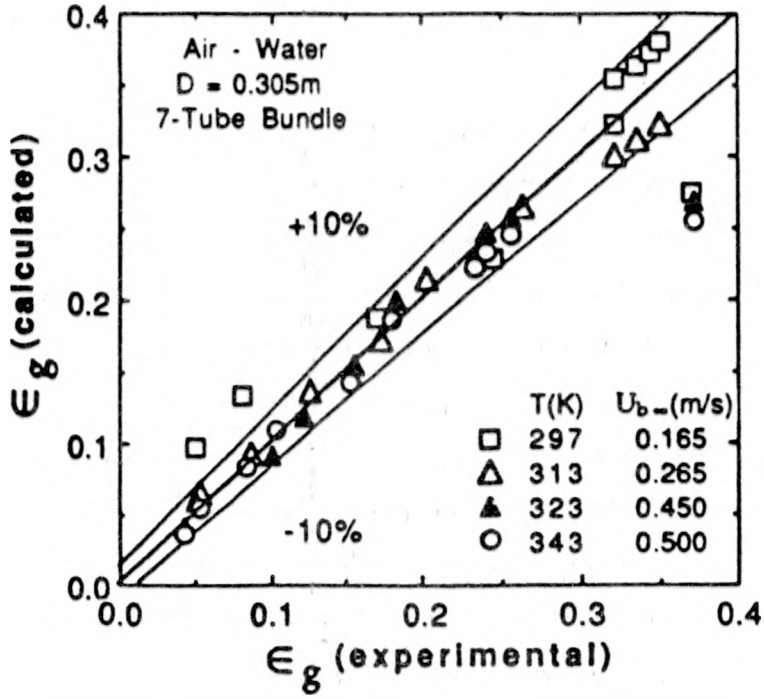

Fig. 5.11. Parity plot for the air-water system gas holdup data. Calculated ϵ_g values are according to Eq. (5.21).

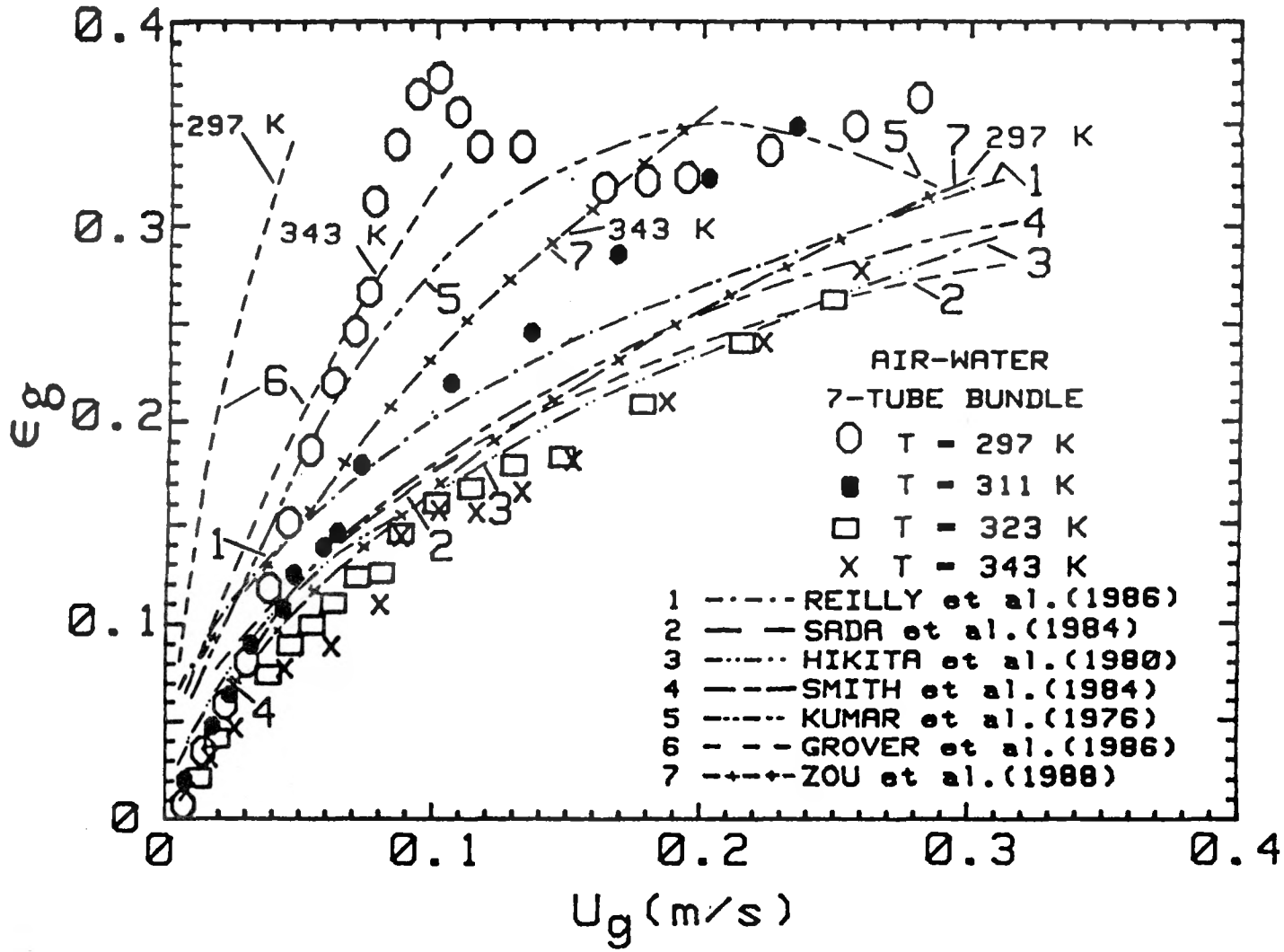

Fig. 5.10. Comparison of experimental air holdup values as a function of air velocity at different temperatures with the predictions based on different correlations.

based on Zou et al. [63] in Fig. 5.10 are seen to be in poor agreement with our data and an opposite qualitative dependence of air holdup on temperature is obvious. It appears that gas holdup data for well defined two-phase systems as a function of temperature will be very useful to develop a quantitative correlation.

Computing values of ϵ_g with $U_{b\infty}$ as an adjustable parameter are compared with the corresponding experimental values in Fig. 5.11. $U_{b\infty}$ values are also listed in this figure for the four temperatures of measurement and it is noted that $U_{b\infty}$ values monotonically increases with increase in temperature. This increase in $U_{b\infty}$ values with temperature suggests larger coalesced bubbles which result in smaller gas holdup. These results are in accordance with the visual observations of bubble size and the measured gas holdup values.

Experimental gas holdup data taken in the larger column with thirty-seven tube bundle as shown in Fig. 4.47 are compared with the predictions of correlations due to Grover et al. [62], Zou et al. [63], Reilly et al. [56], Smith et al. [57], and Roy et al. [64] in Fig. 5.12. The continuous curve 1 is a smooth plot through the four sets of experimental data points at four temperatures. Grover et al. predictions are always appreciably greater than the experimental values and exhibit a different dependence on air velocity. Zou et al. predictions are much lower than the experimental values at 298 K and increase with the increase in temperature much more rapidly than the experimentally observed trend according to which the values decrease with increase in temperature. Reilly, et al. and Smith et al., correlations lead to similar values than the experimental data and further these exhibit almost no temperature dependence in contradiction to the observed trend. Roy et al.correlation does predict the gas holdup values which decrease with increase in temperature in agreement with the observed trend. However, the absolute magnitude of values is appreciably different than the measured values. The drift-flux theory approach, as outlined above, leads to values which are in good agreement with experiment . These are shown in Fig. 5.13 where $U_{b\infty}$ values are also listed.

The experimental data of gas holdup for nitrogen-Therminol taken in the small column [82] with the 19 mm probe presented earlier in Fig. 4.6 are compared with the predictions of three correlations [56, 57, 64] in Fig. 5.14A. Figure 5.14A shows a poor prediction by all the three correlations and the Smith

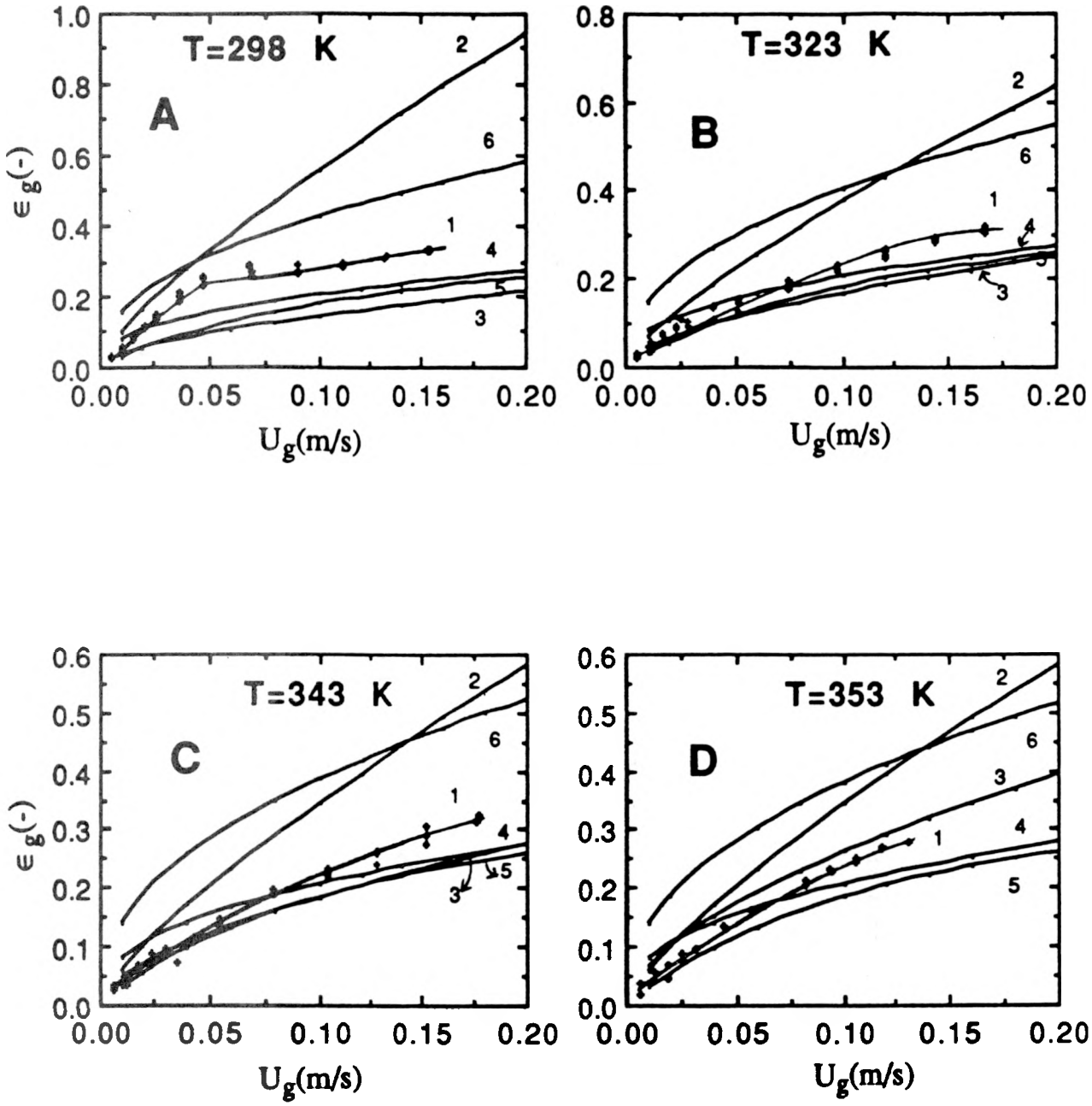

Fig. 5.12. Comparison of the four sets experimental data of air holdup of air - water system with the predictions of different models at four temperatures (1- Experiment, 2 - Grover et al., 3 - Zou et al., 4 - Reilly et al., 5 - Smith et al., 6 - Roy et al.).

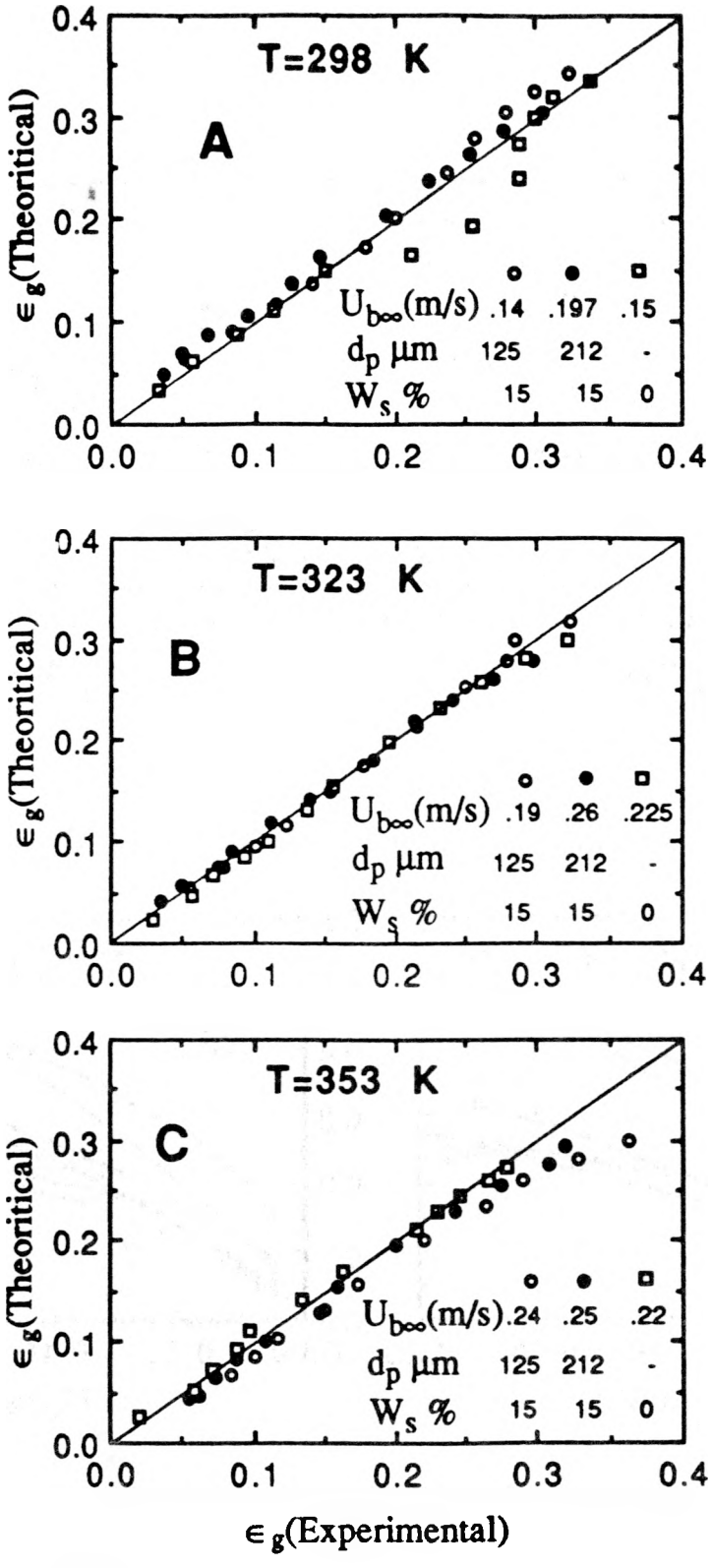

Fig. 5.13. Comparison of experimental air holdup data with the predictions of modified Nicklin's model for air-water and air-water-glass bead systems.

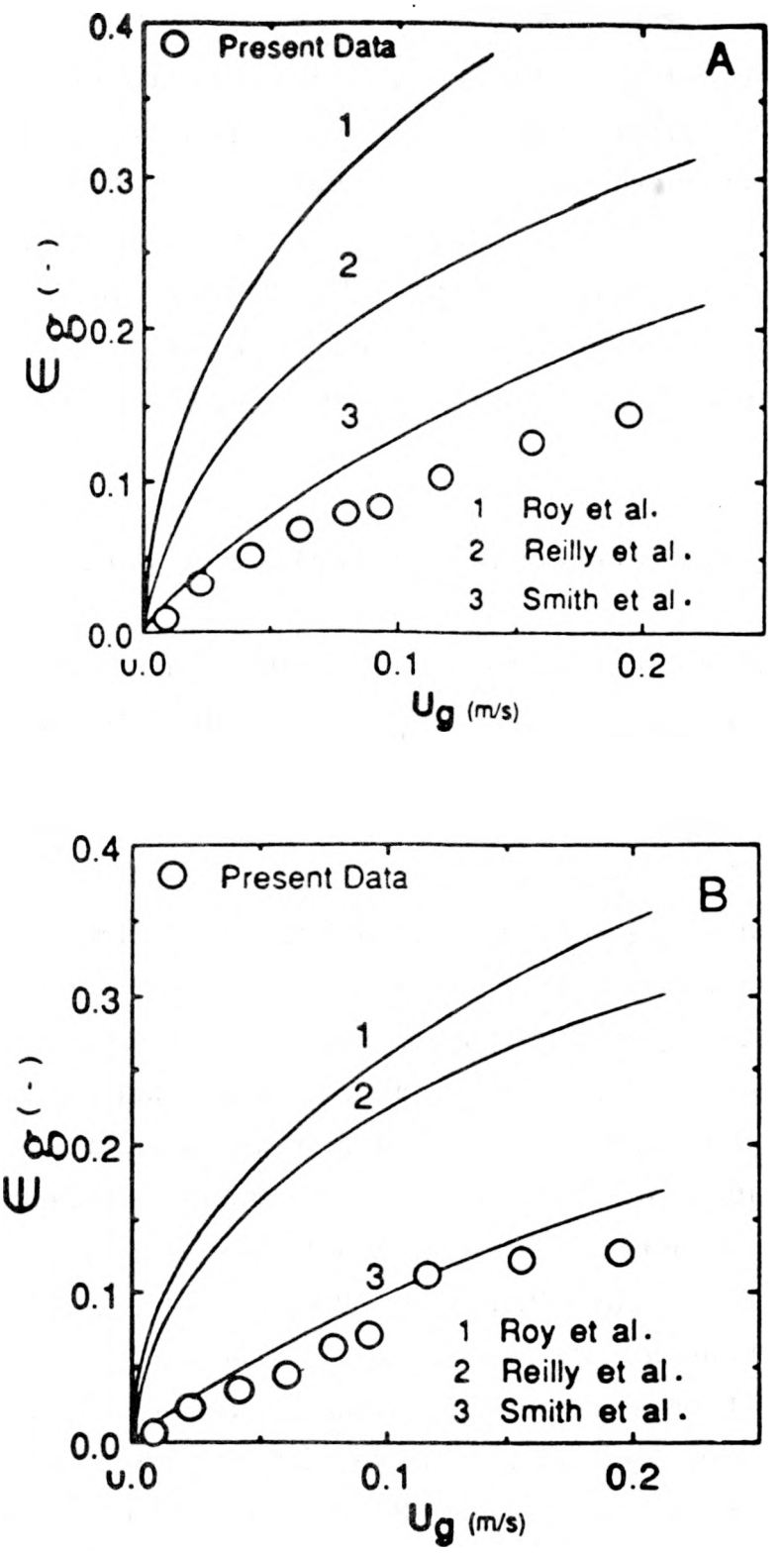

Fig. 5.14. Comparison of 19 mm probe internal nitrogen holdup data with the predictions of correlations for nitrogen-Therminol system: (A) without and (B) with solids.

et al. [57] correlation is the best of all though it overpredicts the data over the entire velocity range. It appears that liquid viscosity is not adequately accounted in these correlations; Reilly et al. [56] and Roy et al. [64] correlations do not have any liquid viscosity term while Smith et al. [57] correlation has only a very weak dependence on liquid viscosity. The drift-flux theory approach leads to satisfactory agreement with experimental data as seen in Fig. 5.15. The $U_{b\infty}$ values obtained for the four different internals in the column are listed in Table 5.2.

5.4 Comparison of Present Three-Phase Data with Theory

Saxena and Patel [80] have correlated their data, Fig. 4.9 and Table 4.8, on the drift-flux theory approach with the results reported in Fig. 5.9. The corresponding $U_{b\infty}$ values are listed in Table 5.1. The agreement between theory and experiment is satisfactory. The various correlations are found to be inadequate for this purpose.

The air holdup data taken in the large column for the air-water-glass bead system are compared with the three correlations [56, 57, 64] in Figs. 4.51 and 4.52. The Reilly et al. [56] correlation exhibits practically no dependence of air holdup on temperature, while those of Smith et al. [57] and Roy et al. [64] predict an increase and decrease of 3 and 5 percent, respectively, in air holdup with increase in temperature in the range of our present measurements. Thus, even the qualitative dependence of air holdup for these systems is not reproduced by these correlations. The quantitative dependence is poor for all the correlations and particularly inadequate for the case of Roy et al. [64]. These correlations developed from data mostly around ambient conditions are incapable of explaining the dependence of gas holdup on temperature and solids concentration. The failure of the Roy et al. [64] correlation is mostly due to the fact that it has column diameter as one of the parameters while measurements, present as well as those available in the literature, have shown that gas holdup is almost independent of column diameter, as long as it is greater than about 10 cm. Further, the correlations due to Reilly at al. [56] and Roy et al. [64] do not include slurry (or liquid) viscosity as a parameter, while our present work suggests it to

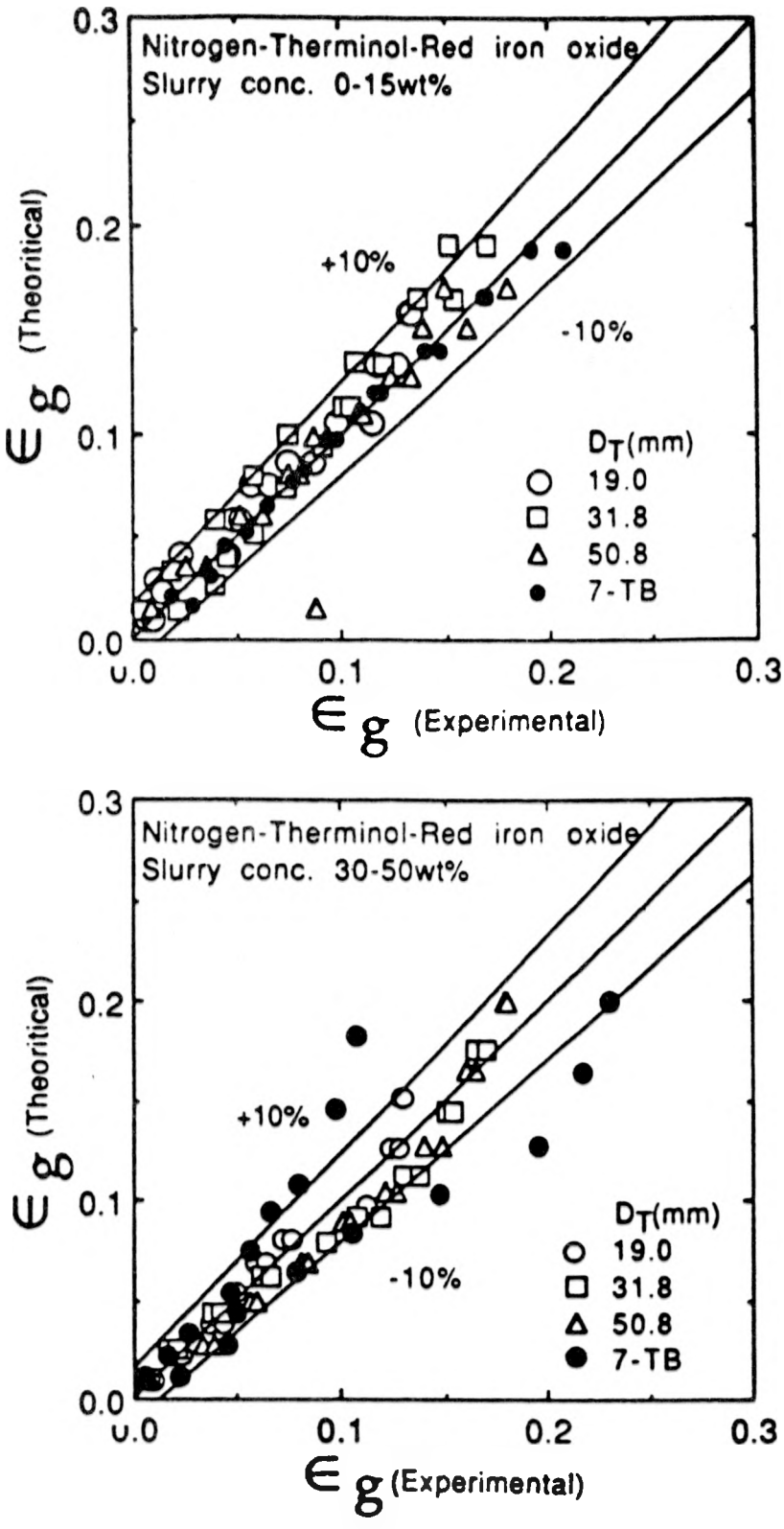

Fig. 5.15. Comparison of experimental nitrogen holdup data for 19 mm probe internal with the predictions based on the drift-flux theory.

Table 5.1. Values of $U_{b\infty}$ based on Eq. (5.21) and determined from experimental gas holdup data for air-water and air-water-glass bead systems at 309K in 0.108 m bubble column.

Single-tube configuration

d_p (μm)	0	50	119	143
w_s (%)	0	10	10	10
$U_{b\infty}$ (m/s)	0.314	0.433	0.420	0.473

Seven-tube bundle configuration

d_p (μm)	0	50	50	119	119	143	143	143	143
w_s (%)	0	5	10	5	10	5	10	20	30
$U_{b\infty}$ (m/s)	0.205	0.236	0.255	0.224	0.233	0.222	0.218	0.291	0.410

Table 5.2. Values of $U_{b\infty}$ based on Eq. (5.21) and determined from experimental gas holdup data for nitrogen-Therminol and nitrogen-Therminol-red iron oxide systems in 0.108 m bubble column at ambient temperature.

Internal	solids concentration (weight percent)			
	0	15	30	50
19.0 mm	0.864	0.998	1.08	1.07
31.8 mm	0.798	0.956	0.841	0.858
50.8 mm	0.796	0.914	0.791	0.749
7TB	0.718	0.812	0.709	0.682

be one of the important parameters in a realistic correlation. The solids concentration in the slurry and temperature seem to be somewhat related parameters as judged from the data of Figs. 4.51A, 4.51B and 4.51C. Slurry viscosity could link all these parameters together and it would follow that sound knowledge of the properties of the phases involved are crucial in the development of an accurate correlation. Experimental data of the nature produced here will help in identifying these parameters.

In Figs. 4.52A and 4.52B are given similar comparisons of theory and experiment for slurries of particle diameters 90 and 50 μm and 5 weight percent respectively as in Fig. 4.51 for slurries of 143.3 μm particles. The disagreements between correlation based air-holdup values and the experimental data are of the same nature as those in Fig. 4.51. None of the three correlations have particle diameter as a parameter, while our data at 297 K show that the gas holdup changes significantly when the size is reduced. In Fig. 5.16, we present the data for the 5 weight percent slurries of two smaller size particles as averaged for the particle size and temperature ranges. The experimental values are consistently smaller than the correlation based values for the entire air velocity range. Smith et al. [57] correlation is most successful of all the correlations in reproducing the data. The Roy et al. [64] correlation leads to a very poor reproduction of experimental data. A modified form of Smith et al. [57] correlation will be appropriate to develop for slurries involving particles smaller than 100 μm as more three-phase data become available.

In Fig. 5.17, these data are shown compared with computed values obtained on the approach based on modified drift-flux theory detailed in section 5.3. It is to be noted that data are well reproduced within ±10 percent. The $U_{b\infty}$ values are also listed in these figures and these again increase with temperature as observed for the two-phase, air-water, system.

The corresponding data [112] of air holdup with thirty-seven tube bundle, reported in Figs. 4.53-4.57, are shown compared with these model predictions in Fig. 5.18. Roy et al. [64] correlation based values are systematically greater than the experimental data, and their dependence on slurry concentration is more pronounced than that observed in the experiments. Reilly et al. [56] predictions are underestimates for air velocity values greater than about 0.07 m/s, and

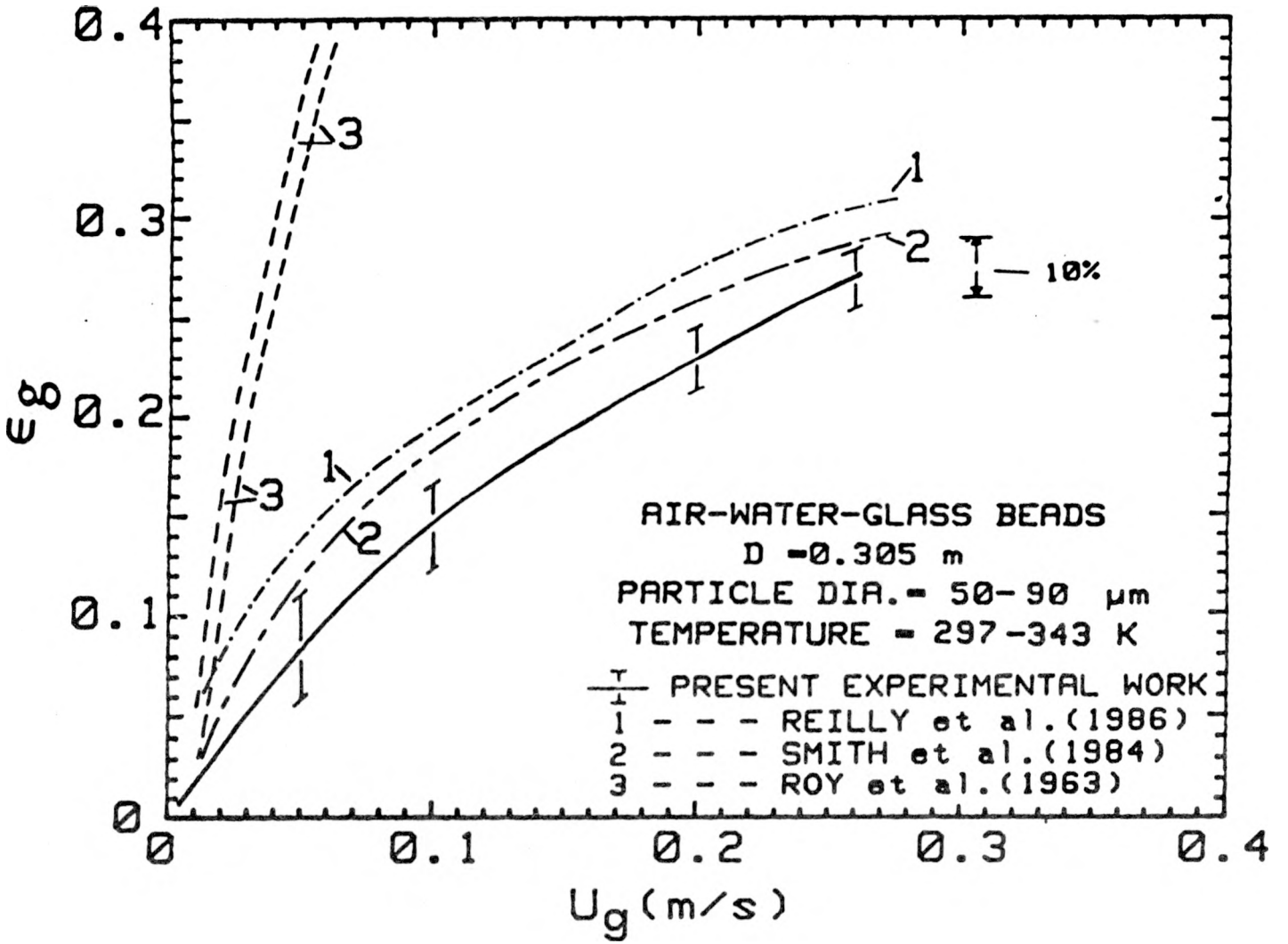

Fig. 5.16. Comparison of the averaged air holdup values for a range of particle sizes, slurry concentrations and temperatures as a function of air velocity with the predictions of different correlations.

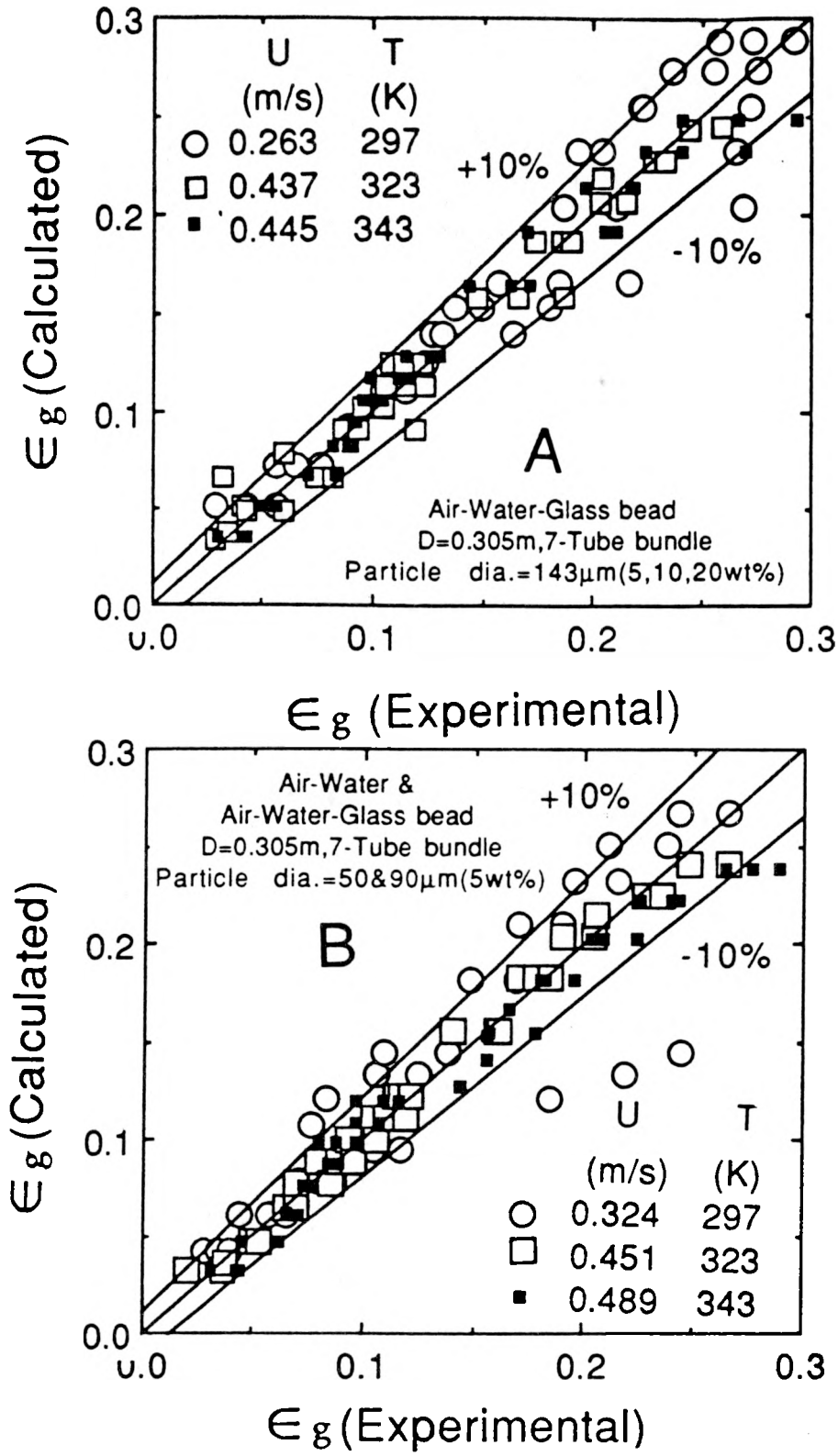

Fig. 5.17. Comparison of experimental air holdup data with the modified drift-flux theory approach.

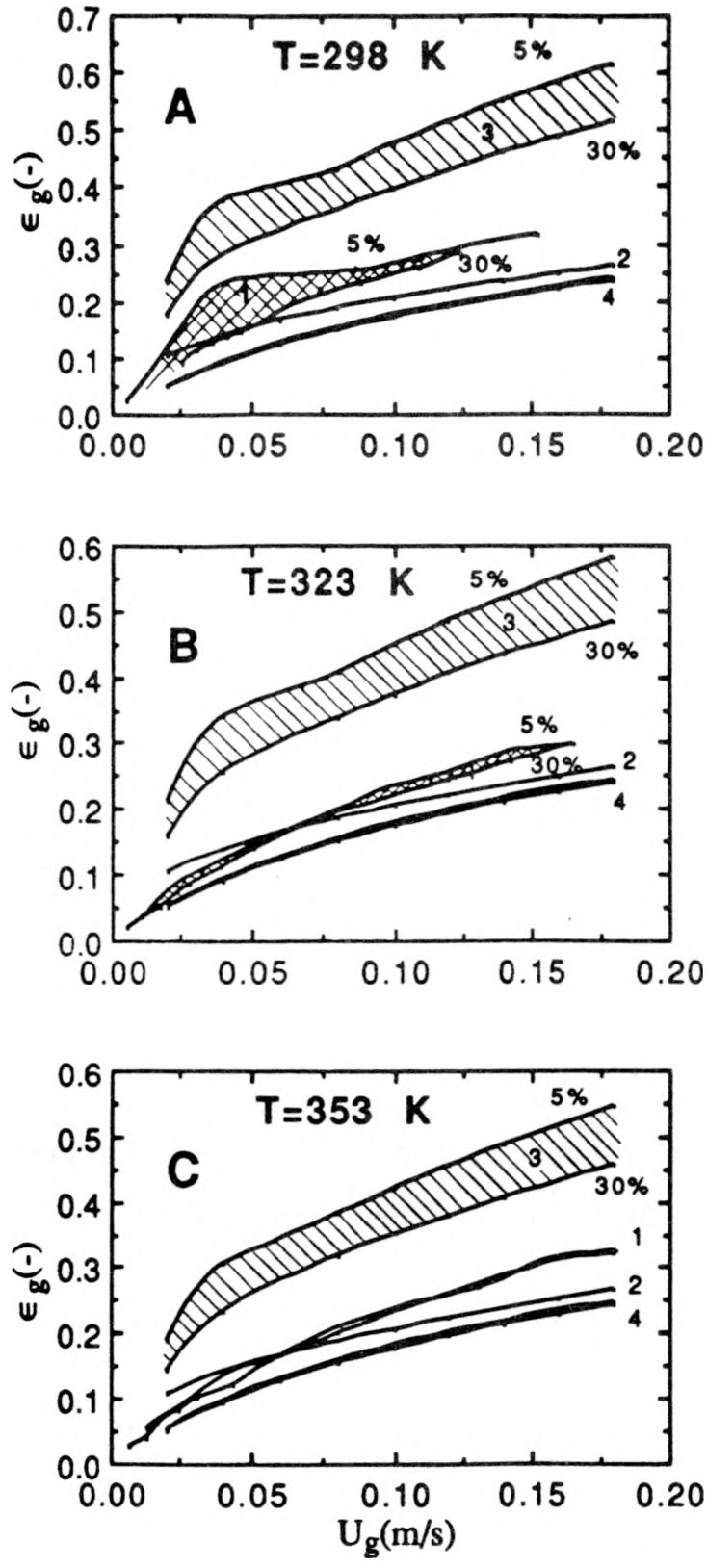

Fig. 5.18. Comparison of experimental air holdup data with the predictions of different models for the air-water-glass bead system (1 - Experimental, 2 - Reilly et al.[56], 3 - Roy et al.[64], 4 - Smith et al.[57].)

predict no dependence of slurry concentration. Smith et al. [57] values are systematically smaller than the experimental values and exhibit a very weak dependence on slurry similar to that implicit in our measured values. These data are shown compared with the modified drift-flux theory approach in Fig. 5.13. The $U_{b\infty}$ variation with temperature is the same as obtained with data on seven-tube bundle.

A comparison of experimental air holdup data for air-water-magnetite system in the small column with a single 19 mm heat transfer probe [105] with the computed values from the three correlations [56, 57, 64] is presented in Figs. 4.10A through 4.10F. In all cases, we find that Roy et al. [64] correlation based values (curves 1) reproduce rather poorly the experimental data and are always greater than the experimental values, the disagreement increases with increase in air velocity. We think that the inclusion of Reynold number based on column diameter is responsible for this discrepancy. Further, this correlation suggests a decrease in the value of gas holdup as solids concentration is increased in the slurry.

Reilly et al. [56] correlation which is based only on gas and liquid properties lead to values (curves 2) which are in fair agreement with the experimental data for slurries of smaller particles and small concentrations over the entire range of air velocities. The reproduction is relatively poorer for larger particles and for higher slurry concentrations. The small dependence of gas holdup found here on particle diameter and slurry concentration is implicitly built into this correlation for data of this nature were employed in the development of this correlation. We recommend this correlation for estimating the upper bound of the gas holdup for three-phase systems based on the present work.

Smith et al. [57] modified correlation of Hughmark [54] leads to values which are underestimates of data for small particles but the reproduction is better as the particle size increases and particularly for the bubbling regime. This correlation also gives a weak dependence on slurry concentration, the gas holdup decreases as the concentration of solids increases in the slurry. Again, based on present data, it appears that this correlation is a good estimate of the lower bound of the experimental gas holdup data.

Computed values from the drift-flux theory approach are shown compared

with the experimental values in Fig. 5.19. The corresponding $U_{b\infty}$ values are listed in Table 5.3. Data of this nature can help in understanding the dependence of $U_{b\infty}$ on d_p and w_s. However, work in this direction could not be pursued in the current contract period.

The experimental data on the larger column, Fig. 4.58 and Saxena et al [113], are shown compared with the predictions of all the four approaches [56, 57, 64 and 76] in Figs. 5.20 and 5.21. It is clear that the correlations of Reilly et al. [56] and Smith et al. [57] predict negligible dependence of gas-phase holdup on temperature, and their predictions at best can be regarded as only in approximate agreement with the experimental data. The correlation of Roy et al. [64] predicts the experimental data rather poorly though it has the right qualitative dependence on temperature. The main reason of the failure of this model is due to the inclusion of column diameter in the correlation. The computed values based on O'Dowd et al.'s [76] approach are given in Fig. 5.21. The agreement between the theory and experiment is good. $U_{b\infty}$ values determined from the experimental data are also reported in Fig. 5.21. These are dependent on temperature for a given slurry-gas system, and at temperatures above the ambient these are also apparently dependent on slurry concentration and particle size. $U_{b\infty}$ values increase with increase in temperature (as in the two-phase system), but decrease with increase in solids concentration in the slurry. The influence of particle size cannot be uniquely established from these data. Probably $U_{b\infty}$ may increase with increase in particle size and further experimental work will be useful.

The air holdup data for the air-water-silica sand system of Saxena et al. [114] graphed in Fig. 4.50 are compared with the computed values based on these four approaches [56,57,64 and 76] in Figs. 5.22 and 5.23. The nature of disagreement between the theory and experiment is almost identical for the two slurry concentrations. The Smith et al. [57] correlation based values give the best agreement with experimental values though these systematically overpredict them.

Reilly et al. [56] values are greater than the experimental results by larger magnitudes than the Smith et al. [57] values. Roy et al. [64] correlation based

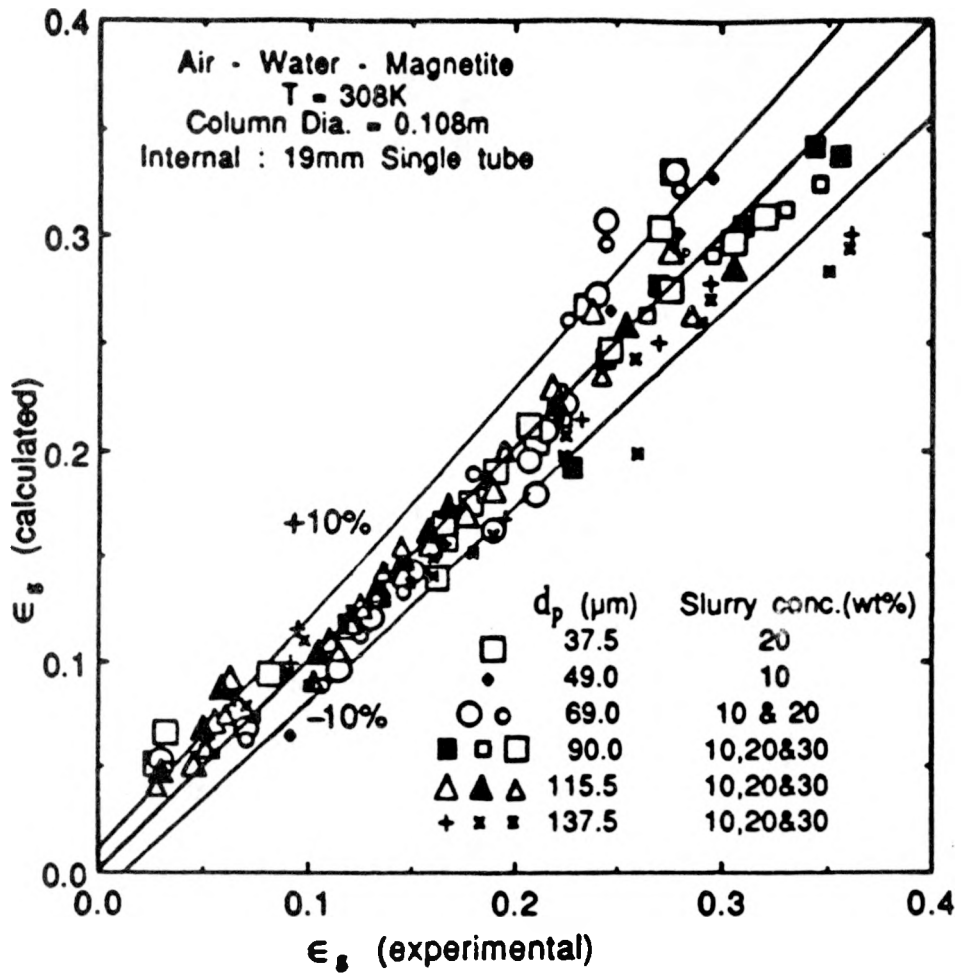

Fig. 5.19. Parity plot for gas holdup. ϵ_g (calculated) are according to the relation of Eq. (5.21).

Table 5.3. Values of $U_{b\infty}$ based on Eq. (5.21) and determined from experimental gas holdup data for air-water magnetite system in 0.108 m in bubble column equipped with a 19 m tube. The data was measured at 308K for particles in the size range 35.7 - 137.5 μm and slurry concentrations in the range 10 - 30 wt%.

Table 1. Values of $U_{b\infty}$ Determined from Experimental Gas Holdup Data

d_p	35.7	49	58	69	69	90	90	90	115.5	115.5	115.5	137.5	137.5	137.5
w_s(%)	20	10	10	10	20	10	20	30	10	20	30	10	20	30
$U_{b\infty}$	0.260	0.265	0.330	0.250	0.275	0.320	0.360	0.410	0.353	0.375	0.450	0.400	0.425	0.460

Table 5.4. Values of $U_{b\infty}$ based on Eq.(5.21) and determined from experimental gas holdup data for nitrogen-Therminol-magnetite system for different internals in 0.108 m bubble column at ambient temperature.

Internal	Solids concentration (weight percent)			
(mm)	0	15	30	50
19.0	0.864	0.875	0.800	0.785
31.8	-	0.888	1.000	1.300
50.8	-	0.800	1.070	1.000

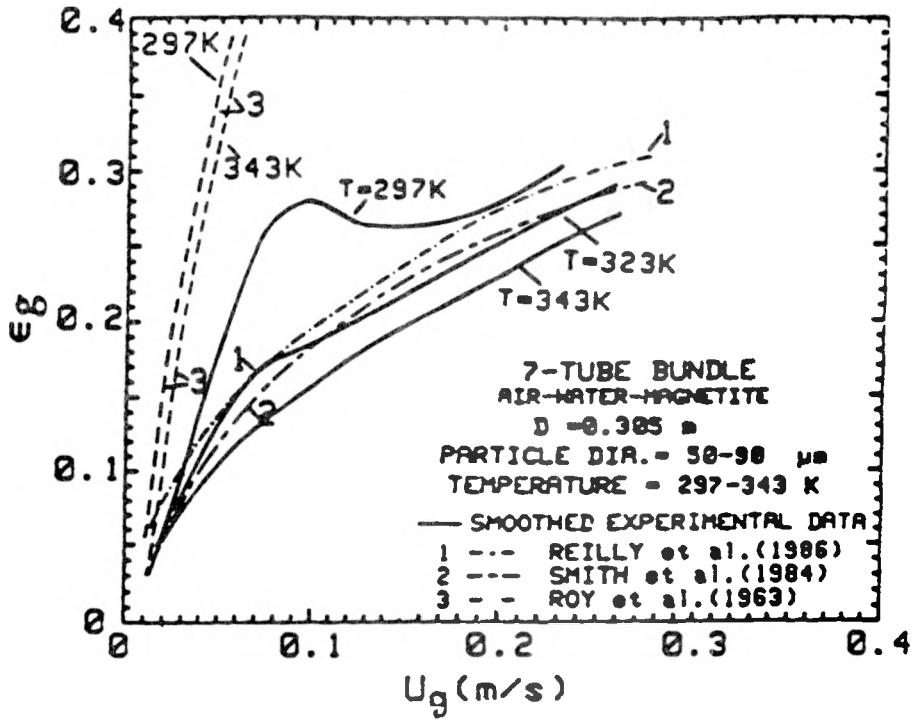

Fig. 5.20. Comparison of averaged experimental air holdup values with the calculated values.

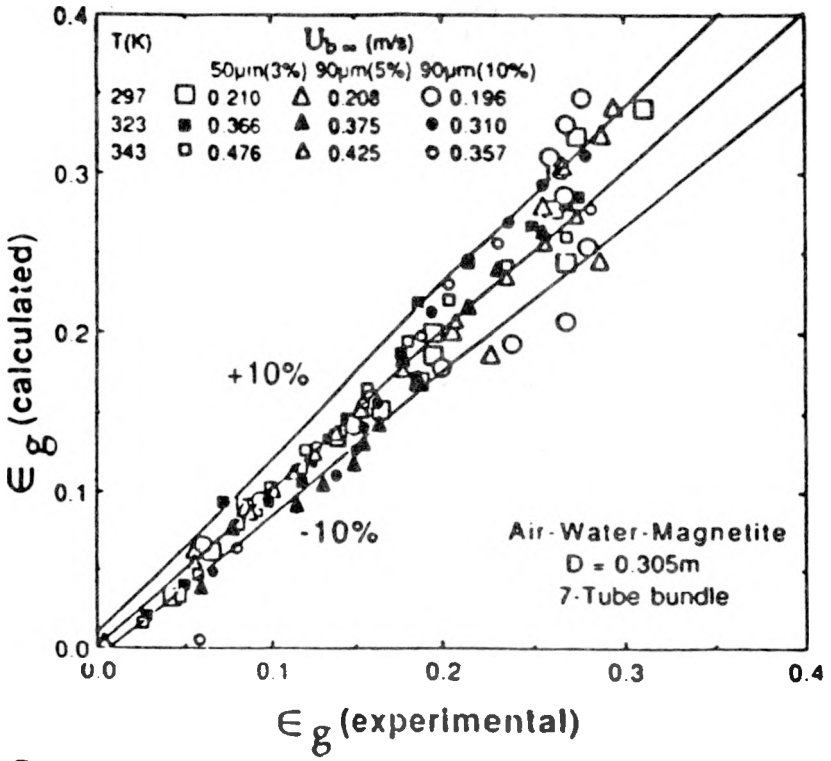

Fig. 5.21. Comparison of experimental and calculated air holdup values on Nicklin's approach.

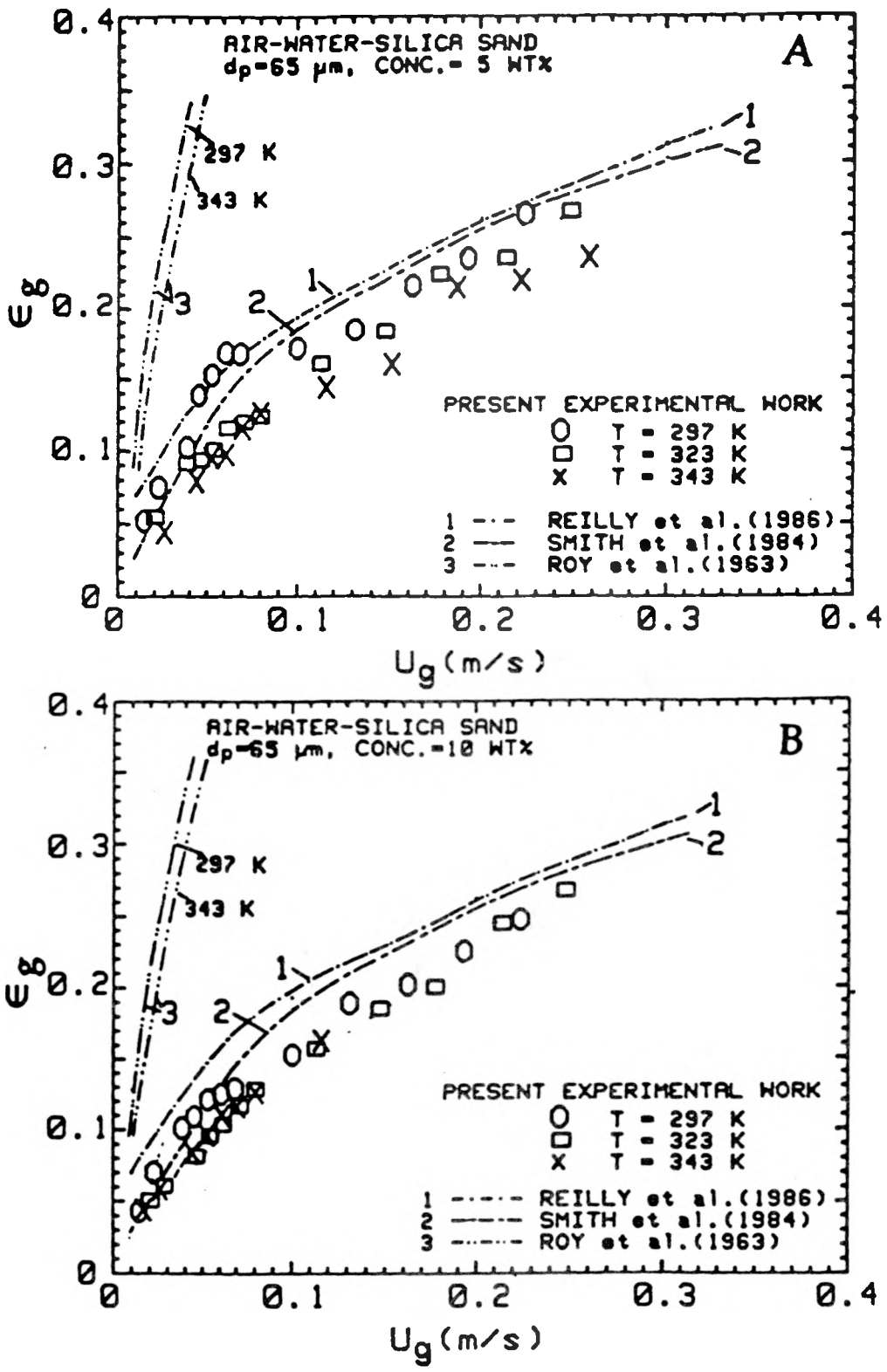

Fig. 5.22. Comparison of air holdup values for air-water-silica sand system over a range of slurry concentrations and temperatures as a function of air velocity with the predictions of different correlations.

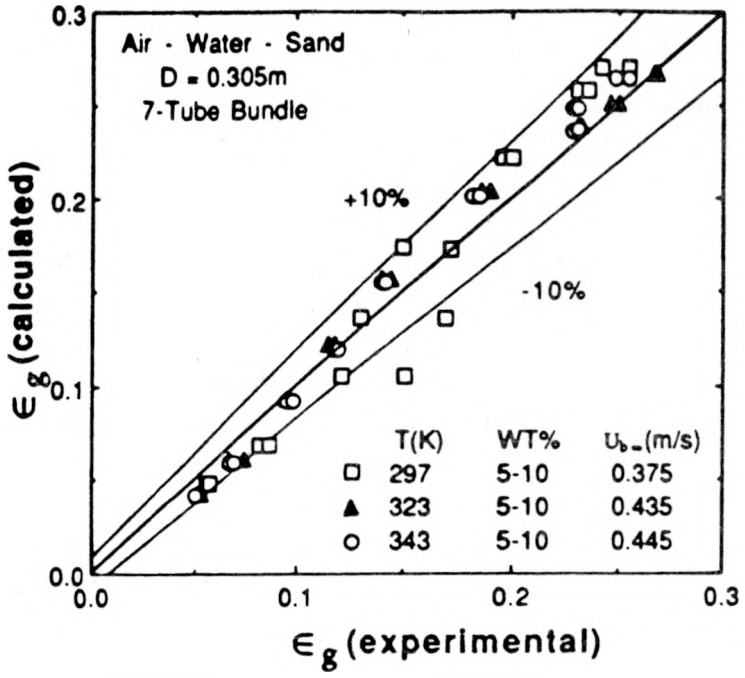

Fig. 5.23. Parity plot for the air-water-silica sand system gas holdup data. Calculated values are based on Eq. (5.21).

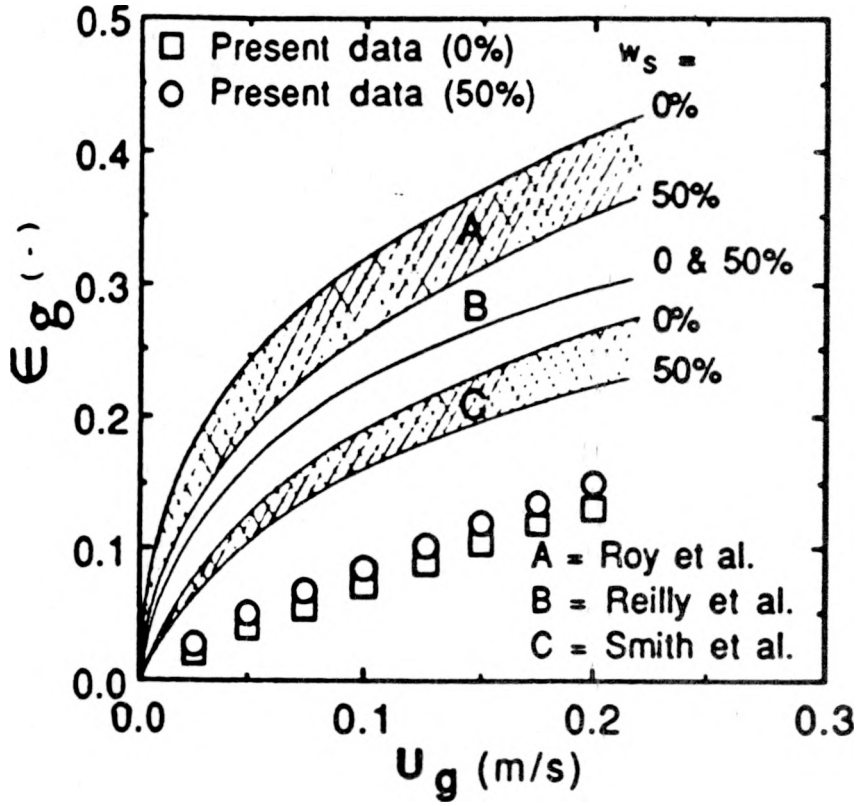

Fig. 5.24. Comparison of experimental data (□ 0%, ○ 50%) for the 19.0 mm probe with the predictions of correlations.

values are in poor agreement with the experimental data both qualitatively as well as quantitatively. This is probably because of the involvement of column diameter as one of the parameters in the correlation.

The drift-flux approach leads to satisfactory results for the air-water-sand system also. The $U_{b\infty}$ values, listed in Fig. 5.23, are again found to be temperature dependent, but these are much less pronounced for the three-phase system than their corresponding two-phase gas-liquid system.

A comparison of nitrogen holdup for the nitrogen-Therminol-red iron oxide system as obtained by Saxena et al. [82] is presented in Fig. 5.14B with the predictions based on the models of Roy et al. [57]. Smith et al.'s correlation [57] is the best of all and reproduces the data satisfactorily. Figure 5.15 presents the comparison of these data with the drift-flux theory [76] which is quite successful. The $U_{b\infty}$ values listed in Table 5.2 exhibit a clear dependence of $U_{b\infty}$ on slurry concentration and its variation with the internal geometry of the column is consistent with its physical meaning.

A comparison of nitrogen holdup data as reported in Figs. 4.15 through 4.17 for nitrogen-Therminol-magnetite system (Saxena et al. [114]) are compared with the model predictions in Fig. 5.24. Two points are to be noted. The experimental data are considerably smaller than the computed results. Further, Roy et al. [64] and Smith et al. [57] correlations predict a larger slurry concentration dependence (0-50 weight percent) than is experimentally observed. Reilly et al.'s correlation [67] has no slurry dependence. It appears that these correlations are not adequate for systems involving highly viscous liquids. A similar shortcoming was observed for nitrogen-Therminol-red iron oxide (1.7 μm) system. Smith et al. [57] correlation gives the best reproduction both as regards to the gas velocity and slurry concentration variations. It may be pointed out that the holdup predictions for less viscous systems, air-water-magnetite [105], by Smith et al.'s [57] correlation were much more satisfactory.

In Fig. 5.25 are presented the computed nitrogen holdup values as compared to the experimental values obtained by following the procedure outlined by O'Dowd et al. [76]. The $U_{b\infty}$ is treated as a disposable parameter and adjusted on the basis of experimental data. These values are listed in Table 5.4 for different size probes and slurry concentrations. The plots in Fig. 5.25 are separated from

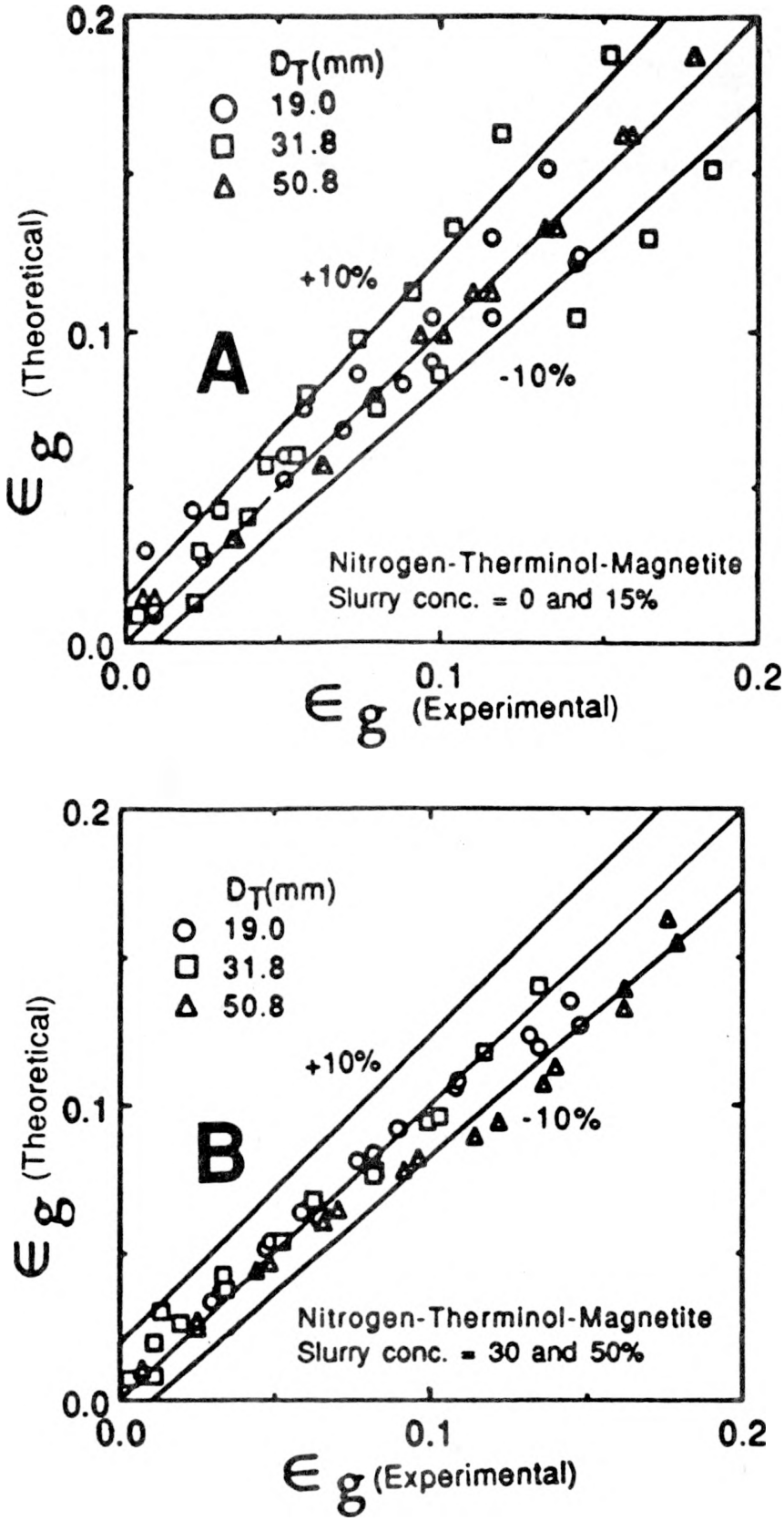

Fig. 5.25. Comparison of experimental and calculated nitrogen holdup values based on drift-flux theory.

one another only to avoid overcrowding. It is clear that this approach could correlate the data within an estimated uncertainty of about ten percent. It appears to be a reasonable approach for data correlation at the present time.

Saxena et al. [115] have also measured the nitrogen holdup for the nitrogen-Therminol-magnetite system in the small column equipped with a seven-tube bundle at ambient conditions and for slurries in the range 0-50 weight percent. These data are compared with the three models [56, 57 and 64] in Fig. 5.26, and with O'Dowd et al.'s [76] approach in Fig. 5.27. In all cases, the models predict the data rather unsatisfactorily. The computed values are much larger than the experimental values and will be poor estimates for any design work. Roy et al.[64] and Reilly et al. [56] fail to predict even the dependence of ϵ_g on w_s. Gas holdup correlations must be developed by taking into account the effect of liquid viscosity. The reproduction by the drift-flux theory is good but real confidence in this theory will have to await a good physical interpretation of the terminal rise velocity of a single bubble in an infinite medium ($U_{b\infty}$) which has been treated here as an adjustable parameter.

5.5 Conclusions and Recommendations

The measurements of gas holdup reported here for two liquids of widely different viscosities in bubble columns equipped with internals of different configurations and employing solids of different sizes and concentrations reveal certain interesting trends, which are mentioned here. Viscosity has a profound influence on gas holdup which decreases as the viscosity increases. The presence of solids also decreases the gas holdup. The temperature has an involved dependence and our data suggest that with increase in temperature the holdup decreases and the magnitude of this decrease reduces with increase in temperature for less viscous liquids. For liquids of high viscosity the above mentioned qualitative trend changes at some temperature beyond which the holdup increases with increase in temperature. These trends can be explained with the changes in the rheology of the system and hence proper knowledge of viscosity for the system under consideration is essential. Viscosity of the suspension influences the bubble dynamics in the column and hence the gas

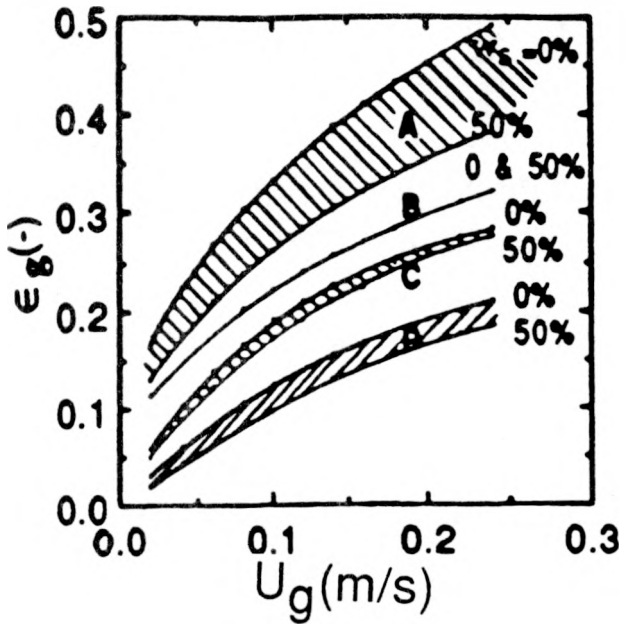

Fig. 5.26. Comparison of ϵ_g with model predictions.
A - [64], B - [56], C - [57], and P- Present data.

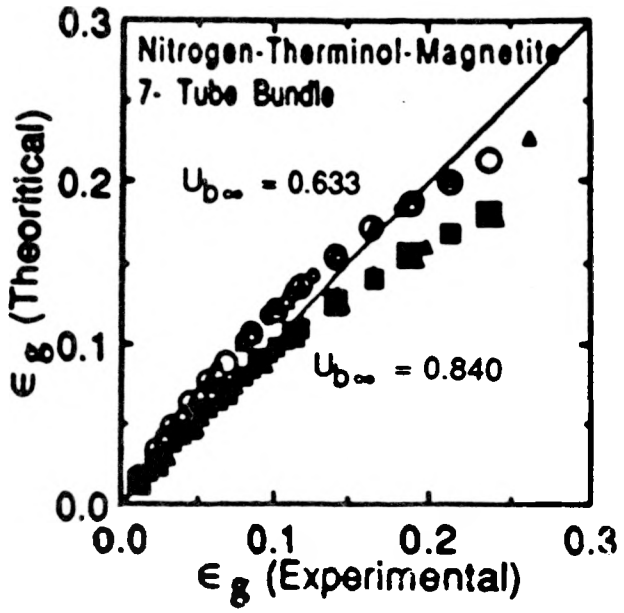

Fig. 5.27. Comparison of experiment and theory [76] for ϵ_g.

holdup. Internals are found to influence the bubble coalescence and thereby the gas holdup. Holdup data in bubble columns are insensitive to column diameter.

Existing correlations are extensively tested and are found to be inadequate to reproduce or predict the gas holdup. The modified drift-flux theory approach is found successful in correlation the experimental data and this success suggests that a more basic approach to develop a sound theory for the evaluation of $U_{b\infty}$ in terms of system and operation parameters is in order. The information generated here will help in achieving this goal. Gas holdup data are important to characterize the slurry bubble column operation, and in establishing the mass transfer and mixing characteristics.

6. DISCUSSION OF EXPERIMENT AND THEORY: HEAT TRANSFER

6.1 Available Data and Correlations for Two-Phase Systems

Heat transfer in air-water system has been widely investigated and serves as an important basis for assessing the relative accuracies of different measurements. All the available data along with smoothed values [83] are displayed in Fig. 6.1. Curve 1 represents the data of Kolbel et al. [84] taken in columns of diameter 19.2 and 29.2 cm fitted with a porous plate distributor and a cylindrical heater of length and diameter 10 cm and 3 cm respectively at 313 K for air velocities in the range 0.0035-1.10 m/s. The present data are in good agreement with their values except for air velocities smaller than about 0.025 m/s. Fair et al. [85] data at 300 K in a 0.457 m diameter column, referring to column wall and air-water dispersion, are shown as curve 2 in Fig. 6.1. Stationary baffles comprised of perforated plates with holes of varying diameters and spacing were placed in the column and water flow of 10 to 13 gallons per minute was maintained. When the baffles were given a reciprocating rapid motion (1050 cycles per minute), heat transfer coefficient values were consistently higher than those shown in Fig. 6.1. Data were also obtained for a 1.07 m diameter column fitted with forty-two tubes of 0.038 m diameter in two concentric circles of diameters 0.98 and 0.88 m. One of the tubes of the bundle served as a heater. Their graphical plot of heat transfer coefficient values showed an appreciable scatter but there was an overall general agreement in the two sets of experimental values which they have represented by simple correlation. They point out a greater uncertainty in their low air velocity data. From Fig. 6.1, it is clear that their data are consistently greater than the present data, the disagreement is about 20% at lower air velocities and it decreases to about 5% at higher air velocities. At least part of this systematic disagreement may be attributed to the liquid flow and presence of baffles in the heat transfer rates for the column wall and an immersed surface.

Burkel's data [86, 87] referring to an immersed surface (coil) in a 0.19 m cylindrical column are shown as set 3 in Fig. 6.1. At higher air velocities his data are differing by about 10% from the present work and this difference is about 15%

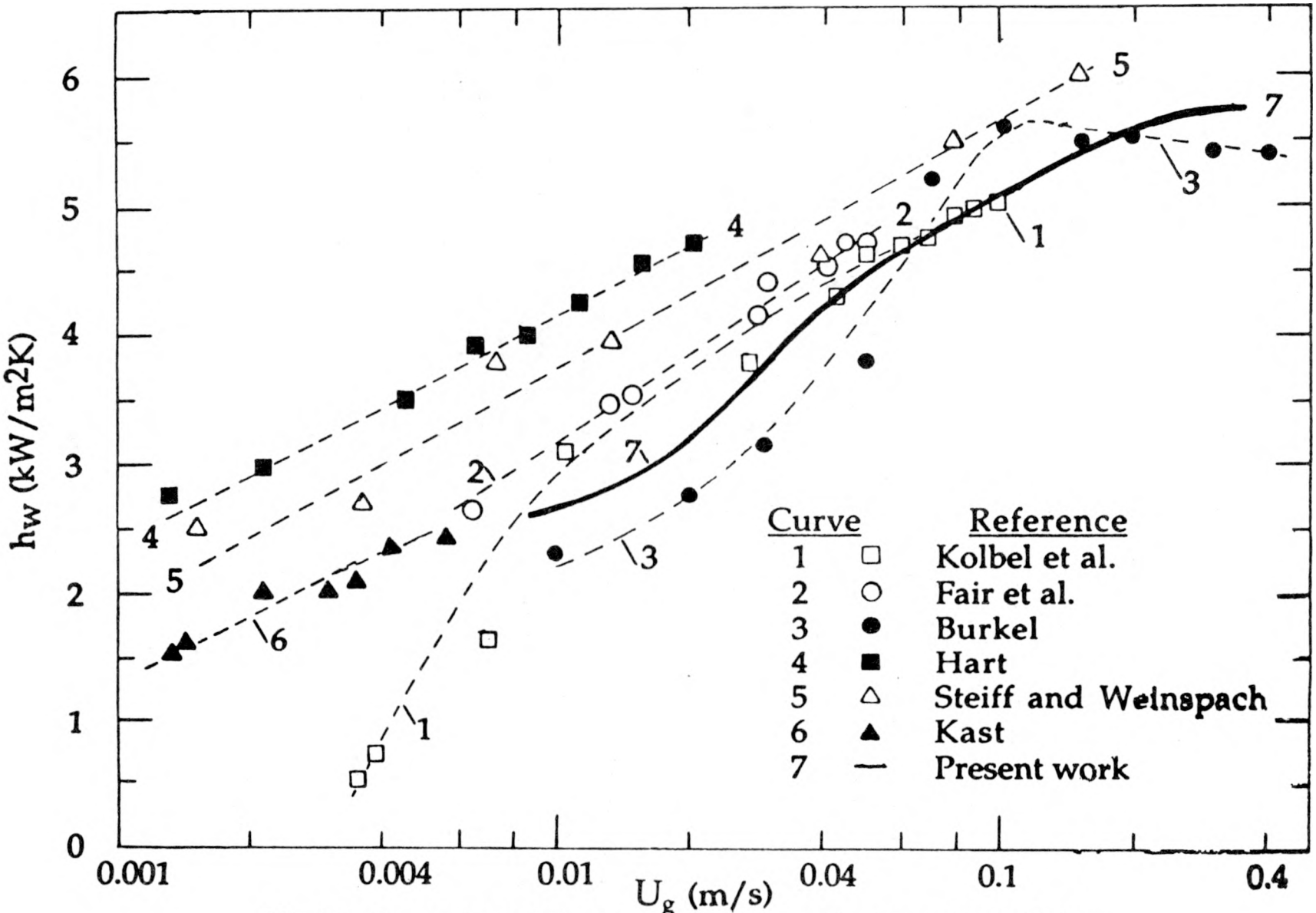

Fig. 6.1. Comparison of the present experimental heat transfer coefficient values with the measurements of other workers for the air-water system as a function of superficial air velocity and temperatures in the range 300-344 K.

at lower air velocities. His values are considered unreliable on the whole in view of their general disagreement from all the available data sets, and their qualitative trend of variation with air velocity. Set 4 of Fig. 6.1 refers to the data of Hart [88] at 344 K taken in a column of 9.9 cm diameter and equipped with a single nozzle of 6.35 mm diameter. Water was allowed to flow with a constant velocity, and column wall to air-water dispersion heat transfer coefficient was measured. The apparent disagreement of these data from present work is due to a higher temperature to which these refer. Hart [88] has empirically correlated his data to show their general agreement with the data of set 2. This will imply that these data [88] like set 2 are consistently greater than sets 1 and 7. Further, this disagreement increases with decrease in air velocity.

Steiff and Weinspach [89] employed a 19 cm diameter column fitted with a sintered plate distributor and measured heat transfer coefficient between the heated column wall and the air-water dispersion at 313 K. The latter was obtained by the cocurrent flow of air and water through the column. These data, Set 5, are consistently greater than all the other data sets. The disagreement with set 7 is 40% at the lowest air velocity and decreases to 10% at the highest air velocity. This disagreement if not attributed to the difference between the measured column wall and an immersed surface heat transfer coefficient in view of the above discussion, then it would suggest that the way these workers have averaged their heated surface temperature and column water temperature might have given rise to systematic error in their computed heat transfer coeffcient values. The inference that these data are not reliable is, however, more conclusive and evident from the analysis of Fig. 6.1.

Kast [80] has reported heat transfer coefficient for 28.8 cm diameter column wall and air-water dispersion as a function of air velocity in the range 0.02 to 0.6 cm/s. His data shown as set 6 in Fig. 6.1, appear to be consistent with the data of Fair et al. [85] (set 2) and probably with Hart [88] (set 4), but are systematically smaller than Steiff and Weinspach [89] (set 5) and greater than Kolbel et al. [84] (set 1). However, for U_g smaller than 0.008 m/s, the bubble induced liquid mixing in the column is sensitive to the column diameter and the nature of the air sparger. As a result one could expect significant differences in the heat transfer values measured for the column wall for an immersed surface. We

think that this is the reason for appreciable differences in the heat transfer rate values reported by different workers in this low air velocity region shown in Fig. 6.1.

The heat Transfer coefficient values obtained as a function of air velocity in the present work and shown in Fig. 6.2 by curve are compared with the predictions of various available correlations and models. Fair et al. [85] on the basis of their data in the air velocity range 0.023 to 0.107 m/s proposed the following empirical correlation:

$$h_w = 8849\ U_g^{0.22} \qquad 6.1$$

The expressions leads to values, curve b in Fig. 6.2 that are in poor agreement with our measured values both at low and high gas velocities . Further, this form for h_w is incapable of reproducing the qualitative feature of heat transfer coefficient according to which h_w approaches a constant value at higher velocities.

Mersmann [91] proposed a correlation for the heat transfer in bubble columns in analogy to the phenomenon of free convection by replacing the Grashof number with the Archimedes number. His [91] final result is

$$h_w = 0.107\ k_L \left(g/v_L \alpha\right)^{1/3} Pr^{0.226} \qquad 6.2$$

Computed values of h_w at 308 K from Eq. (6.2) is 4.21 kW/m^2K is independent of air velocity. The constant h_w value which is invariant with respect to air velocity on the basis of our data is 5.8 kW/m^2K. Thus, it is clear that Mersmann [91] theory predictions are appreciably smaller than the measured values.

Zehner [92] heat transfer model assumes a thinned thermal boundary layer on the heat transfer surface when bubbles are present. The length of the boundary layer was taken to be the same as the distance between successive bubbles, l, and its values was assumed to be constant as 7 mm. The heat transfer through the boundary layer is described as that over a flat heated plate. His final expression for gas velocities up to about 0.1m/s is

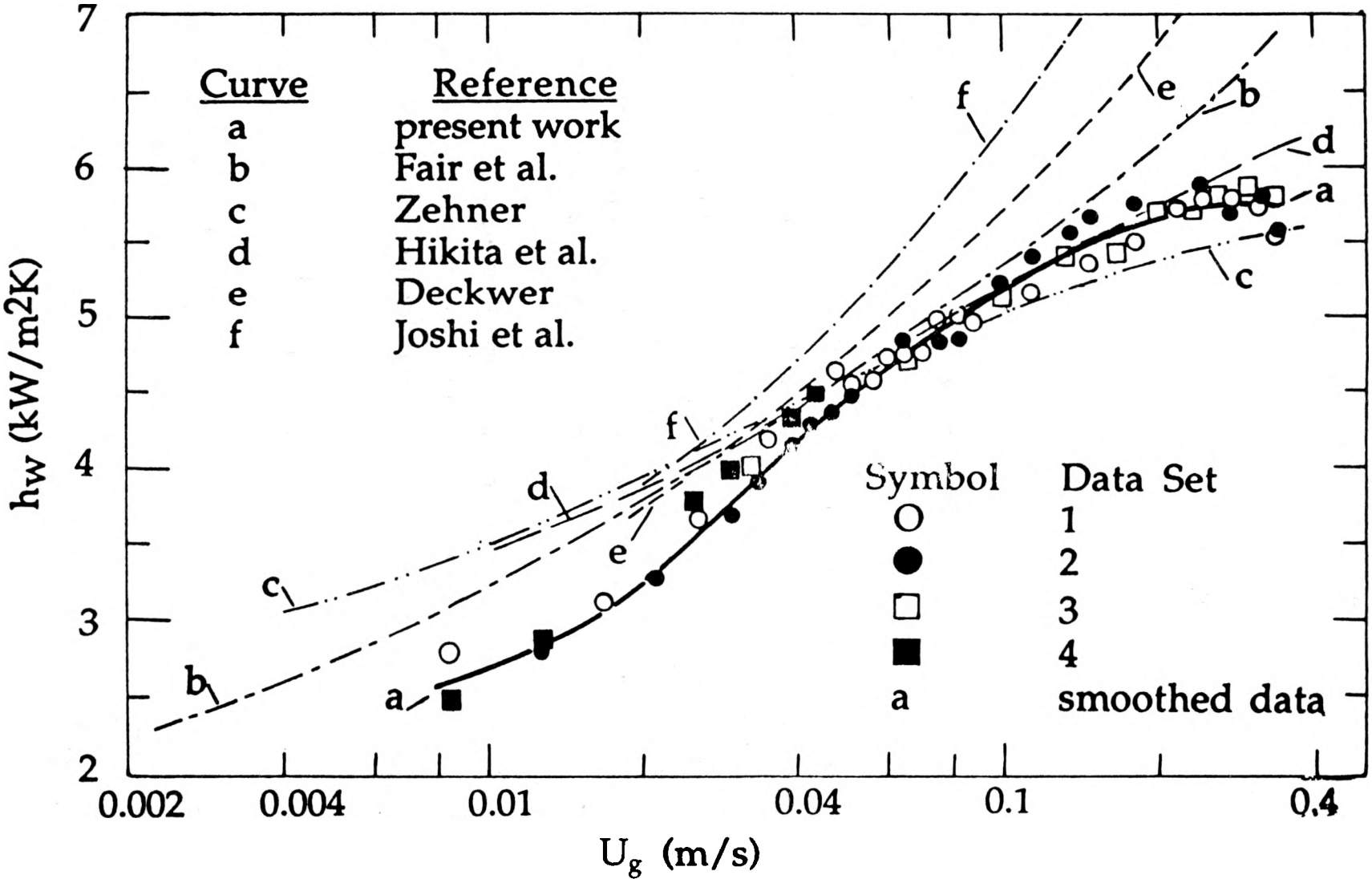

Fig. 6.2. Comparison of experimental heat transfer coefficient with various computed sets for air-water system as a function of superficial air velocity at 309 K.

$$h_w = 0.18(1 - \epsilon_g)\left[k_L^2\ \rho_L^2\ C_{pL}\ V_F^2 / l\ \mu_L\right]^{1/3} \qquad 6.3$$

Where

$$l = d_b(\pi/6\epsilon_g)^{1/3} \qquad 6.4$$

$$V_F = \left[\frac{1}{2.5}\left(\frac{\rho_L - \rho_g}{\rho_L}\right) g\, D_C\, U_g\right]^{1/3} \qquad 6.5$$

and

$$\epsilon_g = U_g\ /\ \left[0.25 \exp\left(5\ \epsilon_g\right)\right] \qquad 6.6$$

Computed values from these relations are shown as set C in Fig. 6.2. In the lower air velocity range (<0.06 m/s), his values are greater than our measured values, but are in good agreement for the range 0.06 to 0.10 m/s. At higher velocities his values approach to a constant value for heat transfer coefficient which, however, is smaller than the experimentally obtained values. The difference is about 8 percent. One important factor to note in this theory is that h_w is dependent on column diameter. Several workers have claimed h_w to be independent of column diameter.

Hikita et al [87] proposed the following empirical correlation based on their data for several liquids having widely different values of viscosity and surface tension for temperatures (295 to 318 K) and air velocities (5.3 to 34 cm/s):

$$\frac{h_w}{\rho_L\ C_{pL}\ U_g}\left(\frac{C_{pL}\ \mu_L}{k_L}\right)^{2/3} = 0.411\left(\frac{U_g\ \mu_L}{\sigma_L}\right)^{-0.851}\left(\frac{\mu_L g}{\rho_L\ \sigma_L^3}\right)^{0.308} \qquad 6.7$$

They also show that if the influence of σ_L on h_w is ignored, the above relation can be simplified to:

$$\frac{h_w}{\rho_L\ C_{pL}\ U_g}\left(\frac{C_{pL}\ \mu_L}{k_L}\right)^{2/3} = 0.268\left(\frac{U_g^3\ \rho_L}{\mu_L g}\right)^{-0.303} \qquad 6.8$$

Alternatively

$$St = 0.268 \left[Re_b\ Fr\ Pr^{2.16}\right]^{-0.303} \qquad 6.9$$

The computed values of h_w form Eq. (6.7) are consistently greater than the experimental values over the entire air velocity range by about 60%. The reason for this large discrepancy lies in the fact that these workers [87] have used their own data in the development of Eq. (6.7). Their data are much higher than the experimental values found by other workers and it could be due to the small size of the heater they have used on the column wall. We adjusted the numerical constant in Eq. (6.7) on the basis of our data to obtain the following relation:

$$\frac{h_w}{\rho_L\ C_{pL}\ U_g}\left(\frac{C_{pL}\ \mu_L}{k_L}\right)^{2/3} = 0.271\left(\frac{U_g\ \mu_L}{\sigma_L}\right)^{-0.851}\left(\frac{\mu_L\ g}{\rho_L\ \sigma_L^3}\right)^{0.308} \qquad 6.10$$

Computed values of Eq. (6.10) are shown in Fig. 6.2 às set d. The data are poorly reproduced in the low as well as in the high gas velocity range.

Kast [90] and many other workers [86-89, 93-96] after him have proposed the calculation of h_w based on an expression of the following general form:

$$St = C_1 \left[Re_b\ Fr\ Pr^{C_2}\right]^{-C_3} \qquad 6.11$$

Different values of C_1, C_2 and C_3 have been recommended. A critical study of Deckwer [93] show that a good compromised choice is,

$$St = 0.1 \left[Re_b\ Fr\ Pr^2\right]^{-0.25} \qquad 6.12$$

when gas velocity is less than 10 cm/s. Computed values of h_w are shown as curve e in Fig. 6.2. The calculated values are consistently greater than the experimental values, the disagreement increases from 8% at 0.03 m/s to 19% at 0.20 m/s. The form of Eq. (6.12) also does not lead to values which approach to a constant h_w at higher gas velocities.

Joshi and Sharma [97] in contrast to Deckwer [93] have argued that the input gas energy is dissipated and consumed mostly in the wakes of the bubbles and only less than 10% is used to create liquid motion in the bubbly flow regime. Assuming ideal inviscid flow behavior and the presence of multiple interacting cells in the axial direction, they have derived the following expression for the average liquid circulation velocity in the bubble column:

$$V_c = 1.31 \left[g D_C \left(U_g - \epsilon_g U_{b\infty} \right) \right]^{1/3} \qquad 6.13$$

The average axial component of this liquid velocity is:

$$V_a = 1.18 \left[g D_C \left(U_g - \epsilon_g U_{b\infty} \right) \right]^{1/3} \qquad 6.14$$

Substituting this value of V_a in the Sieder and Tate equation, Joshi et al [98] proposed the following relation for the calculation of h_w

$$\frac{h_w D_C}{k_L} = 0.031 \left[\frac{D_C^{1.33} g^{1/3} \left(U_g - \epsilon_g U_{b\infty} \right)^{1/3} \rho_L}{\mu_L} \right]^{1/3} \left(\frac{C_{pL} \mu_L}{k_L} \right)^{\frac{1}{3}} \left(\frac{\mu_L}{\mu_w} \right)^{0.14} \qquad 6.15$$

as shown in Fig. 6.2, computed values based on this relation, curve f, are consistently and significantly greater than the experimental values.

6.2 Available Data and Correlations for Three-Phase Systems

Smith et al. [99] have presented an extensive tabulation of existing correlations for three-phase reactors of column wall or immersed surface to a three-phase dispersion. However, here we will discuss only those correlations and models which are appropriate to mimic the operation of a slurry bubble column in which the continuous liquid phase is either stagnant or moving rather slowly and the turbulent mixing and solids dispersion is caused by the gas bubbling through the column.

Kolbel et al. [100] have measured the heat transfer between a heated probe immersed in water with sand particles and air bubbling up to a maximum

velocity of about 12 cm/s. Samples of sand were used with average particle diameter (d_p) as 0.04, 0.075, 0.11 and 0.2 mm. Based on these data, it was proposed that for laminar flow

$$Nu = 222.8\, Re^{0.16}\, (d_p/d_o)^{0.05} \qquad 6.16$$

and for turbulent flow,

$$Nu = 350.8\, Re^{0.108}\, (d_p/d_o)^{0.05} \qquad 6.17$$

These correlations were recommended for

$$1 < (d_p/d_o) < 5 \qquad 6.18$$

with d_o = 0.04 mm.

Further, Nu and Re are defined as [101]

$$Nu = h_w\, d_p/k_L \qquad 6.19$$

and

$$Re = U_g\, \rho_g\, d_p/\, \mu_g \qquad 6.20$$

For the present system and operating conditions, the correlation of Eq. (6.17) is applicable. However, the calculations yielded much greater values than the corresponding experimental values. In view of the involvement of d_p and d_o in the correlation, we consider it only of historical importance and do not use it for detailed calculations and comparison with our experimental data in this work. Further, some ambiguity exists about the calculation of Nu and Re, and these are also defined in terms of the diameter of the heating element in one of their works [102].

For two-phase bubble and droplet columns, Mersmann et al. [103, 91] have

recommended that the maximum heat transfer coefficient, $h_{w\ max}$, is given by

$$h_{w\ max} = 0.12\left(\frac{g^2\rho_L}{\mu_L}\right)^{\frac{1}{6}}\left(\frac{\rho_L-\rho_g}{\rho_L}\right)^{\frac{1}{3}}\left(k_L\rho_L C_{pL}\right)^{\frac{1}{2}} \qquad 6.21$$

Here all quantities are in SI unit system. For the applicability of this relation, the following condition must also be satisfied.

$$Ar \cdot Pr > 10^6 \qquad 6.22$$

where

$$Ar = \frac{d_b^3(\rho_L - \rho_g)g\rho_L}{\mu_L^2} \qquad 6.23$$

and

$$Pr = \frac{\mu_L C_{pL}}{k_L} \qquad 6.24$$

For air-water system in the churn turbulent regime, the product of Ar and Pr is 3.3×10^7 for $d_b = 7$ mm [104, 77]. This validates the applicability of the above correlation to the present work. Calculations revealed that the value of $h_{W\ max}$ is about 4.43 kW/m^{2}K. Our measurements give a value of about 6.2 kW/m^{2}K.

For three-phase systems it is being proposed [105] to examine the validity of this correlation in the following revised form:

$$h_{w\ max} = 0.12\left(\frac{g^2\bar{\rho}}{\bar{\mu}}\right)^{\frac{1}{6}}\left(\frac{\bar{\rho}-\rho_g}{\bar{\rho}}\right)^{\frac{1}{3}}\left(\bar{k}\bar{\rho}\bar{C}_p\right)^{\frac{1}{2}} \qquad 6.25$$

where all the quantities now refer to the three-phase suspension and are computed according to the following relation listed in [51]:

$$\bar{\rho} = v_s\ \rho_s + v_L\ \rho_L \qquad 6.26$$

$$\bar{\mu} = \mu_L (1 + 4.5\, v_s) \qquad 6.27$$

$$\bar{k} = k_L \frac{2k_L + k_s - 2v_s (k_L - k_s)}{2k_L + k_s - v_s (k_L - k_s)} \qquad 6.28$$

$$\bar{C}_p = w_s C_{ps} + w_L C_{pL} \qquad 6.29$$

Following the reasoning given by Deckwer [93] for heat transfer from an immersed surface to liquid agitated by gas in a bubble column, Deckwer et al. [51] have proposed that the heat transfer coefficient from an immersed surface to a three-phase dispersion may be given by the following relation:

$$St = 0.1 \left[Re\ Fr\ Pr^2\right]^{-0.25} \qquad 6.12$$

This expression is valid for gas velocities up to 10 cm/s and thereafter h_w asssumes a constant value. Here

$$St = h_w / \bar{\rho}\, \bar{C}_p\, U_g \qquad 6.30$$

$$Re = U_g\ d_p\ \bar{\rho} / \bar{\mu} \qquad 6.31$$

$$Fr = U_g^2 / g d_p \qquad 6.32$$

and

$$Pr = \bar{C}_p\, \bar{\mu} / \bar{k} \qquad 6.33$$

$\bar{\rho}$, $\bar{\mu}$, $\bar{k}$ and $\bar{C}_p$ in the above equations are as defined by relations of Eqs. (6.26) - (6.29).

Pandit and Joshi [106] while reviewing the heat transfer literature in three-phase gas sparged reactors have mentioned that the difference between heat transfer coefficient for small particles (<100 μm) for gas-liquid and gas-liquid-solid systems is nominal. However, this difference was found to increase with an increase in the solid-phase holdup. h_w increases with d_p and levels off for d_p greater than 3mm. A maximum value of h_w occurred at a specific value of ϵ_s. This value of ϵ_s depends upon the value of d_p. h_w is found to be practically independent of the value of column diameter. They [106] also remarked that the h_w value is the same for the column wall and for a surface immersed in the reactor.

For the case of small particles (<100μm) and in the absence of liquid flow, Pandit and Joshi [106] have proposed the following explicit relation for the estimation of h_w:

$$h_w = 0.087\,(U_g - \epsilon_g U_{b\infty})^{0.266} g^{0.26}\,\bar{\rho}^{\,0.8}\,\bar{C}_p^{\,0.34}\,\bar{\mu}^{-0.33}\,\bar{k}^{\,0.66}\,D_T^{0.06}\,\mu_w^{-0.14} \qquad 6.34$$

Here h_w = 0.087 in kcal/m^2° C h, U_g is in m/s, ϵ_g is fractional gas holdup, $U_{b\infty}$ is the terminal rise velocity of a single bubble in m/s, g is the acceleration due to gravity in m^2/s, $\bar{\rho}$ defined by Eq. (6.26) is in kg/m^3 , $\bar{C}_p$ defined by Eq. (6.29) is in k cal/kg.°C, $\bar{\mu}$ defined by Eq. (6.27) in kg/m s, $\bar{k}$ defined by Eq. (6.28) is in kcal/m°C s, D_T is the column diameter in m, and μ_w is the viscosity of water in kg/m s. The gas-phase holdup was correlated by an equation of the following type.

$$\epsilon_g = \frac{U_g}{a + bU_g} \qquad 6.35$$

for each value of ϵ_s. The constant a was identified with $U_{b\infty}$. They have prepared a table listing the constants a and b as a function of particle diameter and solid-phase holdup.

Kim et al. [107] have synthesized the data of two-phase (liquid-solid) and three-phase fluidized-bed heat transfer on the basis of the following correlation which implies the heat transfer model of the surface renewal type with isotropic turbulence.

$$h_w = 0.0722\left(k_L \rho_L C_{pL}\left\{\left[(U_L + U_g)\left(\epsilon_g \rho_g + \epsilon_L \rho_L + \epsilon_s \rho_s\right) - U_L \rho_L\right] g(\epsilon_L \mu_L)^{-1}\right\}^{\frac{1}{2}}\right)^{\frac{1}{2}} \qquad 6.36$$

For a slurry bubble column with $U_L = 0$, the above relation reduces to:

$$h_w = 0.0722\left(k_L \rho_L C_{pL} \left\{ \left[U_g \left(\epsilon_g \rho_g + \epsilon_L \rho_L + \epsilon_S \rho_S \right) \right] g(\epsilon_L \mu_L)^{-1} \right\}^{\frac{1}{3}} \right)^{\frac{1}{2}} \qquad 6.37$$

Deckwer et al. [51, 93] relation of Eq. (6.12) as applied to two-phase (gas-liquid) bubble column can be rearranged to obtain the following explicit relation for the heat transfer coefficient:

$$h_w = 0.1 \left[\left(k_L \rho_L C_{pL} \right) \left(P_v / \mu_L \right)^{\frac{1}{2}} \right]^{\frac{1}{2}} \qquad 6.38$$

where energy dissipation per unit volume, p_v, is,

$$P_v = g U_g \rho_L \qquad 6.39$$

Suh et al. [108] have derived a similar relation for liquid fluidized beds and proposed the following relation for the energy dissipation term for three-phase fluidized beds:

$$P_v = \left[(U_L + U_g) \left(\epsilon_S \rho_S + \epsilon_L \rho_L + \epsilon_g \rho_g \right) - U_L \rho_L \right] g / \epsilon_L \qquad 6.40$$

Kim et al. [107] in deriving Eq. (6.37) have used the relation of Eq. (6.40). Suh et al. [108] proposed a numerical coefficient of 0.0647 in Eq. (6.37) instead of 0.0722. A recent analysis of Suh and Deckwer [109] shows that the form of Eq. (6.38) with p_v given by Eq. (6.40) is appropriate for slurry bubble columns as well as for three-phase fluidized beds with Newtonian and non-Newtonian fluids. For bubble columns with $U_L = 0$, the expression of Eq. (6.40) for p_v is simplified to

$$P_v = \left[U_g \left(\epsilon_s \rho_s + \epsilon_L \rho_L + \epsilon_g \rho_g \right) \right] g / \epsilon_L \qquad 6.41$$

Combining Eqs. (6.38) and (6.41), we get the h_w equation of Suh and Deckwer [109] for a slurry bubble column as follows:

$$h_w = 0.1\left(k_L \rho_L C_{pL} \left\{ \left[U_g \left(\epsilon_S \rho_S + \epsilon_L \rho_L + \epsilon_g \rho_g \right) \right] g(\epsilon_L \mu_L)^{-1} \right\}^{\frac{1}{3}} \right)^{\frac{1}{2}} \qquad 6.42$$

Suh and Deckwer [109] also proposed that μ_L in Eqs. (6.38) and (6.42) represented the apparent effective bed viscosity (μ_b), and for the case of three-phase systems in Eq. (6.42) μ_L be replaced by μ_b. They [109] further suggested that μ_b be computed by the theoretical expression derived by Vand [52], Eq. (4.4). Equation (6.42) is indeed similar to Eq. (6.37) except for the numerical constant and m_b instead of μ_L.

Kato et al. [110] have reported values of heat transfer coefficient between the column wall and fluidized beds of air-water-glass beads. The fluidized beds used were 5.2 and 12.0 cm internal diameter transparent acrylic columns and glass beads of diameter 420 μm, 660 μm, 1.2 mm and 2.2 mm. The heat transfer section for the 5.2 cm column consisted of a 3 cm long and 2 mm thick copper pipe, while for the 12.0 cm column it was 10 cm long and 1 mm thick copper pipe. The heater section was located 25 cm above the distributor and sheath nichrome wire was wound around the outer surface of the pipe. The heat flux through the copper surface was calculated from the power consumption of the electric heater. The temperature difference between the heat transfer surface and the fluidized bed was 0.8 - 3 K. The temperature of the heat transfer surface was maintained close to the ambient temperature and the temperature at the entrance of the bed was 283-301 K, and was kept constant during the experiment to + 0.12 K. The water velocity was varied in the range 0.3 to 10 cm/s while the air velocity was chosen at 2.0 and 10 cm/s.

In the 0.12 m internal diameter column, the influence of gas velocity, liquid velocity and particle size on heat transfer coefficient for gas-liquid-solid fluidized beds was investigated. With increasing liquid velocity, the heat transfer coefficient initially increased, passed through a maximum and a minimum, increased rapidly, and then the degree of the increase in heat transfer coefficient decreased with further increase in liquid velocity. In this region, the flow state of the gas-liquid-solid fluidized bed was stable. The liquid velocity at which the bed became stable was represented by $\overline{U}_{13}$. The small of $\overline{U}_{13}$ increased with increasing particle size and gas velocity for small particles, but it was hardly influenced by gas velocity for large particles.

The heat transfer coefficient for liquid velocities greater than $\overline{U}_{13}$ was influenced by the gas flow velocities. The influence was significant at lower

liquid velocities as the gas flow induced a significant contribution by creating an internal circulation of liquid flow. The data were correlated by the following relation:

$$Nu' = 0.044\,(Re'\,Pr)^{0.78} + 2.0\,Fr^{0.17} \qquad 6.43$$

Here

$$Nu' = h_w d_p \epsilon_L / k_L\,(1-\epsilon_L) \qquad 6.44$$

$$Re' = \rho_L U_L d_p / \mu_L (1-\epsilon_L) \qquad 6.45$$

$$Pr = C_{pL}\mu_L / k_L \qquad 6.46$$

and Fr is defined by Eq. (6.32). For zero superficial liquid velocity, the above relation simplifies to the following:

$$Nu' = 2.0\,Fr^{0.17} \qquad 6.47$$

or

$$h_w = \frac{2.0 k_L (1-\epsilon_L)\, U_g^{0.34}}{\epsilon_L d_p^{1.17} g^{0.17}} \qquad 6.48$$

The relation of Eq. (6.48) will be examined for its appropriateness in representing our heat transfer data for slurry bubble column with zero liquid flow velocity. It can be seen a priori that Eq. (6.48) will not be very appropriate for reproducing the experimental data in view of its pronounced dependence on d_p while experimentally determined h_w values are almost independent of d_p.

6.3 Comparison of Present Two-Phase Data with Theory: Air-Water System

Our extensive heat transfer data for the air-water system as obtained in the smaller column with a single probe [67 - 69] are discussed [83] and the same are reported in the previous section 6.1. Saxena and Patel [80] have taken similar

data for the seven-tube bundle and these values are systematically greater than single tube values, Fig. 4.23. The analysis presented in section 6.2. clearly demonstrated the inability of the existing correlations to reproduce these experimental data. Our analysis revealed that power and semi-logarithmic functions can correlate the data satisfactorily. Figure 6.3 presents this analysis with the following explicit expressions for the two functions.

$$h_w = 10{,}050\ U_g^{0.28} \qquad 6.49$$

and

$$h_w = 7{,}710 + 1.10 \ln U_g \qquad 6.50$$

Heat transfer coefficient taken in the larger column with a single probe [116] are displayed in Fig. 6.4, set g. These are compared with five different correlations as a function of air velocity. In general, the agreement between the experimental (curve g) and theoretical values (curves a-f) is poor in as much as neither the qualitative nor the quantitative dependence of h_w on air velocity is accurately reproduced. The predicted values based on correlations of Fair et al. [85] and Hikita et al. [87], shown as curves a and b respectively in Figure 6.4, under- and over-estimate the experimental data respectively. It would be very useful to develop an accurate correlation which could reproduce the characteristic variation of experimental h_w, viz. a rapid increase in h_w values at lower values of U_g and approaching a constant value at higher values of U_g.

The curve c based on Deckwer's model [93] and strictly valid for values of U_g up to 10 cm/s only, gives a poor reproduction of experimental data. The latter values are consistently underestimated and the model does not have even the qualitative feature of the variation of h_w with U_g. Joshi and Sharma [97] have proposed a circulation cell model, and Joshi et al. [98] have presented two correlations based on analogies with mechanically agitated contactors and with flow pipes. Predictions based on these two correlations are shown as curves d and e respectively in Figure 6.4. In these computations $V_{b\infty}$ is taken as 0.23 m/s following Joshi and Sharma [117] which is based on bubbles of diameters in the

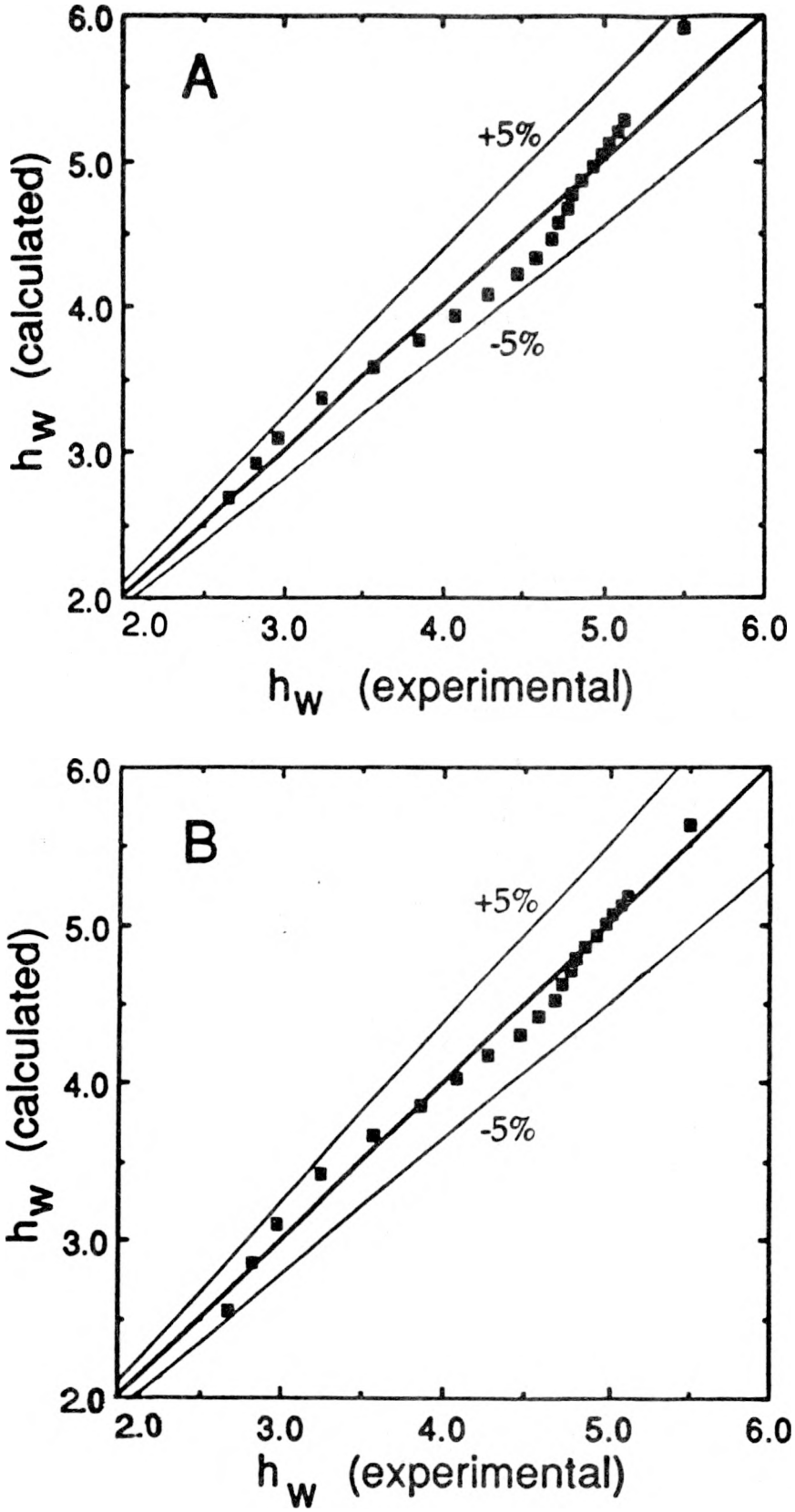

Fig. 6.3. Parity plot of h_W (kW/m^{2}K) for air-water system: (A) power function and (B) logarithmic function.

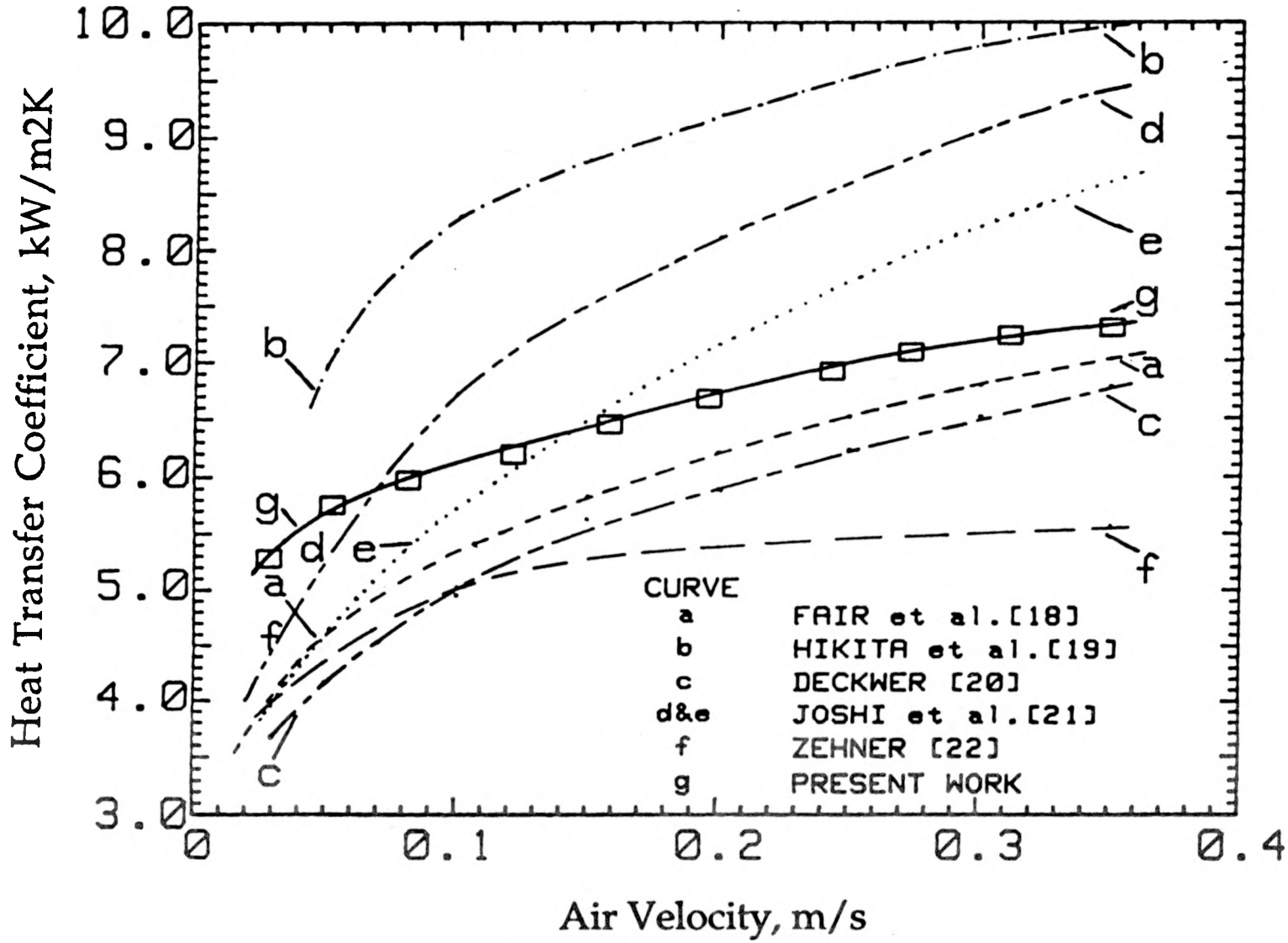

Fig. 6.4. Comparison of the variation of heat transfer coefficient as observed in the larger column for the air-water system at 297K with the predictions of the available correlations and models as a function of air velocity.

range 6 to 7.2 mm and U_g in the range 0.05 to 0.30 m/s. ϵ_g is estimated from the relation developed by Mashelkar [118] for the air-water system. Both sets of values fail to reproduce the experimental data satisfactorily. The set f values are based on the model of Zehner [92, 119] wherein a constant value of 7 mm is assumed for the length of the boundary layer, l. Zehner [92] proposed to use his correlation only up to about 0.1m/s and assumed h_w to be constant thereafter. This model also poorly reproduces the experimental results and the difference between the two sets of values is considerable.

The heat transfer measured with the seven-tube bundle in the larger column [111] at several temperatures are compared with the predictions of relatively successful correlations due to Hakita et al. [87], Pandit and Joshi [106], Kim et al. [107], and Suh and Deckwer [109] in Figure 6.5. The computations performed at the two extreme temperatures, 297 and 343 K, are shown in Figure 6.5, to avoid over crowding. The computed values based on Hikita et al. [87] correlation lead to values which are in poor qualitative agreement with the experimental data. The calculated values of heat transfer coefficient, while smaller than the experimental values at the lower temperature. The Pandit and Joshi [106] correlation based values are considerably smaller than the experimental values at the higher temperatures over the entire air velocity range. On the other hand, at the lower temperature, the computed values are smaller than the experimental values at low air velocities and this trend reverses with the increase in air velocity. In general, the correlation would appear to be inadequate. The Kim et al. [107] correlation predicts values which are consistently smaller than the experimental values, and the disagreement seems to increase rapidly with increase in temperature. The qualitative shape of the dependence of heat transfer coefficient on air velocity is adequately reproduced. However, this correlation will need substantial refinement before reliable predictions may be possible. One such effort was made by Suh and Deckwer [109]. This did improve the agreement between theory and experiment but still the differences are large enough to warrant further refinement of theory. We think this will be in order as some more data on different systems become available.

Zehner [92, 119] proposed a heat transfer model for two-phase systems in the discrete bubbling regime and computed values of heat transfer coefficient from

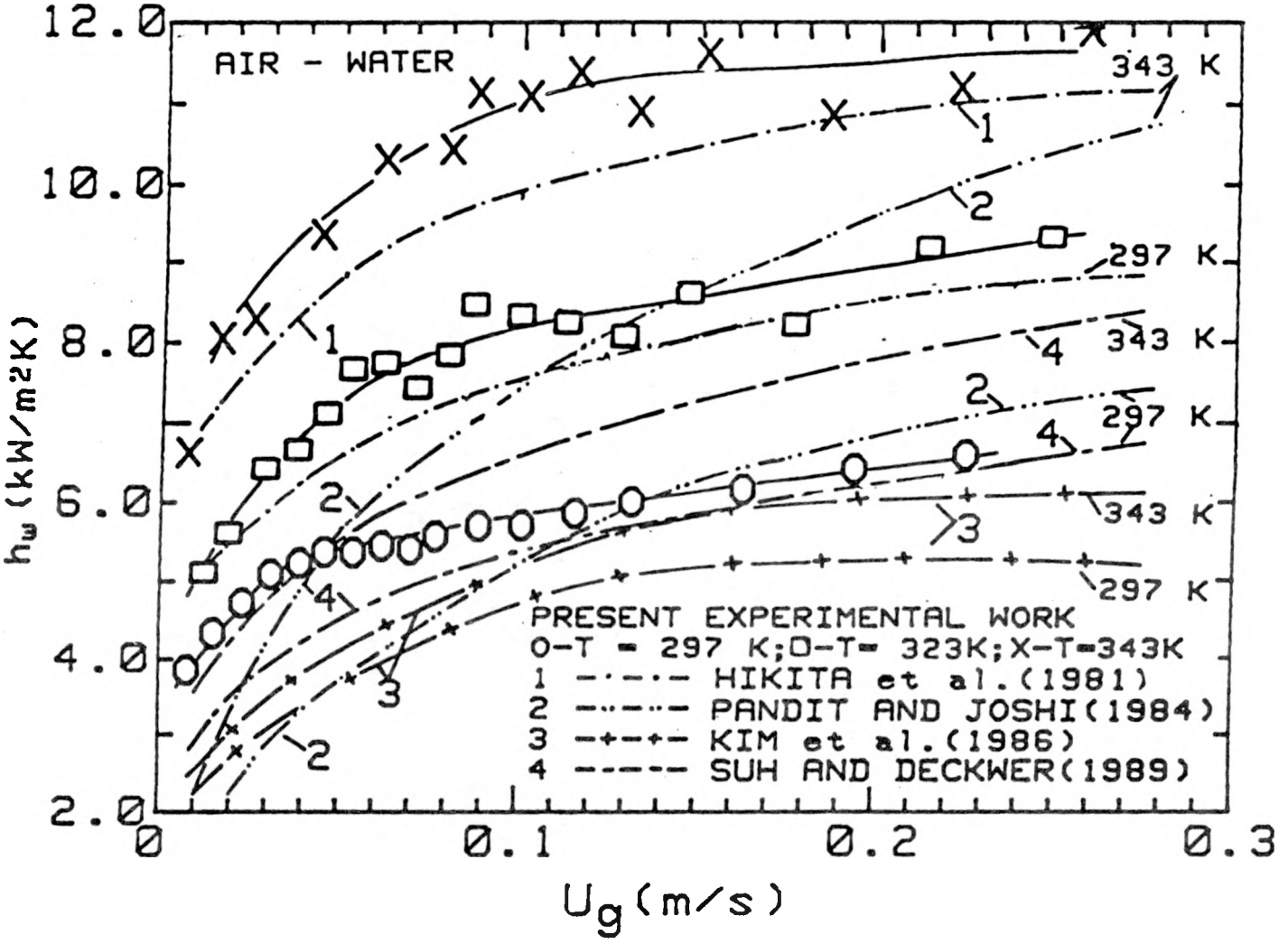

Fig. 6.5. Dependence of heat transfer coefficient for the air-water system on air velocity and temperature. Comparison of experimental data with the predictions of different correlations.

his expressions for the data of Fig. 6.5 are much smaller than the experimental values. At 303 K, the values range between 0.578 to 4.13 kW/m^2K for the air velocity range of 0.01 to 0.30 m/s. For the same air velocity range at 343 K, the values range between 0.765 to 5.47 kW/m^2K. Thus, the predicted values are an order of magnitude smaller at low air velocities and are about half as large at the highest air velocity. One would have expected a better agreement at lower air velocities and the agreement to deteriorate as the air velocity increases due to bubble coalescence and increasing turbulence.

The Mersmann [103] correlation developed for the maximum heat transfer coefficient in analogy to the phenomenon of free convection predicts values in this temperature range which vary from 4.22 to 4.87 kW/m^2K. These values are somewhat smaller than our experimental values and the difference increases as the temperature increases. This conclusion is in agreement with our [83] earlier finding at ambient temperature in Figure 6.1.

It may be recalled that h_w data for single, five and seven-tubes do not differ much from each other as also evident from the data plotted in Figure 4.63. This is understandable because the tubes occupy only a small fraction of the column in the center. This will not be the case for the thirty-seven tube bundle where the baffling is appreciable and is uniform throughout the column cross-section. In Figure 6.6A, these h_W data are displayed at 25° C where values for the thirty-seven tube bundle are different and more importantly exhibit a different dependence on air velocity. A similar trend in general is evident at a higher temperature shown in Figure 6.6B at 70°C. It appears that increasing temperature bring about relatively more pronounced changes in h_w as compared to ambient temperature operation. In contrast to gas holdup, heat transfer coefficient is influenced more by the liquid mixing and liquid circulation patterns established by bubbles as the bubble diameter decreases with increase in the number of tubes in the column. Small bubbles inhibit liquid circulation to some extent in a well baffled bubble column.

In Fig. 6.7 the heat transfer for air-water (probe 3) are compared with the predictions of Kim et al. [107], Deckwer [93], Suh and Deckwer [109], and Pandit and Joshi [106]. These data are reported in greater detail in Fig. 4.72A and Fig. 4.74. The models poorly estimate the data and always underpredict the

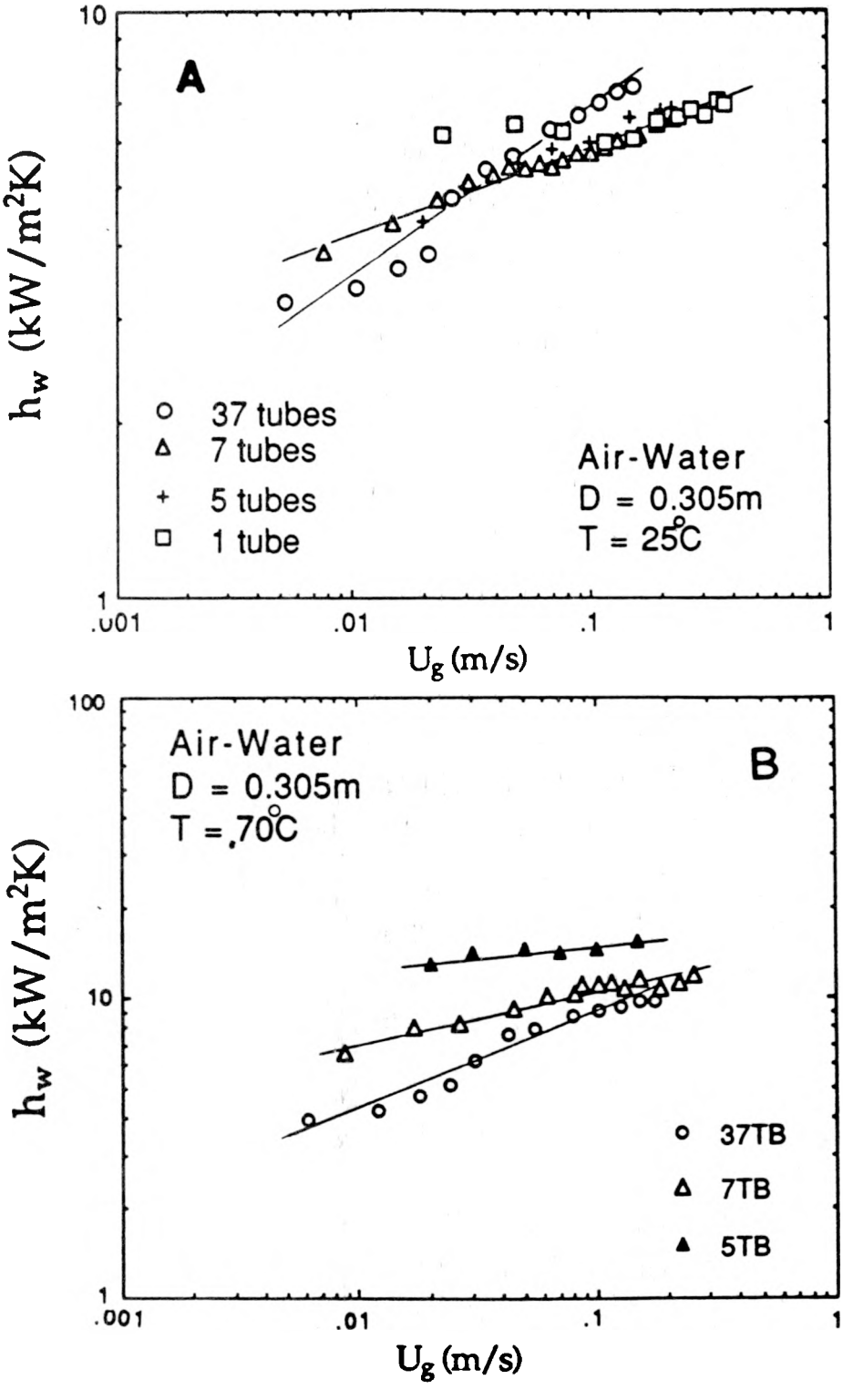

Fig. 6.6. Comparison of h_W for a bubble column equipped with tube bundles of different sizes.

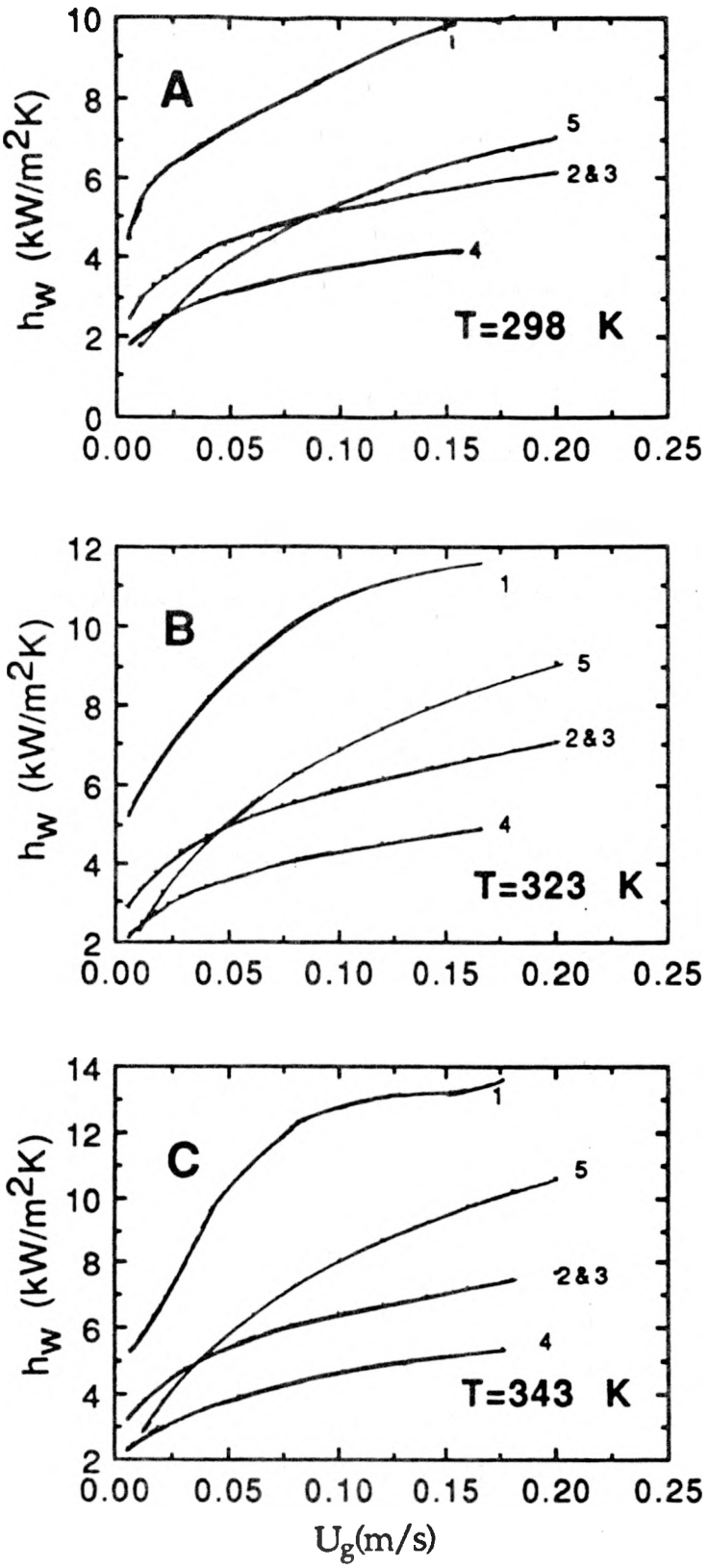

Fig. 6.7. Comparison of experimental heat transfer coefficient data (probe 3) of air-water system with the predictions of different models at four temperatures. (1-Experimental, 2-Deckwer, 3-Suh and Deckwer, 4-Kim et al., 5-Pandit and Joshi).

experimental values. This failure of theory is in conformity with the seven-tube bundle data. These heat transfer data are correlated with a power function in U_g with the results reported in Fig. 6.8.

In Fig. 6.9A the h_w data for 19 mm probe, reported in Fig. 4.38, are compared with the predictions of theoretical expressions due to Deckwer et al. [51], Suh and Decker [109], Kim et al. [107], and Pandit and Joshi [106]. The theoretical expressions of Deckwer et al. [51] and Suh and Deckwer [109] are identical for two-phase systems and hence curves 1 and 2 are the same in Fig. 6.9A. However, these models [51, 109] overestimate the experimental data while models of Kim et al. [107] and Pandit and Joshi [106] underestimate the data. The departure of theoretical curves for the three-phase system (treated here as an effectively two-phase system) from the experimental data are presented in Fig. 6.9 B and these are similar to those found for the two-phase system in Fig. 6.9 A. The Suh and Deckwer [109] correlation based values reproduce the data satisfactorily. This, however, is to be regarded as somewhat fortuitous as this model fails in Fig. 6.9 A. Hence , the need to develop a reliable heat transfer model is obvious. In this context an empirical approach is adopted here following Saxena et al. [120] and is briefly discussed in the following.

The 19 mm heat transfer probe data up to U_g = 0.15 m/s are fitted to an empirical relation of the following type

$$h_w = aU_g^b \qquad 6.51$$

for nitrogen-Therminol system. This yielded a = 1.204 and b = 0.316. Similarly, the three-phase system data for slurry concentrations of 15, 30 and 50 weight percent could be represented by Eq. (6.51) except a and b values are different for each set. Figure 6.10 presents a comparison of these four sets of experimental values with corresponding computed values. One set of a and b values could not represent the entire data for the four sets. This for such fine powder slurries as discussed earlier [120] is due to the changing viscosity of the slurry with the changes in slurry concentration. Hence following our earlier approach, we correlated the data for the four sets by the following relation:

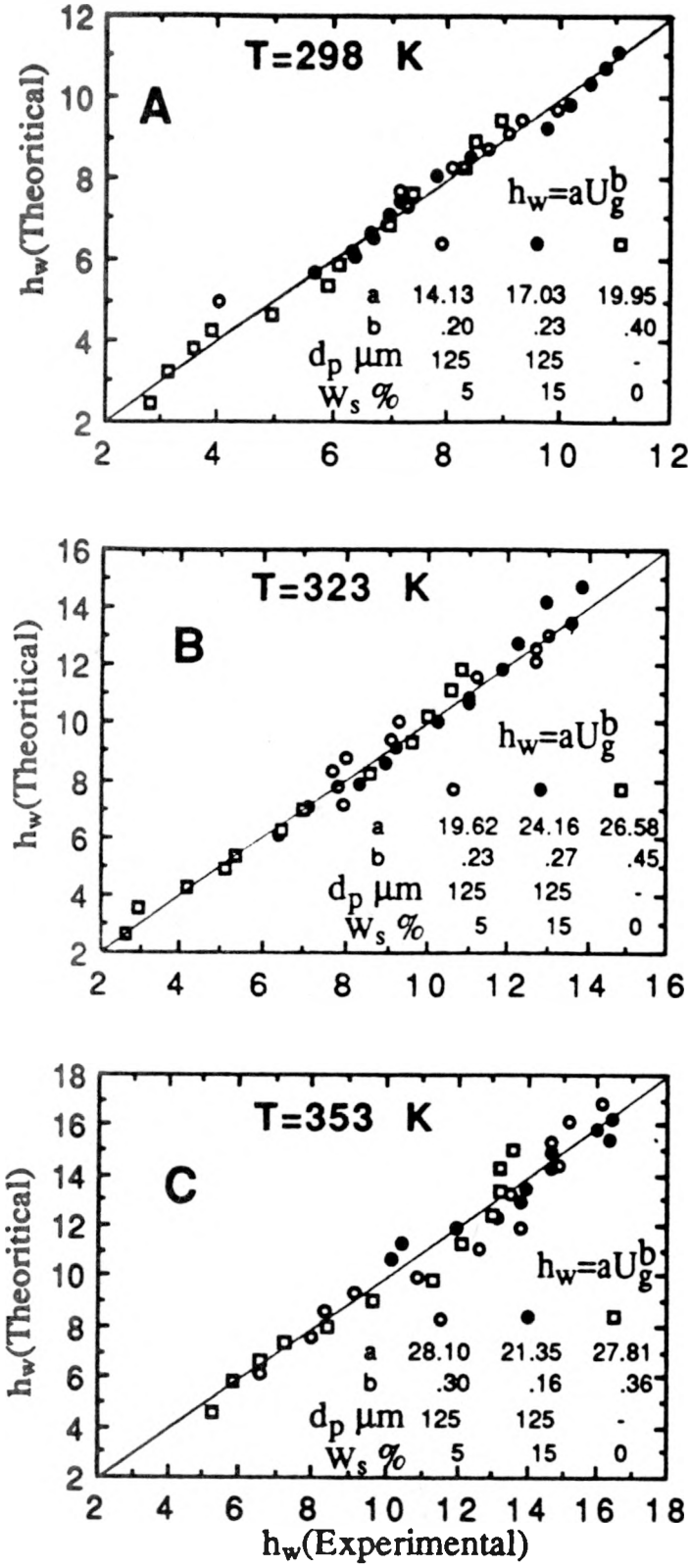

Fig. 6.8. Comparison of experimental heat transfer coefficient data for probe 3 with the predictions of the proposed semi-empirical correlation.

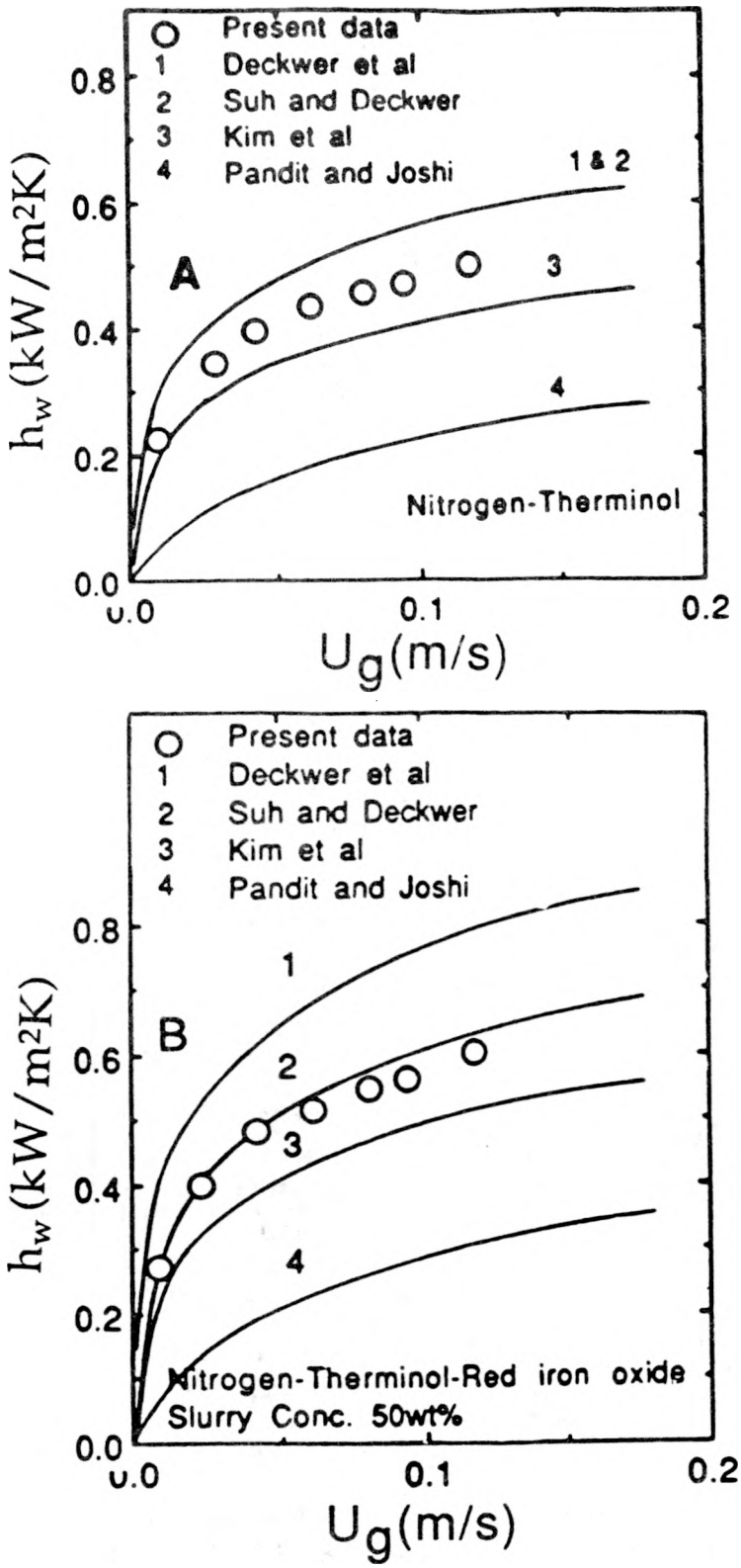

Fig. 6.9. Comparison of experimental h_W data for the 19 mm probe internal with the predictions of different correlations.

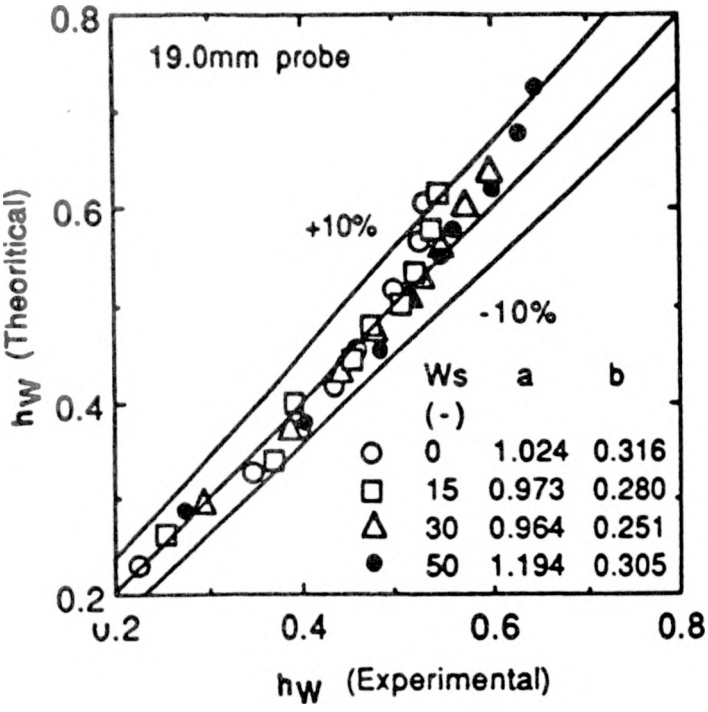

Fig. 6.10. Comparison of experimental h_W data for 19 mm probe internal with the predictions based on Eq. (6.51).

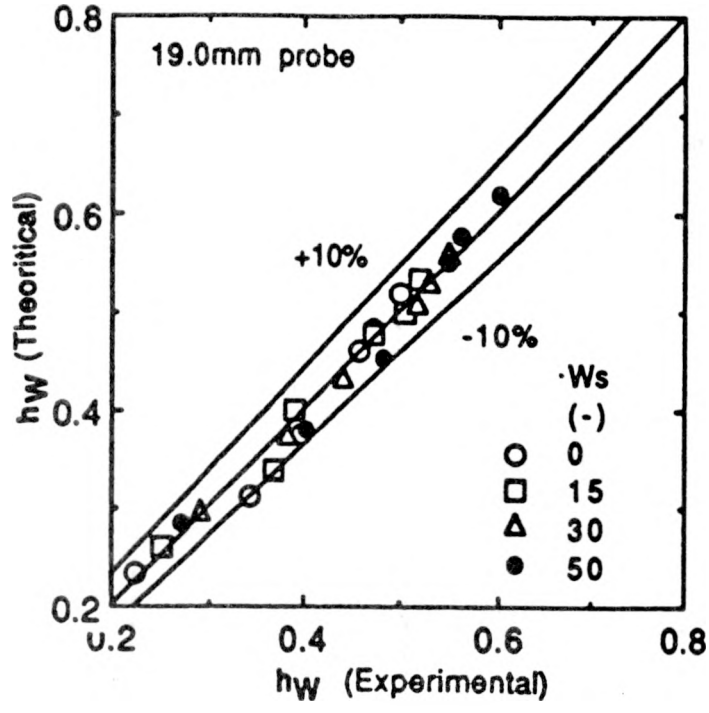

Fig. 6.11. Comparison of h_W for 19mm probe internal with those based on Eq. (6.52).

$$h_w = 1024 \left(\mu_L / \mu_{sL}\right)^{-0.34} U_g^{0.316} \qquad 6.52$$

where

$$\mu_{sL} = \mu_L (1 + 4.5 v_s) \qquad 6.53$$

In the limit when $\mu_{sL} = \mu_L$, Eq. (6.52) reduces to Eq. (6.51). Figure 6.11 presents a comparison of all the four sets of data with the computed values based on Eq. (6.52). The good agreement between the computed and experimental values is a good testimony of the fact that slurry rheology is an important feature in correlating heat transfer data for three-phase systems.

Nitrogen-Therminol system heat transfer data of Saxena et al. [121], Fig. 4.66, for the thirty-seven tube bundle are synthesized in Fig. 6.12 on the basis of an empirical equation of the type (6.51). The exponent b is seen to be dependent upon temperature and decreases monotonically with increase in temperature. This effectively implies that our present data are not adequately represented by the theory of Deckwer et al. [51, 93].

6.4. Comparison of Present Three-Phase Data with Theory

The experimental data of Saxena et al. [122] for the air-water-red iron oxide are reported in Figs. 4.26 and 4.27 for a single probe in the small column at ambient conditions. In Figs. 6.13, these data are shown compared with the predictions of four models. On the whole, agreement between theory and experiment is poor and inadequate.

It is clear from Fig. 6.13 that none of the models can represent even qualitatively the experimental variation of h_w with U_g. The experimental values clearly display a trend of decreasing rate with increasing U_g and may even approach a constant value as the value of U_g is further increased. On the other hand all the models suggest an initial rapid and then a relatively gradual increase in h_W values with increasing U_g values. This failure of theory to predict even the qualitative trend of h_w dependence on U_g for slurries involving

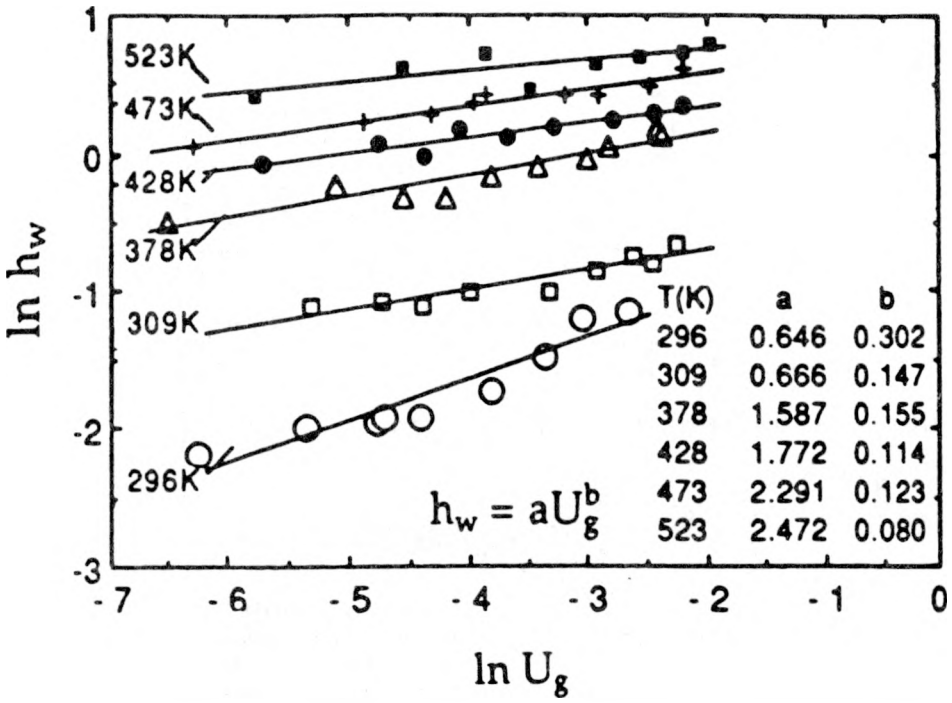

Fig. 6.12. A plot of heat transfer coefficient (probe 1) versus nitrogen velocity shown in logarithmic coordinates at different temperatures. Solids concentration = 0 wt%.

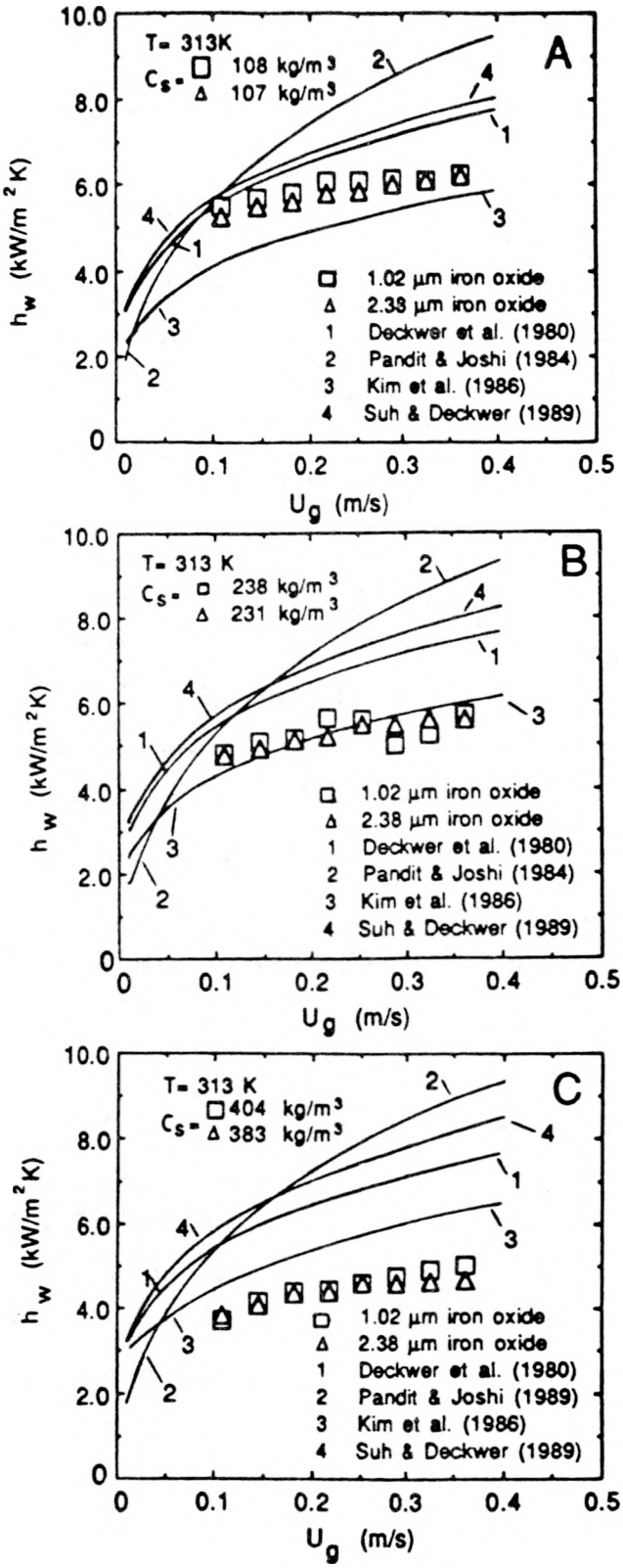

Fig. 6.13. Comparison of experimental h_W values as a function of U_g with the predictions of four theoretical models for slurries of two different average size particles at concentrations of (A) 107 and 108, (B) 231 and 238, and (C) 383 and 404 kg/m^3.

fine powders is a significant indicator for probing the differences in mechanistic details of heat transfer for slurries of small and large particles.

The quantitative predictions of these models are also in unsatisfactory agreement with the experimental values of heat transfer coefficient. The computed values based on Deckwer et al. theory (curves 1) are consistently and systematically greater than the corresponding experimental values. The degree of disagreement increases with increase in velocity beyond 0.1 m/s where the three-phase dispersion is in churn turbulent regime. Pandit and Joshi [106] correlation based values (curves 2) are always greater than Deckwer et al. [51] correlation based values for experimental values. However, their trend of reproduction of experimental data with respect to slurry concentration and gas velocity is disturbing. At the lowest slurry concentration, the computed values underestimate the experimental results over the entire air velocity range; at a still higher concentration in Fig. 6.13B the experimental data are somewhat satisfactorily reproduced; while at the highest slurry concentration in Fig. 6.13C, the calculated values (curves 3) overestimate the experimental data over the entire air velocity range.

Several empirical forms have been examined to represent the experimental data sets. The two successful empirical forms are those of Eq. (6.51) and

$$h_w = c + d \ln U_g \qquad 6.54$$

Heat transfer data for each slurry concentration and particle size were synthesized by the method of least-squares for the above mentioned two functional forms. The two constants a and b of Eq. (6.51) and c and d of Eq. (6.54) thus obtained are listed in Table 6.1 along with the range of air velocity. Also shown in this table are the values of average percentage absolute deviation and the range of percentage absolute deviation for h_w in each case. From the magnitudes of these deviations, it is clear that both of these functions are appropriate to represent the present data. The adequacy of these two functions to represent the heat transfer data is shown by the two parity plots of Figs. 6.14 and 6.15. In all cases, the heat transfer data are adequately represented by these two functions within the limits of experimental uncertainty of $\pm$ 5 percent.

Table 6.1. Constants of Eqs. (6.51) and (6.54) as determined from the experimental h_W values for air-water-red iron oxide system at 313K and measured in 0.108 m bubble column equipped with 19 mm heat transfer probe.

System	d_p (μm)	C_s (kg/m^3)	Velocity range (m/s)	Constants		% Abs. Dev. Avg.	% Abs. Dev. Range
Equation 1:		$h_W = a\ U_g^b$		a	b		
Air - Water -	1.02	108	0.108 - 0.362	6.97	0.103	0.91	0.32 - 2.43
Iron oxide	1.02	238	0.108 - 0.362	6.09	0.093	3.74	0.09 - 8.50
(313 K)	1.02	404	0.108 - 0.362	6.34	0.228	1.11	0.19 - 2.38
	2.38	107	0.108 - 0.362	7.09	0.134	0.36	0.01 - 0.73
	2.38	231	0.108 - 0.362	6.52	0.139	0.80	0.17 - 2.06
	2.38	383	0.108 - 0.362	5.64	0.164	1.10	0.04 - 2.12
	All Data Based Global Constants			6.42	0.144	10.6	0.83 - 24.4
Equation 2:		$h_W = c + d \ln U_g$		c	d		
Air - Water -	1.02	108	0.108 - 0.362	6.88	0.610	0.88	0.22 - 2.35
Iron oxide	1.02	238	0.108 - 0.362	6.04	0.490	3.72	0.10 - 8.64
(313 K)	1.02	404	0.108 - 0.362	6.02	1.000	1.09	0.30 - 1.96
	2.38	107	0.108 - 0.362	6.95	0.770	0.39	0.02 - 0.83
	2.38	231	0.108 - 0.362	6.39	0.726	0.80	0.02 - 1.96
	2.38	383	0.108 - 0.362	5.48	0.706	0.97	0.00 - 2.00
	All Data Based Global Constants			6.29	0.716	10.5	0.01 - 25.3

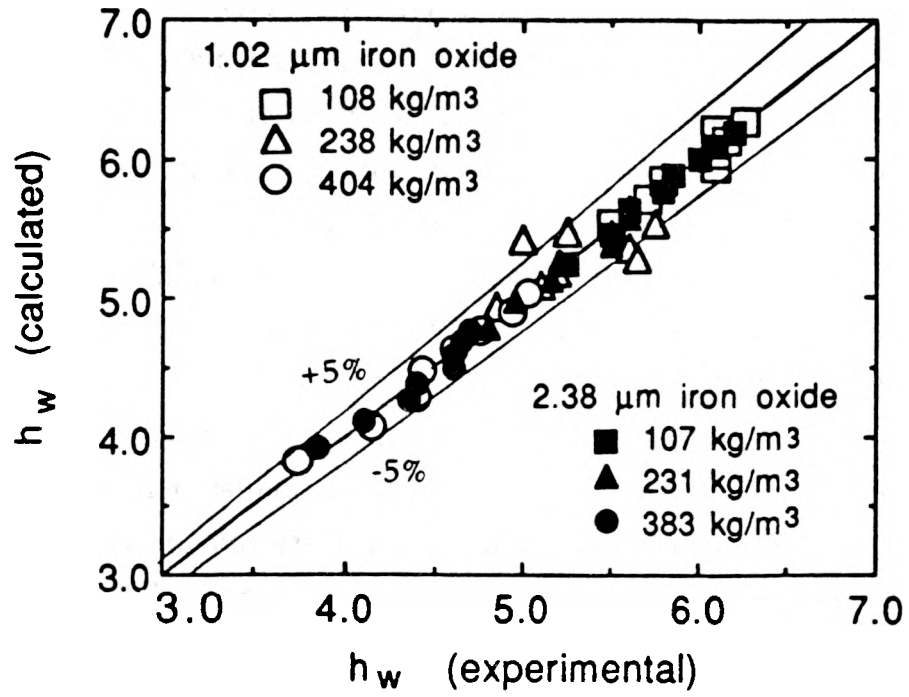

Fig. 6.14. Parity plot of h_W (kW/m^{2}K) for air-water-red iron oxide based on Eq. (6.51), power function, with the values of the constants listed in Table 6.1.

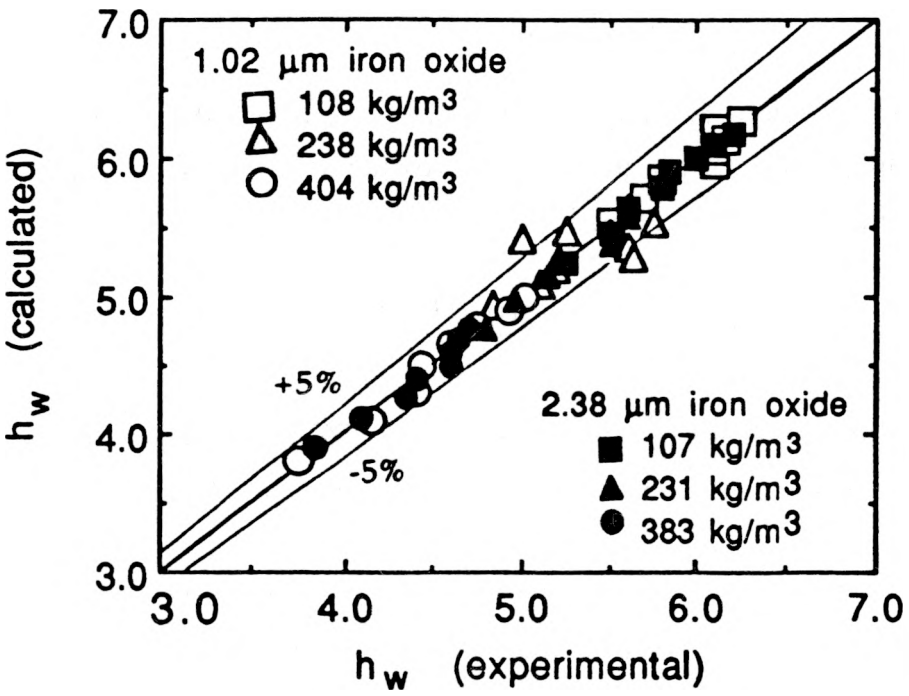

Fig. 6.15. Parity plot of h_W (kW/m^{2}K) for air-water-iron-oxide based on Eq. (6.54), logarithmic function, with the values of the constants listed in Table 6.1.

Next, an attempt was made to represent the entire data referring to two particle sizes, three concentrations for each particle size, and over the entire air velocity range by the two functions of Eqs. (6.51) and (6.54) but with only one set of constants for each function. This yielded the results graphed in Fig. 6.14A for the power function, and in Fig. 6.16B for the logarithmic function. The constants a and b, and c and d are listed in Table 6.1, and are referred to as global constants. It is clear that the reproduction is poor and unsatisfactory. The maximum deviation ranges up to as much as twenty-five percent.

To discover the reason for this large discrepancy we examined the role of suspension rheology in heat transfer process. Particles smaller than 10 μm but closer to 1 μm are generally considered colloidal and these remain more or less dispersed in suspension under gravity, Probstein and Sengun [123]. These authors have proposed that the rheology characteristics of a suspension is largely controlled by the volume fraction of the colloidal particles. Hence, it will be appropriate to introduce the suspension viscosity term in the above empirical expression to account for the changing heat transfer behavior as the slurry concentration is altered. Hence Eq. (6.51) is rewritten in the following form:

$$h_w = a' \, \mu_s^e \, U_g^b \qquad 6.55$$

Here, the suspension viscosity, μ_{SL}, is defined in terms of the liquid phase viscosity, μ_L, by the relation of Eq. (6.27). A regression analysis of the entire data leads to the following explicit relationship:

$$h_w = 8.13 \, (\mu_L / \mu_s)^{1.14} \, U_g^{0.144} \qquad 6.56$$

The adequacy of the proposed relationship of Eq. (6.56) is to be judged by the parity plot of Fig. 6.17 giving the calculated and experimental heat transfer coefficients.

Air-water-glass bead system data [69, 127], as obtained in the small column with a single probe and for slurries of different size particles and concentrations is compared with the predictions of different models in Fig. 6.18. Kim et al. [107] correlation based values (curve 3) are always smaller while those of Pandit and

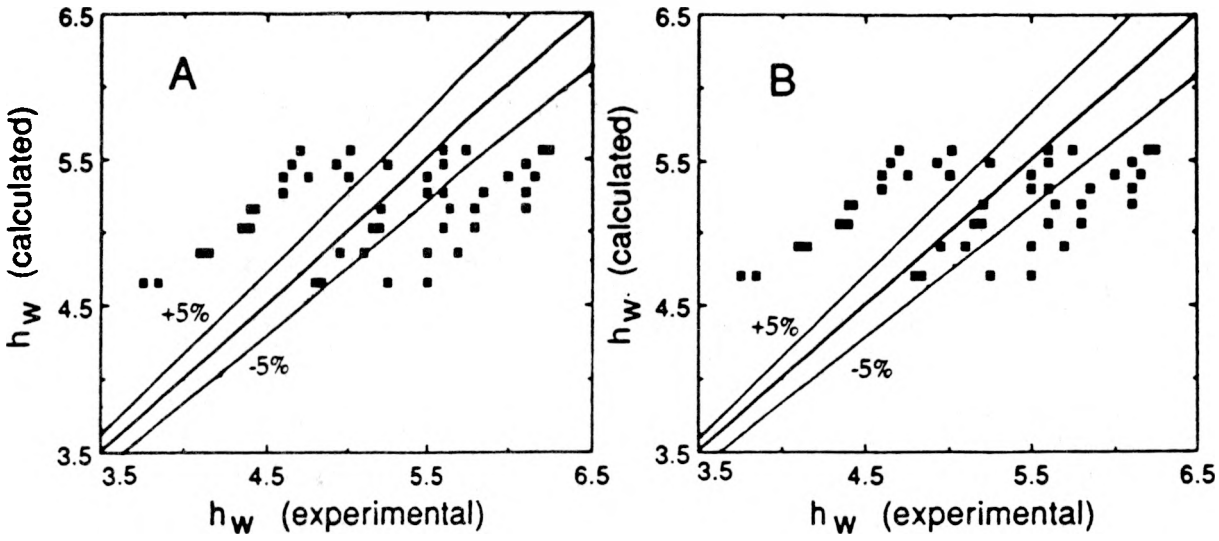

Fig. 6.16. Parity plot of h_W (kW/m^{2}K) for air-water-iron-oxide system with global constants: (A) power function, and (B) logarithmic function.

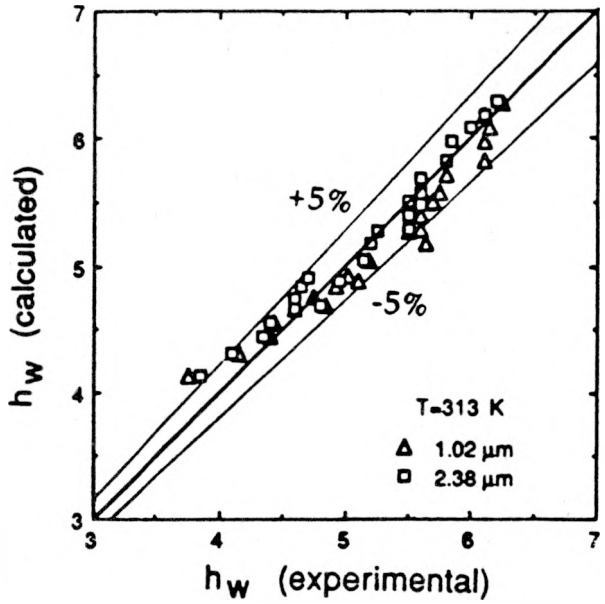

Fig. 6.17. Parity plot of h_W (kW/m^{2}K) for air-water-iron oxide system based on Eq. (6.56).

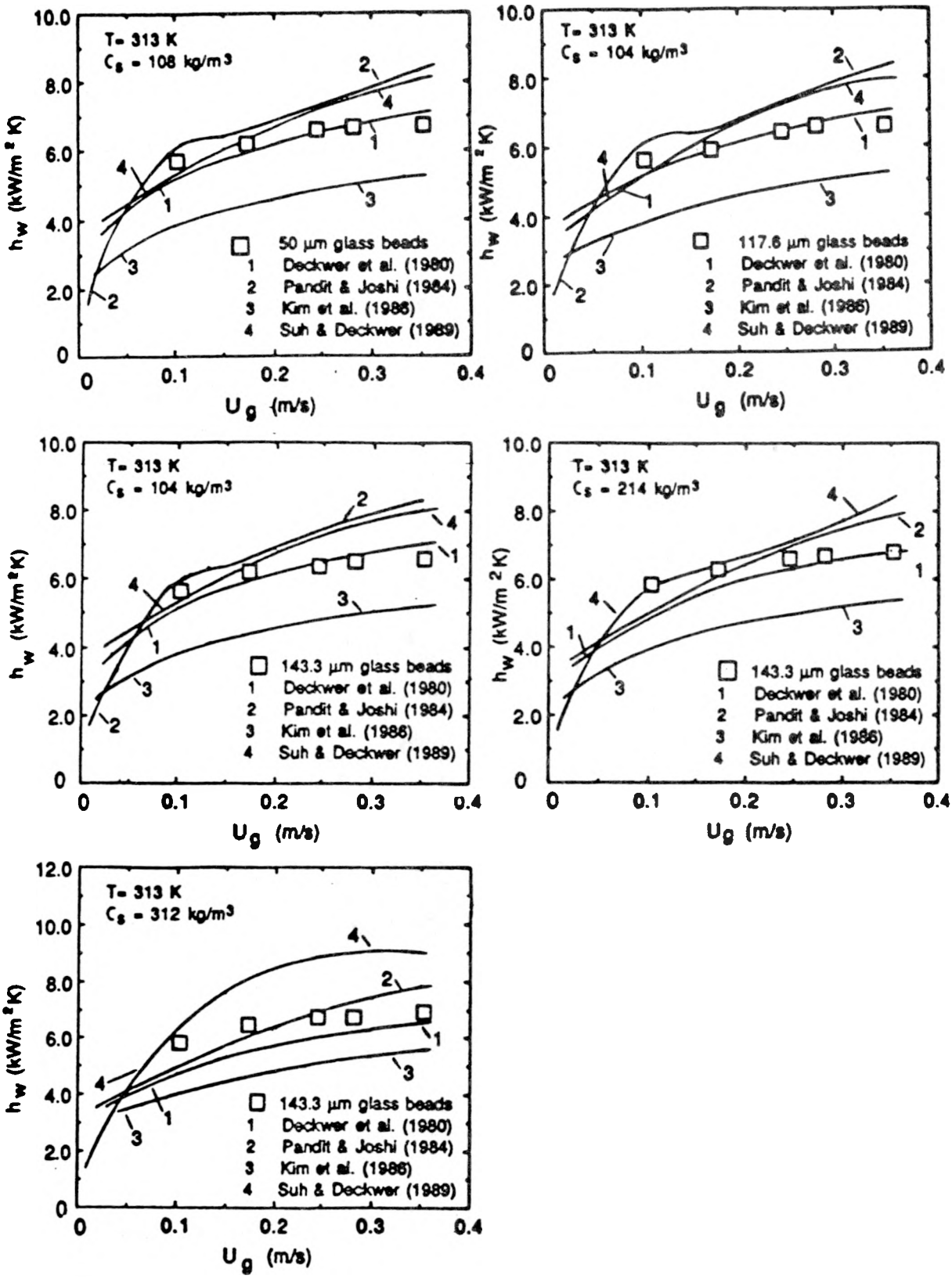

Fig. 6.18. Comparison of h_W data for air-water-glass bead system with different models.

Joshi [106] correlation based values (curve 2) are almost always greater than the experimental values. Deckwer et al. [51], and Suh and Deckwer [109] correlations lead to values which also fail to reproduce the experimental data except the former [51] does slightly better than the latter [109]. However, the agreement between the experimental data and the predictions based on Deckwer et al. [51] correlation consistently worsens as the solids concentration in the slurry increases. In view of the failure of existing correlations, Saxena et al [125] synthesized these data on the basis of Eqs. (6.51) and (6.54) with the constants a, b, c and d listed in Table 6.2. This approach as shown in the concentration and particle dependence of these data on the four constants is rather insignificant and therefore a global fit was tried with the results reported in Table 6.3. The accuracy with which these constants can reproduce the data is also outlined in the last two columns.

Additional data taken for this system for a single probe and a seven-tube bundle [80] were also analysed in a similar fashion with the results reported in Table 6.4. The global constants yielded the following relations:

$$h_w = 8.723\ U_g^{0.194} \tag{6.57}$$

and

$$h_w = 8.108 + 1.508\ \ln U_g \tag{6.58}$$

Here, h_w is in kW/m^2K and U_g in m/s. Comparison of the 130 experimental data points with the corresponding computed values from Eqs. (6.57) and (6.58) is presented in Figs. 6.20 and 6.21 respectively. The agreement is certainly satisfactory in view of the simplicity of relations and neglect of powder size and slurry concentration.

Saxena and Patel [126] have reported data for three single probes of different diameters and correlated the same on the basis of Eq. (6.58). They have proposed a correlation of their data involving a dimensionless hydraulic diameter and air velocity. The final form is:

$$h_W = 9.5\ [1 - (D_T/D_C)]^{0.25}\ U_g^{0.20} \tag{6.59}$$

Table 6.2. Values of the constants of Eqs. (6.51) and (6.54) as determined from the experiemntal h_W values for three different systems in the temperature range 308 - 316K and measured in 0.108 m bubble column equipped with 19 mm heat transfer probe.

System	d_p (μm)	C_s (kg/m^3)	Air Velocity Range (m/s)	Equation (1) a	Equation (1) b	Equation (2) c	Equation (2) d	% Abs. Dev. in h_W Avg.	% Abs. Dev. in h_W Range
Air - Water	-	-	0.103 - 0.353	6.92	0.099	-	-	1.04	0.7 - 2.6
	-	-	0.103 - 0.353	-	-	6.84	0.578	1.03	0.1 - 2.5
Air - Water Magnetite	43.6	107	0.108 - 0.362	7.48	0.109	-	-	1.34	0.2 - 3.0
		167	0.108 - 0.362	8.21	0.164	-	-	1.50	0.1 - 3.4
		258	0.108 - 0.362	7.94	0.131	-	-	1.84	0.3 - 4.9
	43.6	107	0.108 - 0.362	-	-	7.39	0.691	1.32	0.2 - 3.0
		167	0.108 - 0.362	-	-	8.00	1.042	1.52	0.2 - 3.6
		258	0.108 - 0.362	-	-	7.79	0.837	1.78	0.4 - 4.9
Air - Water - Glass Bead	50.0	108	0.103 - 0.353	7.97	0.145	-	-	1.11	0.4 - 1.9
		108	0.103 - 0.353	-	-	7.77	0.901	0.97	0.2 - 1.7
	117.6	104	0.103 - 0.353	7.77	0.142	-	-	1.35	0.4 - 1.8
		104	0.103 - 0.353	-	-	7.59	0.867	1.34	0.5 - 2.1
	143.3	104	0.103 - 0.353	7.61	0.126	-	-	0.92	0.2 - 1.6
		214	0.103 - 0.353	7.81	0.126	-	-	0.60	0.5 - 2.7
		312	0.103 - 0.353	8.07	0.137	-	-	1.01	0.3 - 1.5
	143.3	104	0.103 - 0.353	-	-	7.46	0.769	0.85	0.3 - 1.4
		214	0.103 - 0.353	-	-	7.66	0.791	0.50	0.4 - 2.6
		312	0.103 - 0.353	-	-	7.89	0.875	0.89	0.3 - 1.3

Table 6.3. Global constants of Eqs. (6.51) and (6.52) as determined from the experimental h_W values for air-water-magnetite and air-water-glass bead systems in the temperature range 308 - 316K and measured in 0.108 m bubble column equipped with 19 mm heat transfer probe.

System	a	b	c	d	% Abs. Dev. in h_W Avg.	Range
Air - Water -	7.89	0.136	-	-	1.8	0.02 - 6.2
Magnetite	-	-	7.74	0.865	1.8	0.01 - 6.1
Air - Water -	7.84	0.135	-	-	1.7	0.10 - 4.0
Glass Bead	-	-	7.68	0.841	1.7	0.01 - 4.2

Table 6.4. Values of the constants of Eqs. (6.51) and (6.54) as determined from the experimental h_W values for air-water and air-water-glass bead systems at 393K and measured in 0.108 m bubble column equipped with a 19 mm single tube and a seven-tube bundle.

	d_p (μm)	w_s (%)	a	b	% Abs. Dev.		c	d	% Abs. Dev.	
					Avg.	Range			Avg.	Range
SINGLE TUBE	-	0	8.224	0.193	4.188	1.44-6.85	7.55	0.958	3.224	1.68-6.01
	50	10	7.645	0.170	0.902	0.09-2.28	7.269	0.890	1.297	0.03-2.85
	119	10	8.611	0.181	0.990	0.04-2.40	8.156	1.052	1.373	0.10-2.94
	143	10	8.516	0.172	1.433	0.03-3.07	8.08	0.994	1.046	0.02-2.16
SEVEN-TUBE BUNDLE	-	0	8.645	0.197	3.101	1.12-6.84	8.00	1.050	1.780	0.02-4.53
	50	5	8.706	0.190	2.067	0.33-5.68	8.07	1.021	1.135	0.19-4.48
	50	10	9.207	0.203	2.793	0.41-5.87	8.446	1.113	1.335	0.10-4.51
	119	5	8.980	0.205	2.335	0.31-5.12	8.291	1.127	1.400	0.22-3.79
	119	10	8.953	0.194	2.027	0.17-4.59	8.360	1.105	2.082	0.11-3.78
	143	5	8.732	0.195	2.060	0.16-4.94	8.099	1.052	1.214	0.18-3.85
	143	10	8.619	0.193	2.137	0.54-4.54	8.036	1.044	1.175	0.03-2.97
	143	20	9.263	0.208	2.618	0.07-5.58	8.444	1.135	1.818	0.31-3.92
	143	30	9.189	0.209	2.334	0.01-5.37	8.401	1.144	1.827	0.57-4.28

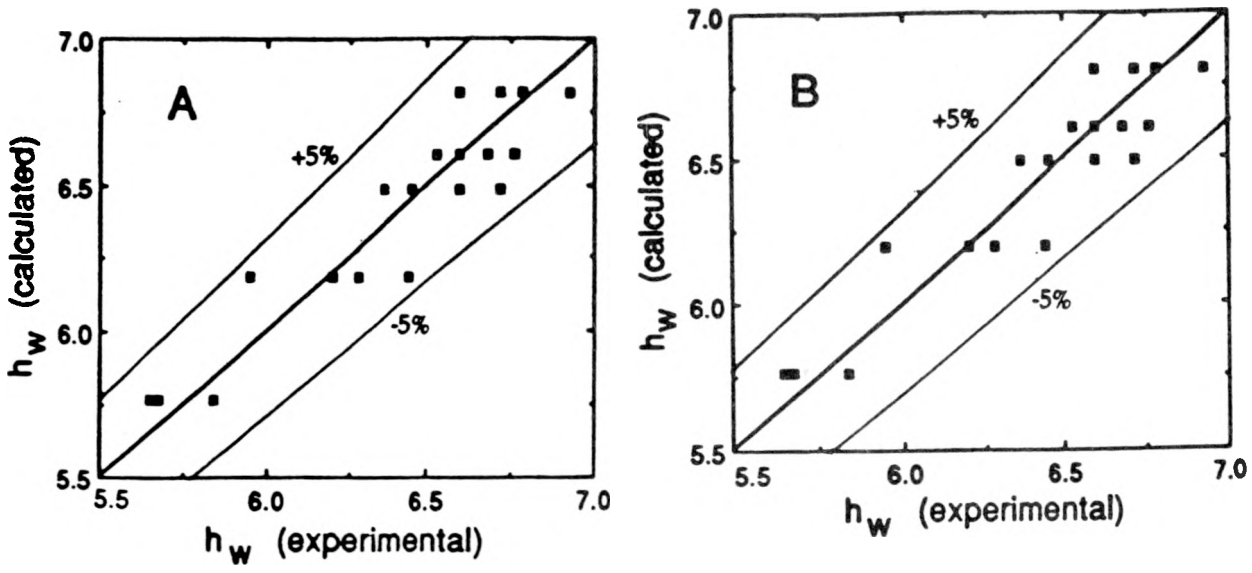

FIG 8.

Fig. 6.19. Parity plot of h_W (kW/m^{2}K) for air-water-glass bead system: (A) power function, and (B) logarithmic function.

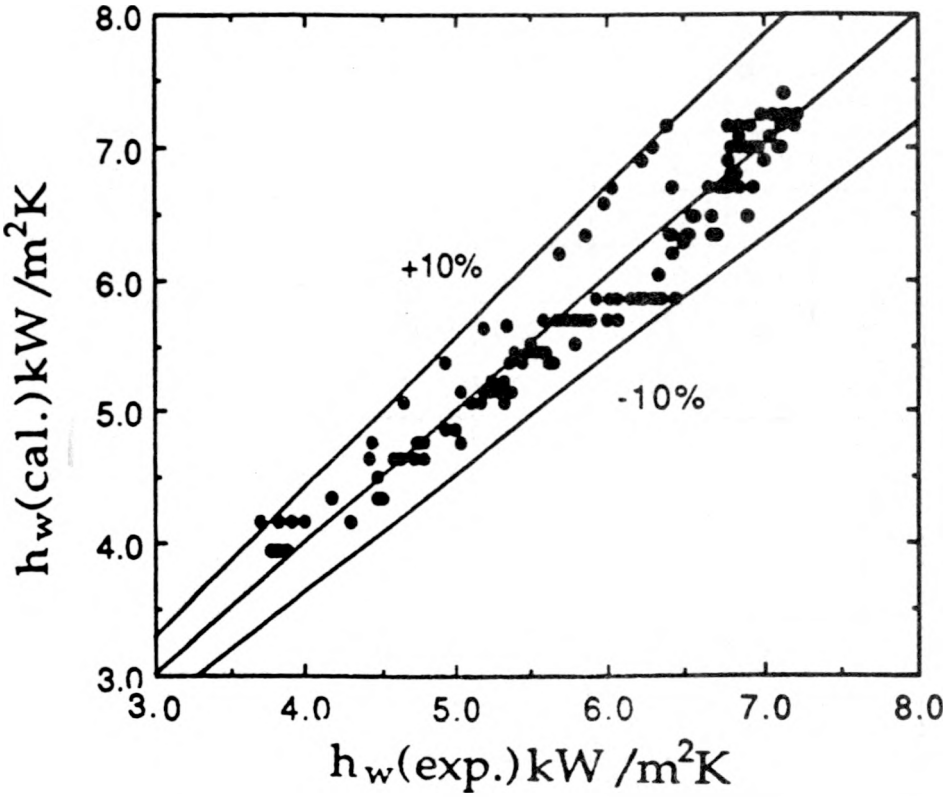

Fig. 6.20. Comparison of experimental and calculated heat transfer coefficient values with global constants for power function, Eq. (6.57).

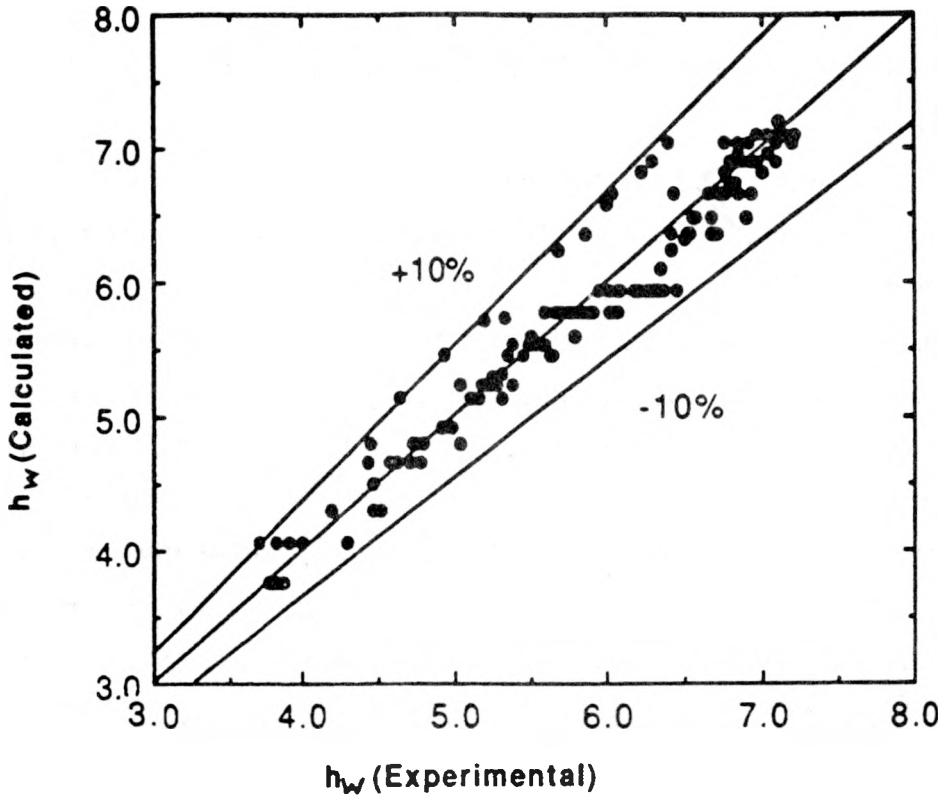

Fig. 6.21. Comparison of experimental and calculated heat transfer coefficient values with global constants for semi-logarithmic function, Eq. (6.58).

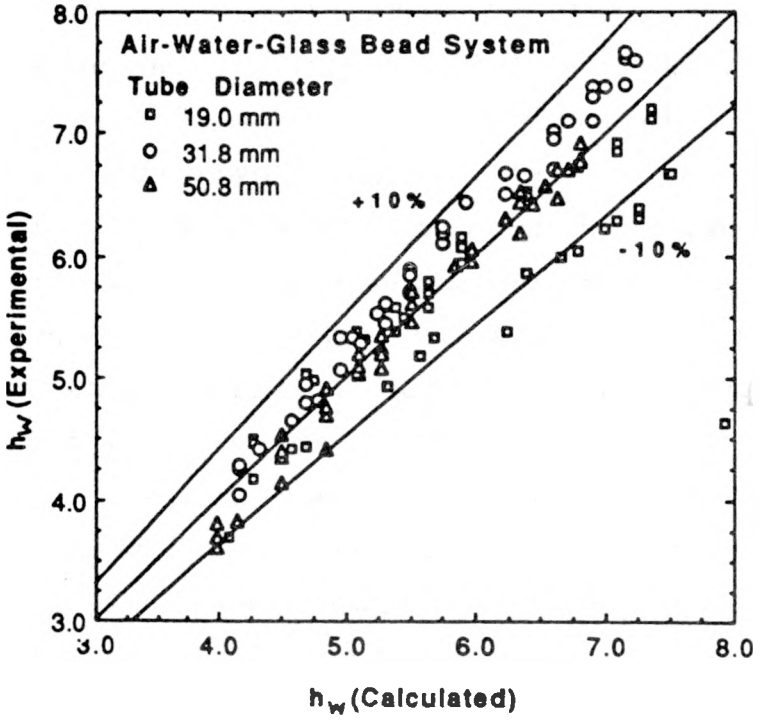

Fig. 6.22. Comparison of experimental and calculated values of heat transfer coefficient on the basis of the proposed correlation.

Comparison of data with the corresponding predictions based on Eq. (6.59) is presented in Fig. 6.22.

In the larger column air-water-glass bead system has been investigated [111, 112] with seven- and thirty-seven tube bundles, and the same are presented in Figs. 4.69 through 4.74.

The heat transfer coefficient values for the seven-tube bundle averaged over the slurry concentration and particle size range, as shown in Fig. 6.23, are compared with the predictions of four models. The Pandit and Joshi correlation [106] has the same deficiency for this three-phase system at all the three temperatures as discussed earlier for the two-phase (air-water) in connection with Fig. 6.5. The correlation underpredicts the data and has an improper qualitative dependence on air velocity. The Deckwer et al. correlation [51] leads to values which are increasingly smaller than the experimental values as the temperature increases. However, the shape of qualitative dependence of heat transfer coefficient on air velocity is well reproduced. The Kim et al. model [107] leads to values which are still smaller than the predicted values based on the Deckwer et al. correlation [51]. Attempts of Suh and Deckwer [109] to improve the correlation of Kim et al. [107] seem to be only partially successful. This correlation does reproduce the qualitative shape of the dependence of heat transfer coefficient on air velocity, and quantitatively leads to values which are in the best agreement with the experimental data of all the four correlations. However, the degree of disagreement between theory and experiment is large and the predictions are systematically smaller than the observed values. It would be appropriate to refine this model as more data become available.

Kolbel et al. [100] and Kato et al. [110] have proposed correlations which also include the particle size. We discuss these correlations for slurry bubble columns because our measurements suggest very small dependence on particle diameter. Both these correlations predict much higher values than the experimental data. The Mersmann et al. correlation [103] as generalized by Saxena et al. [105] for the three-phase systems leads to the maximum heat transfer coefficient values which are smaller than the experimental values. The disagreement, which is about 35 percent at 303 K, increases to about 60 percent at 343 K. In summary, the available heat transfer models and correlations are inadequate to predict the

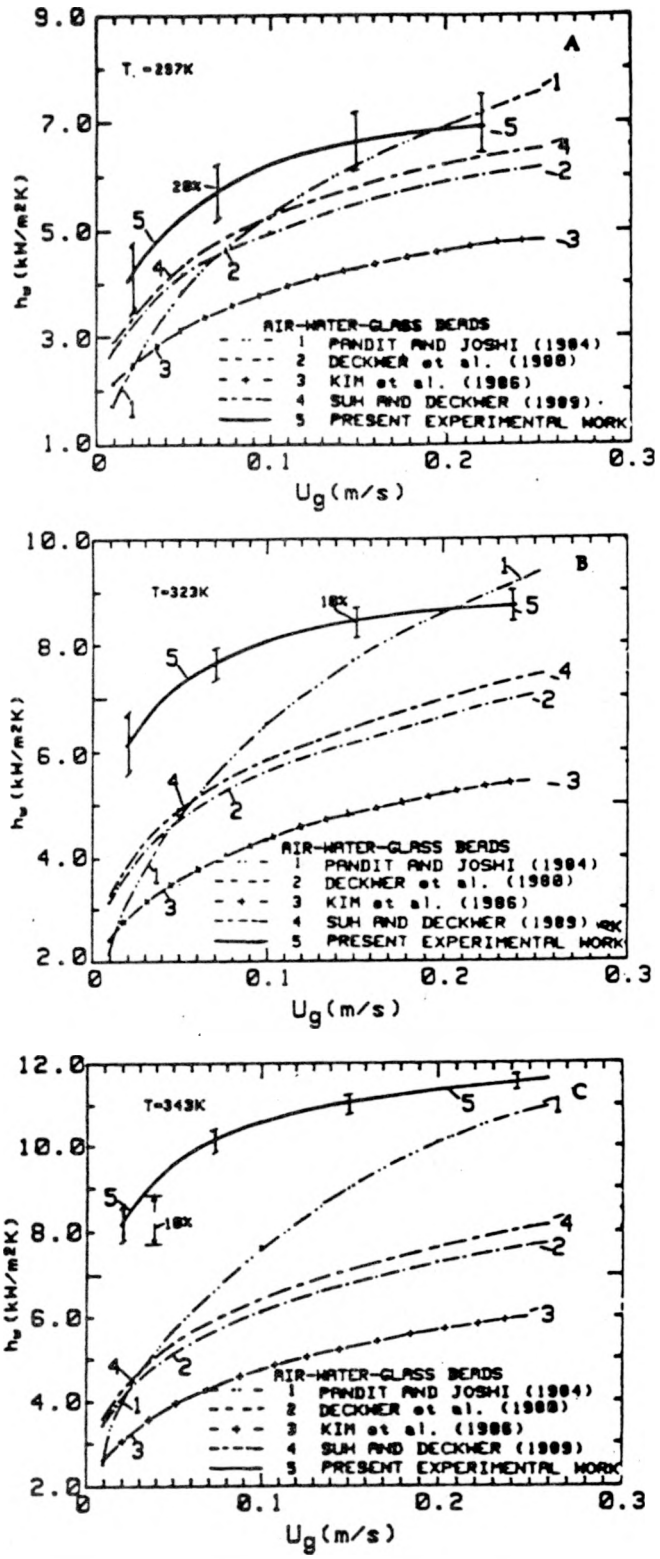

Fig. 6.23. Comparison of averaged heat transfer coefficient values as a function of air velocity with the predictions of different correlations at (A) 297, (B) 323, and (C) 343K.

experimental data, particularly as the temperature increases above the ambient.

The heat transfer data obtained for the thirty-seven tube bundle are compared with the four model predictions in Fig. 6.24. In all cases, the theoretical values are consistently and appreciable smaller than the experimental values. The models either predict very small or no dependence on slurry concentration. In view of the failure of models, a semitheoretical correlation is presented in Fig. 6.8. The computed values are in good agreement with the experimental values in all cases and it is recommended as a good empirical correlation.

The comparison of h_w values [105, 128] for the air-water-magnetite system for a single probe in the small column, Fig. 4.34, are compared with the predictions of five models in Fig. 6.25.

Computed values of h_w from Deckwer et al. correlation [51] are shown in Fig 6.25 (curves 1) as a function of air velocity and for two extreme compositions of the solids in the slurry. The computed values exhibit a continuous increase in the values of h_w with increase in U_g. For values of U_g greater than 0.1 m/s, the experimental values are almost constant, and therefore the agreement between the experimental and calculates values worsens with increase in air velocity. The experimental data show almost no dependence on solids concentration in the slurry while the calculated values exhibit an increase in the value of h_w with increase in solids concentration over the entire range of air velocities. The theory is a reasonable representation of experimental data at air velocities smaller than 0.1 m/s.

Computed values of heat transfer coefficient from the correlation of Pandit and Joshi [106] are shown in Fig. 6.25 (curves 2) as a function of air velocity. h_w values increase with U_g for all particle sizes in disagreement with the experimental data which exhibit an almost constant value for all velocities greater than 0.1 m/s. The computed data also show a dependence on solids concentration, h_w values are greater for slurries containing a larger weight fraction of solids. This difference in h_w values is also dependent upon the size of solids and increases appreciably for slurries containing particles of average diameter of 90.5 μm and greater. The reproduction of h_w by this model is inferior to that of Deckwer et al. model [51] over the entire air velocity range.

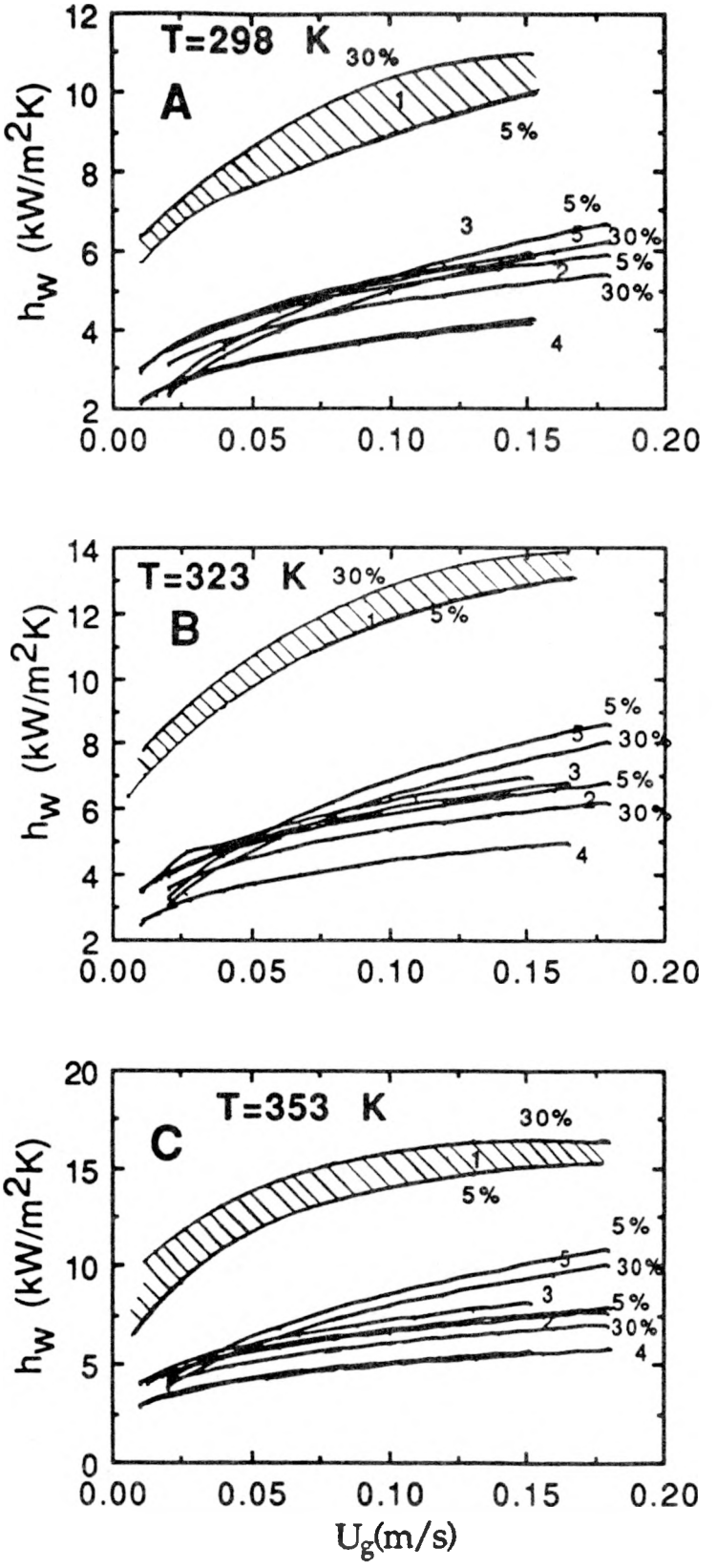

Fig. 6.24. Comparison of experimental heat transfer coefficients with the predictions of different models for the air-water-glass bead system, (1-Experimental, 2-Deckwer, 3-Suh and Deckwer, 4-Kim et al., 5-Pandit and Joshi).

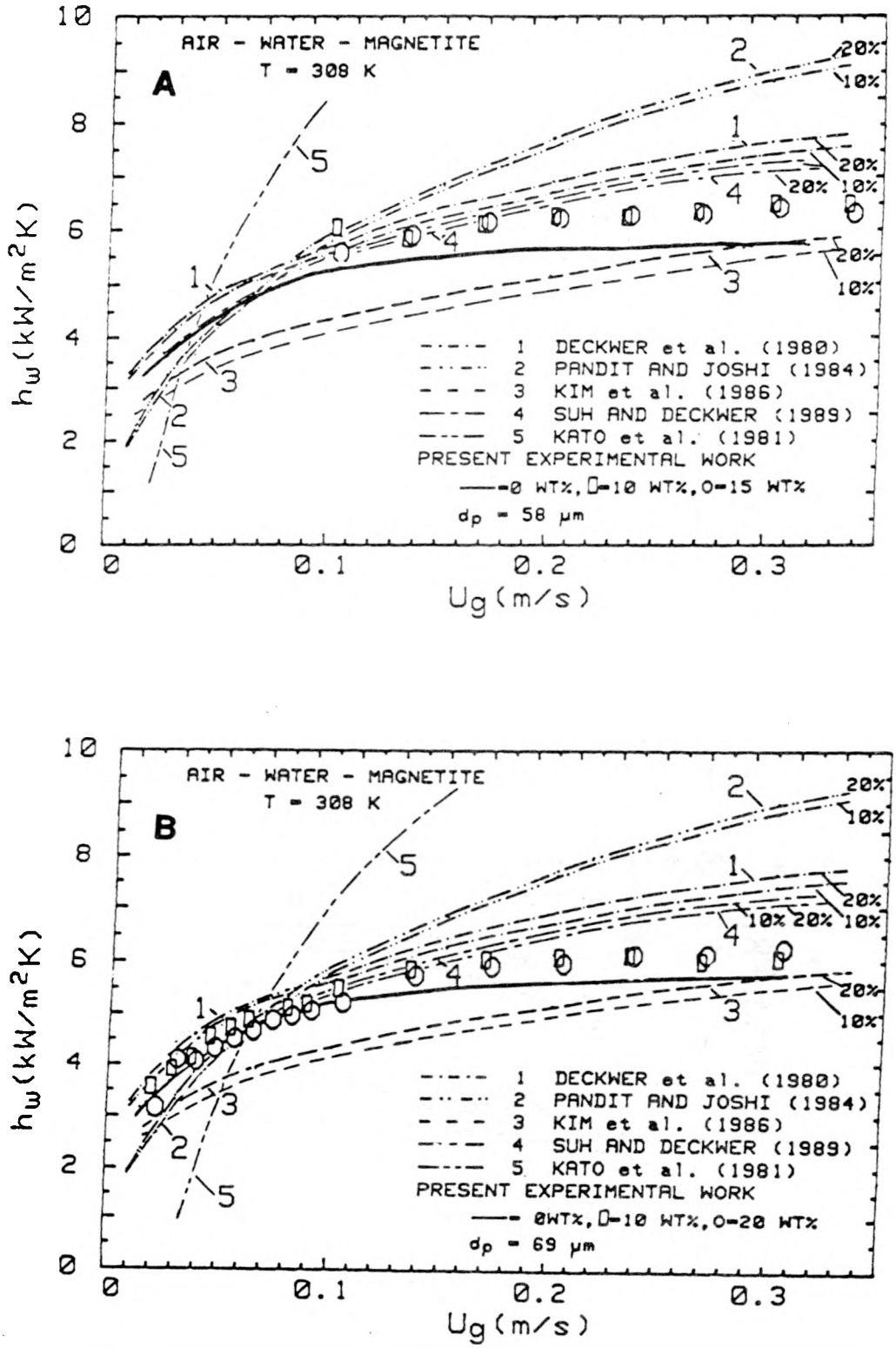

Fig. 6.25. Comparison of heat transfer data with the predictions of different models.

The qualitative shape of h_w dependence on U_g for air velocities smaller than 0.1 m/s is different as predicted on this model than found in present experiments.

Computed values of h_w from Kim et al. correlation [107] as a function of air velocity are shown in Fig. 6.25 (curves 3), and these are in unsatisfactory agreement with the experimental values. The correlation based values exhibit a dependence on solids concentration in the slurry, the values exhibit a dependence on solids concentration, the increase is more for particles of average diameter 90.5 μm and greater. These trends are not exhibited by the experimental data. The calculated values are invariably smaller than the experimental values over the entire air velocity range. This correlation which is primarily developed for liquid fluidized beds appear to be inadequate for slurry bubble columns.

Computed values from Suh and Deckwer [109] of h_w (curves 4) are in somewhat better agreement with experimental data at lower air velocities (smaller than 0.1 m/s) than from Kim et al. correlation [107]. At higher air velocities, the computed values are greater than the experimental values, while those based on Kim et al. [107] are smaller than the experimental values. Other trends for the two sets of values are indeed identical.

It can be seen apriori that Eq. (6.48) will not be very appropriate for reproducing the experimental data in view of its pronounced dependence on d_p while experimentally determined h_w values are almost independent of d_p. In Fig. 6.25 are graphed the computed h_w values from Eq. (6.48) for different experimental conditions as a function of air velocity. In each case the calculated values are poor representation of the experimental data. The calculated h_w values increase much faster with air velocity and fail completely to reproduce the experimental data. The relatively better reproduction of the experimental values as the particle size increases is a consequence of the procedure adopted in developing the correlation. In general, this correlation is regarded as inadequate for representing the experimental heat transfer data for slurry bubble columns.

Computed values of $h_{w\,max}$ from the relations of Eq. (6.25) for 10, 10 and 30 weight percent of solids in the slurry are 4.50, 4.64 and 5.03 kW/m^{2}K. The corresponding experimental values range between 6.0 to 6.4 kW/m^{2}K. This agreement of theory and experimental is regarded as fair and reasonable but not

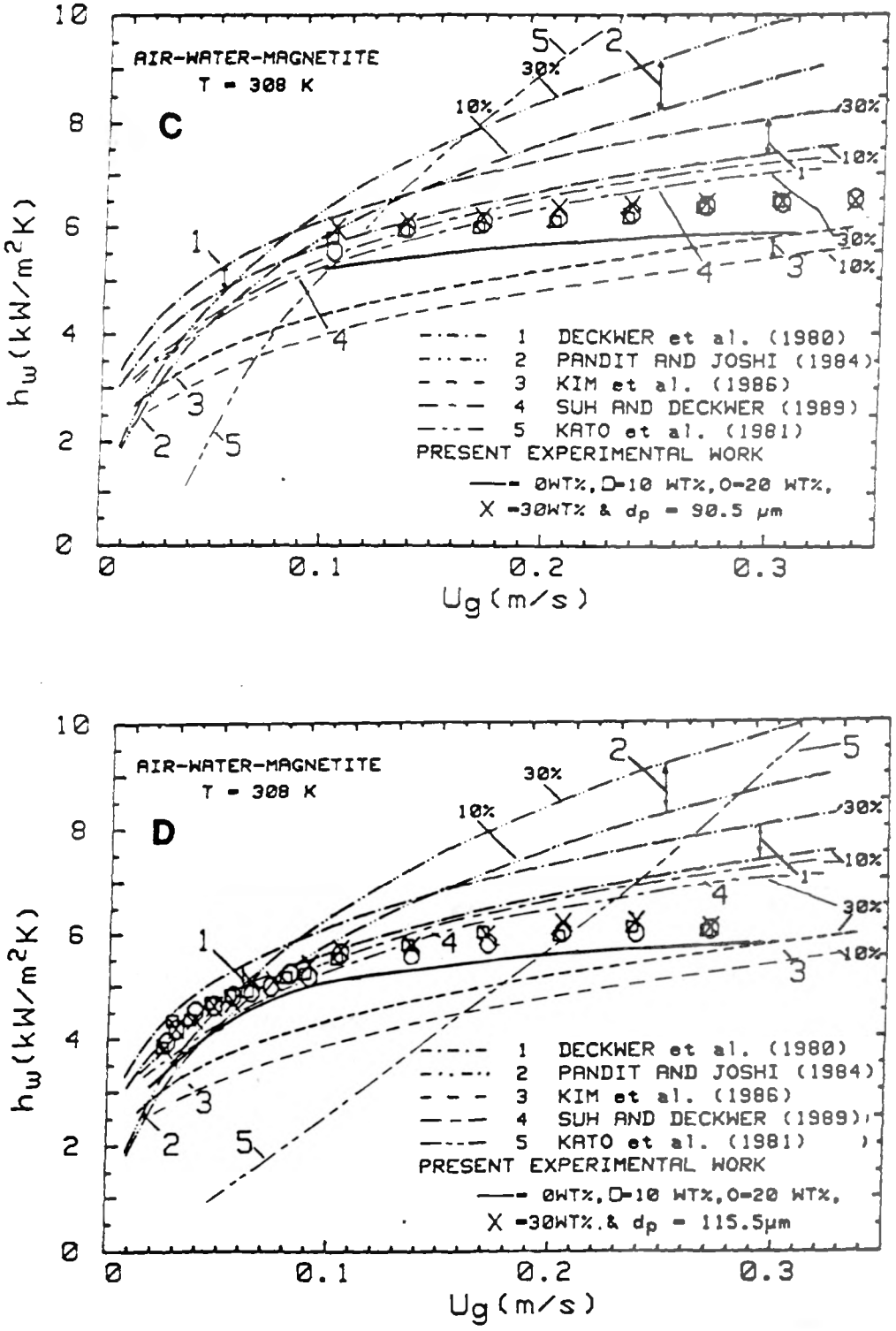

Fig. 6.25. Comparison of heat transfer data with the predictions of different models.

satisfactory.

In view of the failure of these models to represent h_W data, the empirical Eqs. (6.51) and (6.54) were employed to correlate the data with the results reported in Table 6.5 and in Figs. 6.26 and 6.27. The agreement of theory and experiment is quite good, the deviations between the two sets of values are always within the estimated uncertainty of 5%. The maximum percentage average absolute deviations for the 102 data points are 1.4 and 1.3 respectively for the power and semi-logarithmic functions. The corresponding percentage maximum deviations are 4.3 and 4.1 respectively. Experimental h_w data are considered up to a maximum gas velocity of 0.15 m/s where h_w invariably gets to a constant value.

Since the constants of Eqs. (6.51) and (6.54) so not differ significantly with the change of particle size and concentration in the slurry, a global fit based on the entire data was tried with the following results:

$$h_w = 9.206\ U_g^{0.233} \qquad 6.60$$

and

$$h_w = 7.805 + 1.056 \ln U_g \qquad 6.61$$

Based on these two relations, comparison of experimental and calculated h_w values is presented in Figs. 6.28 and 6.29. The functions of Eqs. (6.60) and (6.61) are adequate to estimate h_w data within an average absolute and maximum deviations of 2.9 and 2.7, and 15 and 12 percent respectively. This is quite remarkable as the small dependencies of h_w on d_p and w_s are ignored in this correlation.

From Table 6.5, this exponent has an average value of 0.244 for slurries containing particles of 69 μm average diameter and smaller, while its value is 0.20 for slurries having average diameter of 115.5 μm and larger. This would suggest that for at least larger particles the assumed energy dissipation by viscous forces due to micro-scale eddies in the radial direction which are locally isotropic is not completely valid. Further, as pointed out by Deckwer and coworkers the

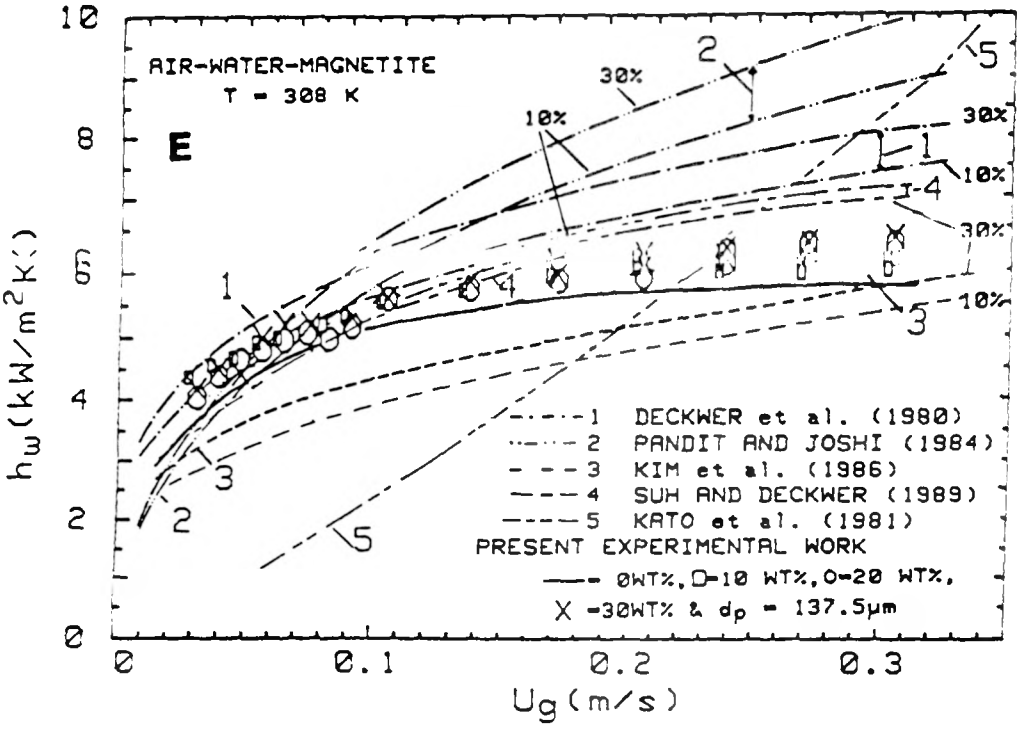

Fig. 6.25. Comparison of heat transfer data with the predictions of different models.

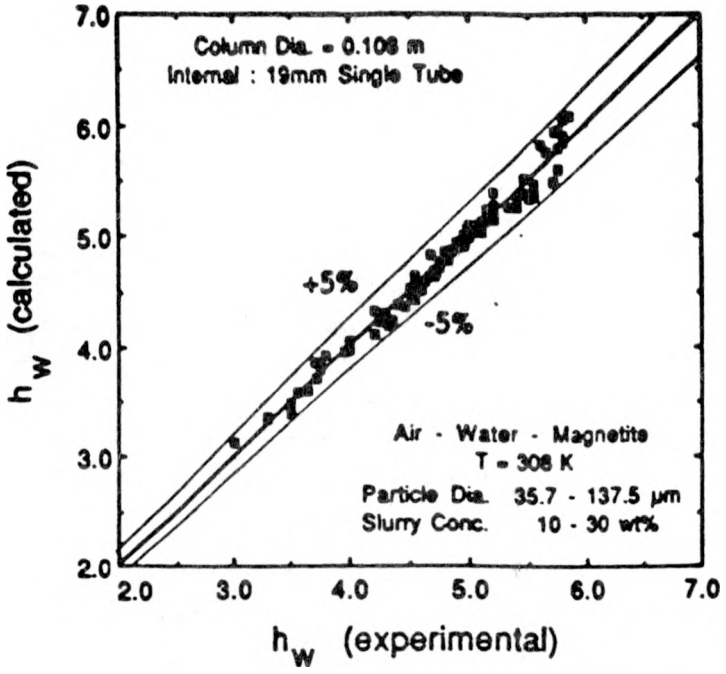

Fig. 6.26. Parity plot for heat transfer coefficient (kW/m^2K). Calculated values are based on Eq. (6.51).

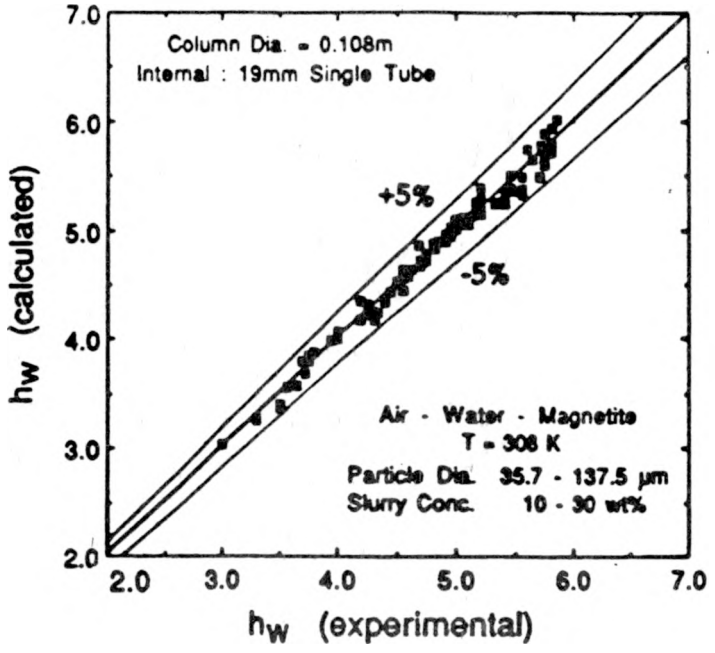

Fig. 6.27. Parity plot for heat transfer coefficient (kW/m^2K). Calculated values are based on Eq. (6.54).

Table 6.5. Values of the constants of Eqs. (6.51) and (6.54) as determined from the experimental h_W values for air-water-magnetite system at 308K and measured in 0.108m bubble column equipped with a 19 mm single heat transfer probe.

d_p	w_s			% Abs. Dev.				% Abs. Dev.	
(μm)	(%)	a	b	Avg.	Range	c	d	Avg.	Range
35.7	10	9.92	0.274	1.67	0.16-4.3	7.93	1.164	1.08	0.22-3.7
49.0	10	9.07	0.236	1.06	0-3.3	7.64	1.039	1.15	0.03-4.1
69.0	10	8.69	0.218	1.12	0.13-2.2	7.49	0.974	1.34	0.03-4.1
69.0	20	9.50	0.249	1.45	0.34-3.6	7.86	1.096	1.13	0.05-3.8
115.5	10	8.47	0.201	1.72	0.19-4.2	7.49	0.940	1.65	0.67-3.1
115.5	20	8.44	0.196	1.62	0.03-3.9	7.49	0.925	1.48	0.35-2.5
115.5	30	9.21	0.223	1.55	0.05-4.1	7.94	1.059	1.39	0.40-3.7
137.5	10	8.40	0.193	0.75	0.27-1.6	7.60	0.959	0.64	0.11-1.8
137.5	20	8.69	0.200	1.63	0.09-3.9	7.80	1.008	1.76	0.18-3.8
137.5	30	8.92	0.203	1.74	0.19-3.8	7.98	1.036	1.75	0.27-2.8

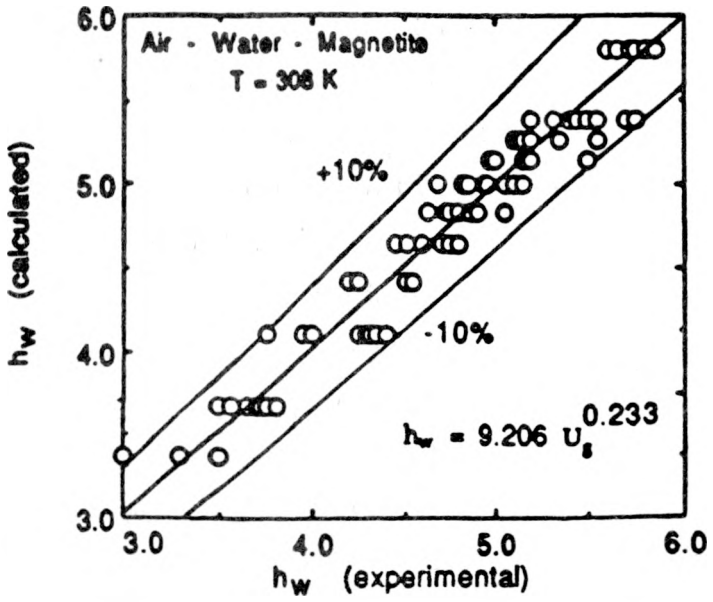

Fig. 6.28. Comparison of experimental and calculated heat transfer coefficient (kW/m^2K) based on Eq. (6.60).

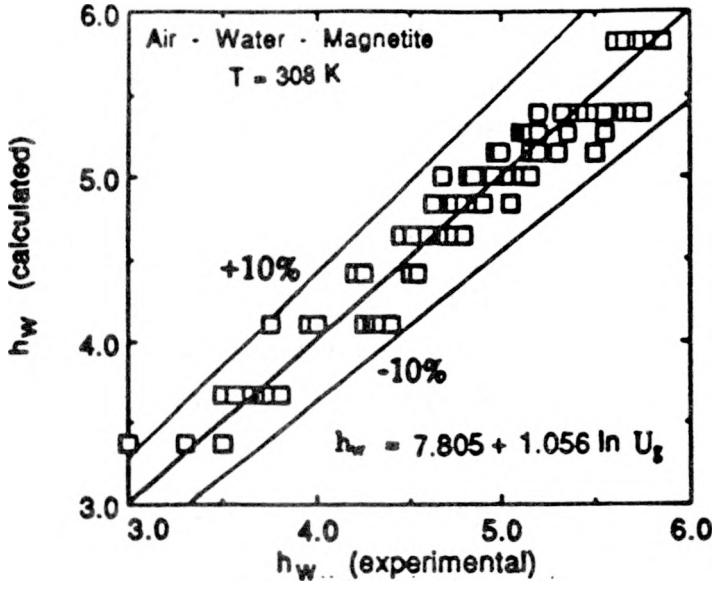

Fig. 6.29. Comparison of experimental and calculated heat transfer coefficient (kW/m^2K) based on Eq. (6.61).

heat transfer for large particles can be augmented by the direct participation of solid particles which will enhance the exchange frequency of fluid elements at the heat transfer surface. On the other hand for small particles the suspension is more homogenous and the variations in h_w will be caused more by the changing thermophysical properties and the experimental work, with micron-size particles, seem to indicate that viscosity of the slurry plays an important role and an empirical multiplicative term is essential.

The air-water-magnetite data [122] for 43.6 μm particles are shown compared with the predictions of various models. It is clear from Fig. 6.30 that the models are inadequate. The empirical Eqs. (6.51) and (6.54) could reproduce the data satisfactorily as seen from Table 6.2. The global constants given in Table 6.3 could reproduce the data as shown in Fig. 6.31.

Experimental data taken for this system in the larger column with a seven-tube bundle are compared with the predictions of various correlations in Figs. 6.32 and 6.33. The experimental data are almost considerably greater than the model based values and both the qualitative and quantitative agreement between theory and experiment is totally unsatisfactory. The empirical relation of Eq. (6.51) on the other hand accomplishes this satisfactorily as shown in Fig. 6.33, which also includes air-water system. The values of the two constants are listed in Table. 6.6.

The experimental data taken in the small column for nitrogen-Therminol-magnetite for a 19 mm single probe [114] are shown compared with the predictions of four models in Fig. 6.34. Deckwer et al. [51] model predicts the data reasonably well. Suh and Deckwer [109] reproduce the two-phase data but fail to reproduce the slurry concentration dependence. Kim et al. [107], and Pandit and Joshi [106] fail to reproduce the experimental data completely in as much as the predictions are too low and the concentration dependence is much less than what is observed experimentally. In Fig. 6.35, the experimental data are compared with the predictions of an empirical Eq. (6.51), where a and b are listed in Table 6.7 for each slurry concentration and three single probes. The reproduction is considered satisfactory.

Next an attempt was made to correlate all the data for the three-probes by a single correlation involving properties of the system and dimensions of the

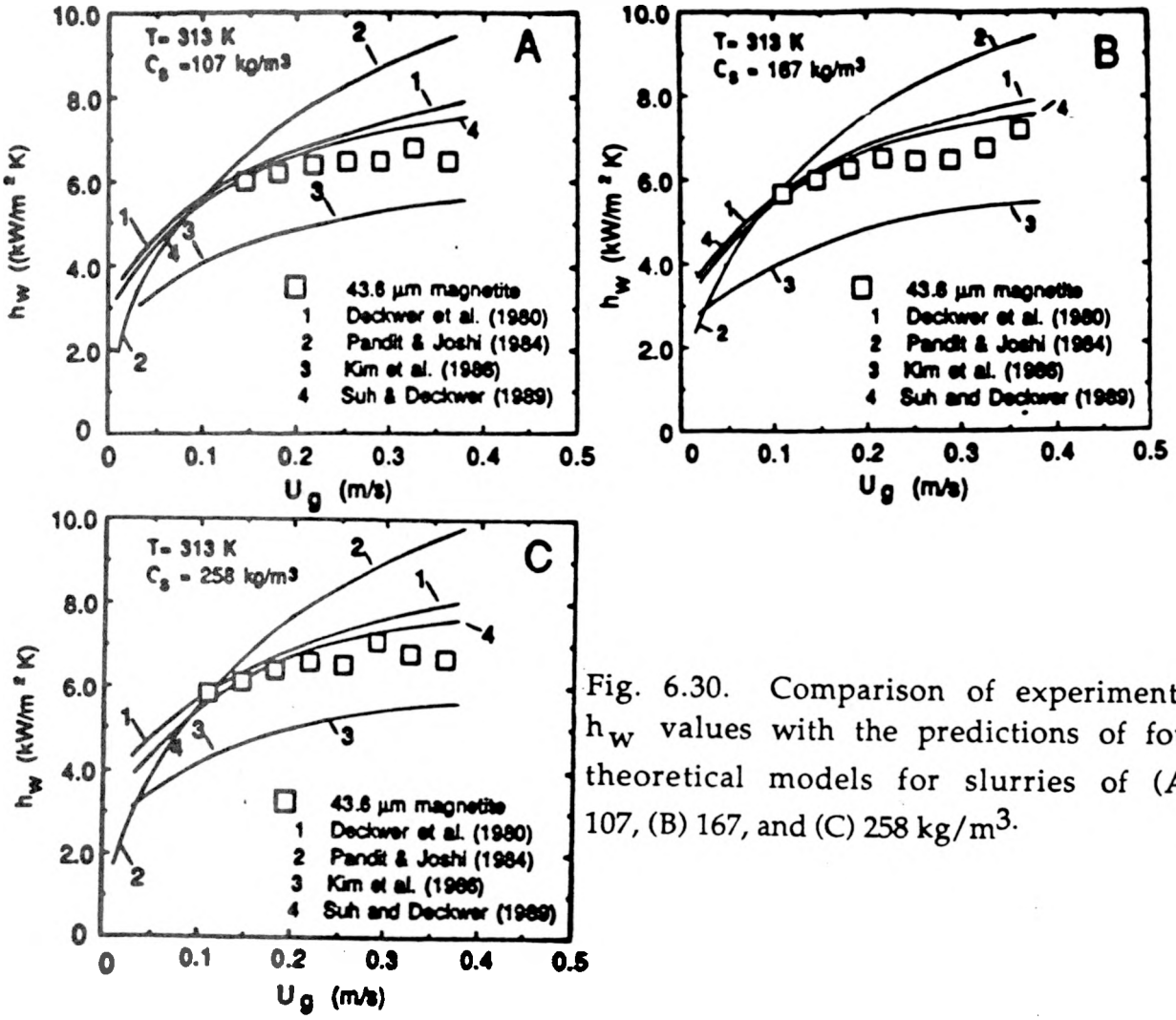

Fig. 6.30. Comparison of experimental h_w values with the predictions of four theoretical models for slurries of (A) 107, (B) 167, and (C) 258 kg/m^3.

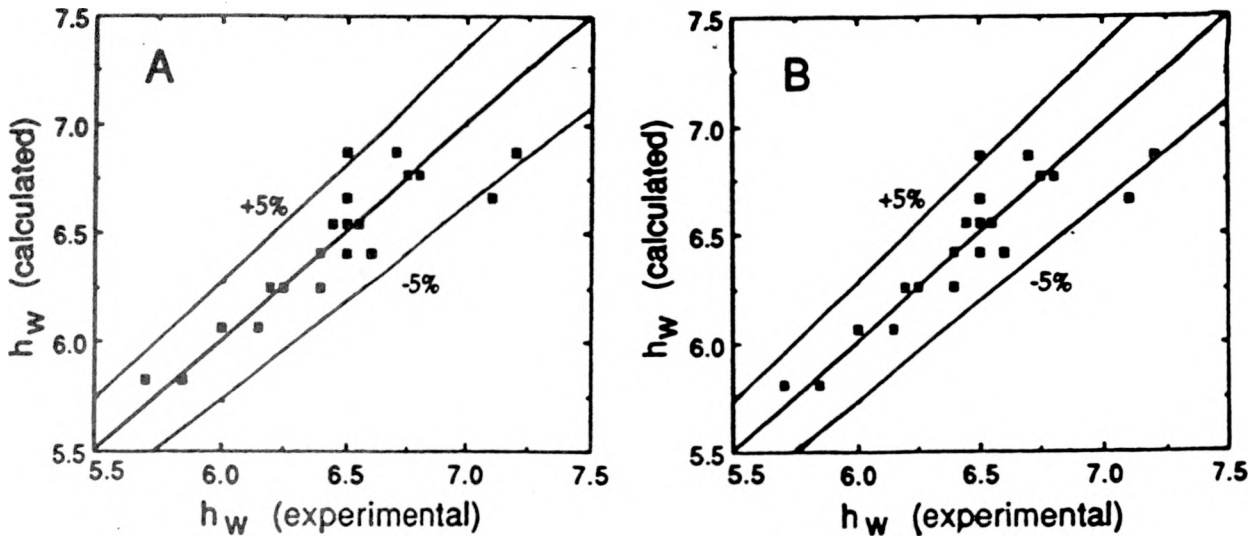

Fig. 6.31. Parity plot of h_W (kW/m^{2}K) for air-water-magnetite system: (A) power function, and (B) logarithmic function.

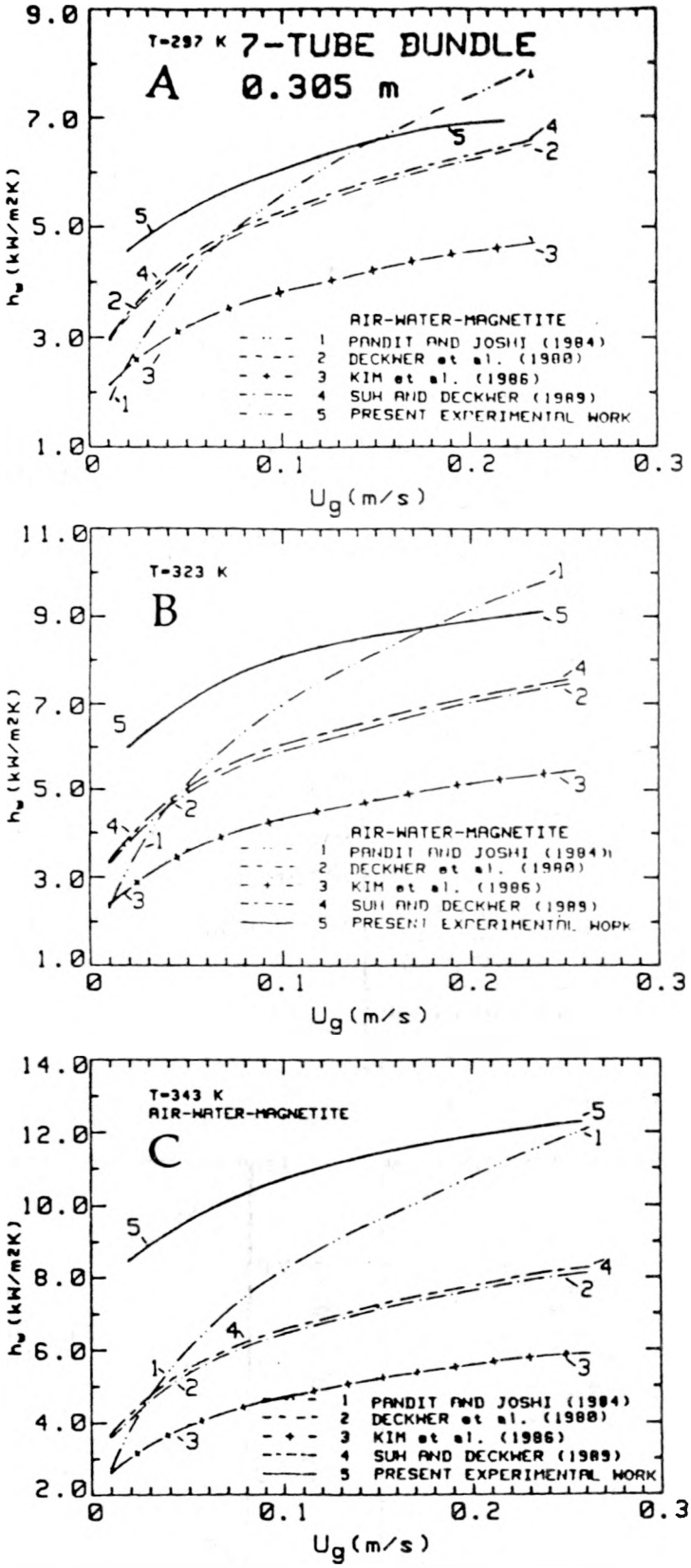

Fig. 6.32. Comparison of averaged experimental heat transfer coefficient with the predictions of different correlations at (A) 297, (B) 323, and (C) 343K.

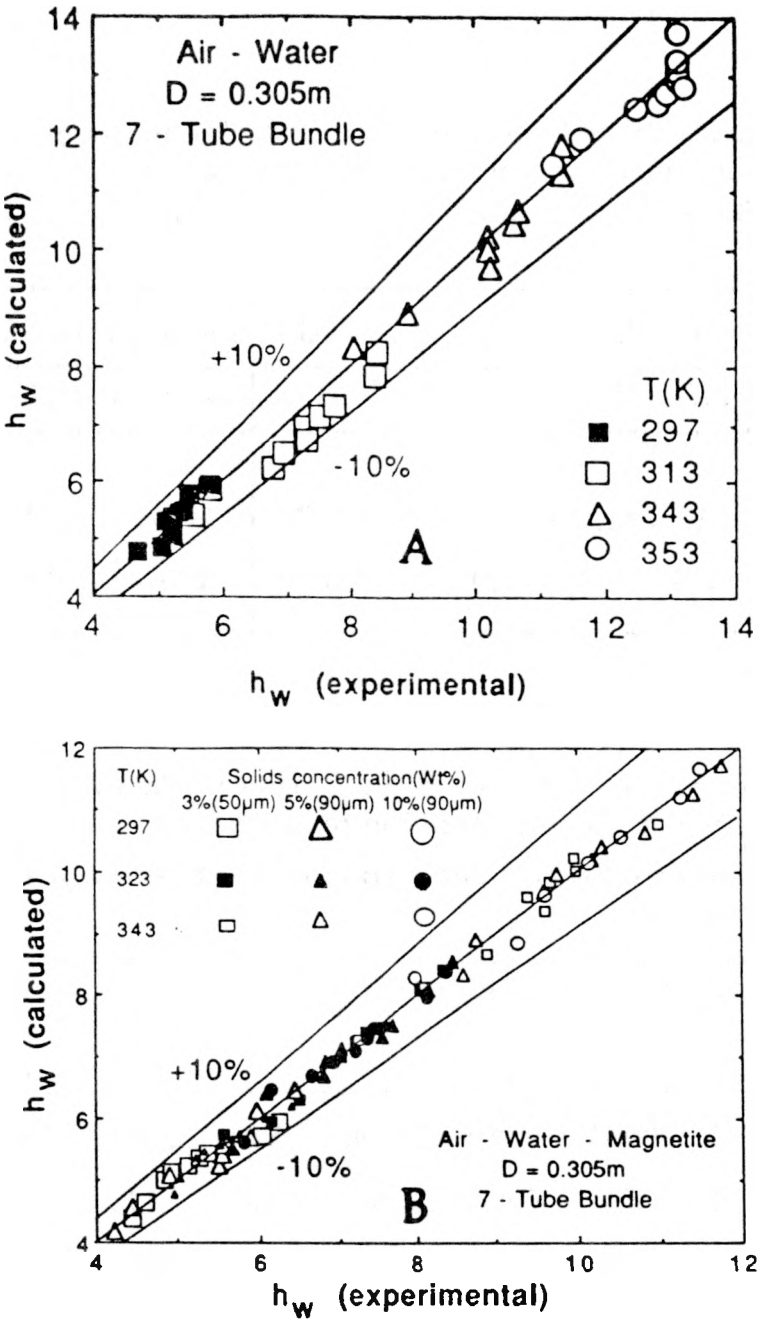

Fig. 6.33. Correlation of heat transfer data on Eq. (6.51) for (A) air-water, and (B) air-water-magnetite systems.

Table 6.6. Values or the constants of Eq. (6.51) as determined from the experimental h_W values for air-water and air-water-magnetite systems and measured in 0.305 m bubble column equipped with a seven-tube bundle.

Constant	Air-Water System			Air-Water-magnetite System		
	297K	313K	343K	297K	323K	343K
a	7.32	12.27	15.87	8.77	11.42	15.41
b	0.11	0.20	0.16	0.16	0.16	0.15

Table 6.7. Values of the constants of Eq. (6.51) as determined from the experimental h_W values for nitrogen-Therminol-magnetite system at 306 - 312K and measured in 0.108 m bubble column equipped with three single heat transfer probes.

Probe Diameter	$w_S = 0$		$w_S = 15$		$w_S = 30$		$w_S = 50$	
mm	a	b	a	b	a	b	a	b
19.0	0.913	0.283	0.969	0.266	1.037	0.261	1.265	0.276
31.8	0.810	0.238	0.856	0.287	0.933	0.295	1.284	0.340
50.8	0.656	0.268	0.800	0.295	0.745	0.242	1.016	0.340

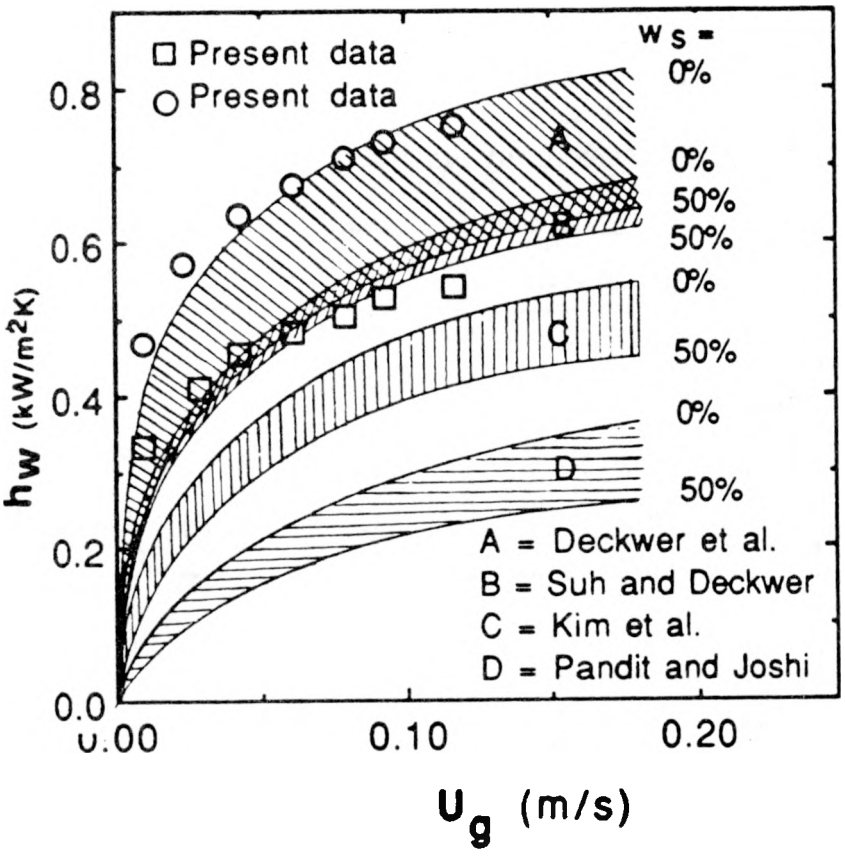

Fig. 6.34. Comparison of experimental data (□-0%, O-50%) for 19.0 mm probe with the theoretical predictions. A: Deckwer et al. [51], B: Suh and Deckwer [109], C: Kim et al. [107], and D: Pandit and Joshi [106].

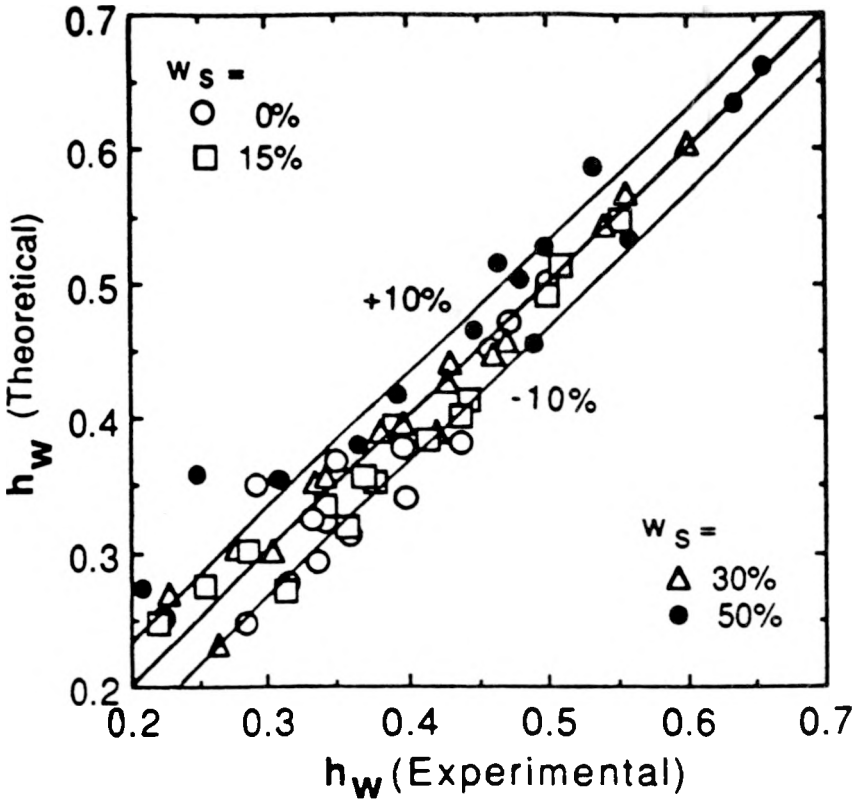

Fig. 6.35. Comparison of experimental and computed h_W values according to Eq. (6.51).

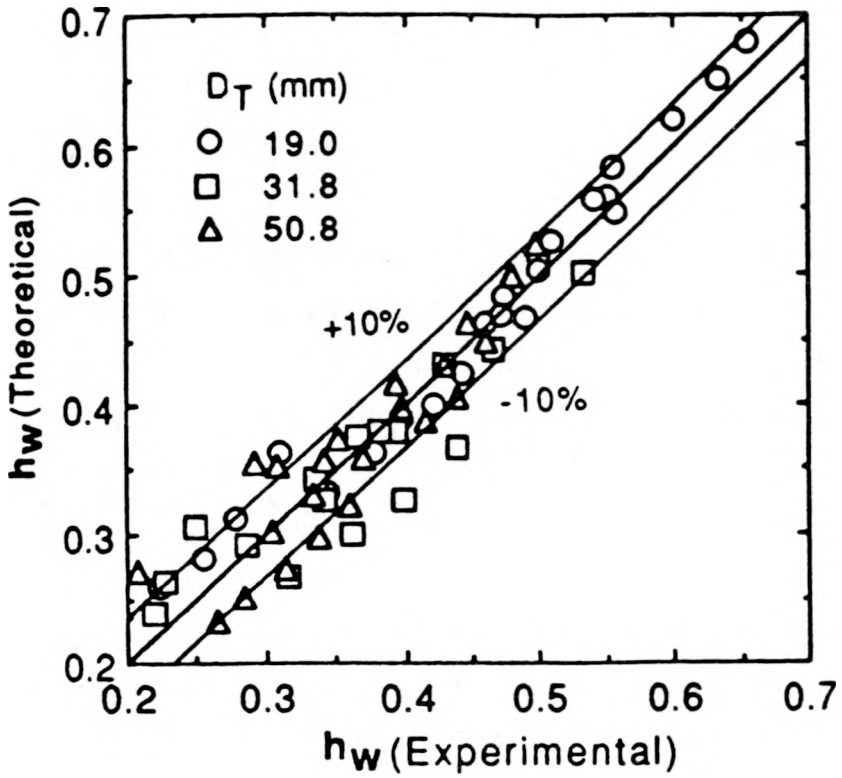

Fig. 6.36. Comparison of experimental and computed h_W values according to Eq. (6.62).

baffled bubble column. Calculations revealed that such properties as thermal conductivity, density and heat capacity change in such a fashion that their product is approximately constant. Hence viscosity essentially plays a dominant role. Further, on the basis of Table 6.7 a mean value of 0.27 was taken for the exponent of U_g. This yielded a correlation of the following form:

$$h_w = 1.05 \, (\mu_L/\mu_{SL})^{-0.6} \, (U_g)^{0.27} \, [\, (D_C - D_T) / D_C \,]^{0.65} \qquad 6.62$$

Explicit comparison of experimental data points with the predictions of Eq. (6.62) is shown in Fig. 6.36 and it is regarded as quite satisfactory.

The experimental data for the seven-tube bundle and magnetite powders of average diameters 27.6 and 36.6 μm [115] are shown compared with the model predictions in Fig. 6.37. Again, the models fail to predict the experimental data. The form of Eq. (6.51) on the other hand could synthesize the data as shown in Fig. 6.38. It is seen that the exponent of U_g varies appreciably and the coefficient of U_g even more. The latter is because of the changes in the rheology of the system and Deckwer's theory [51, 93] does not simulate these changes in slurry properties with composition.

The experimental data for the nitrogen-Therminol-magnetite (d_p = 36 μm) system taken in the larger column with thirty-seven tube bundle [121] are shown plotted in Fig. 6.39 as a function of U_g in log-log plot. Each data set referring to a particular temperature can be represented by an empirical relation of the type of Eq. (6.51). The values of the two constants are listed at each temperature in Fig. 6.39. b is strongly temperature dependent and much different from 0.25. It increases with temperature in the foaming region (T>423 K) and decreases with temperature in the nonfoaming region (T<423 K).

The experimental data [114] for the air-water-silica sand system are reported in Fig. 4.68 for a seven-tube bundle in the larger column at three different temperatures and two slurry concentrations. In Fig. 6.40, the data are shown compared with the predictions of four models. The nature of disagreement between the calculated and experimental h_w values is dependent on temperature and it gets poorer as the temperature increases.

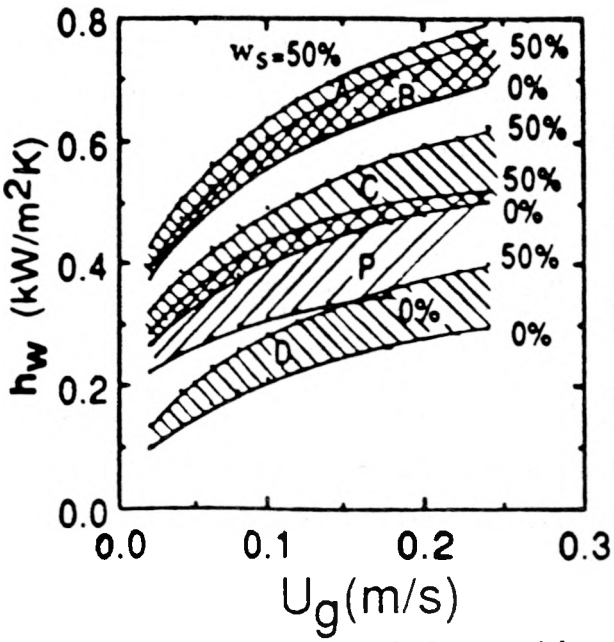

Fig. 6.37. Comparison of h_w with model predictions. A-[51], B-[109], C-[107], D-[106] and P- Present work.

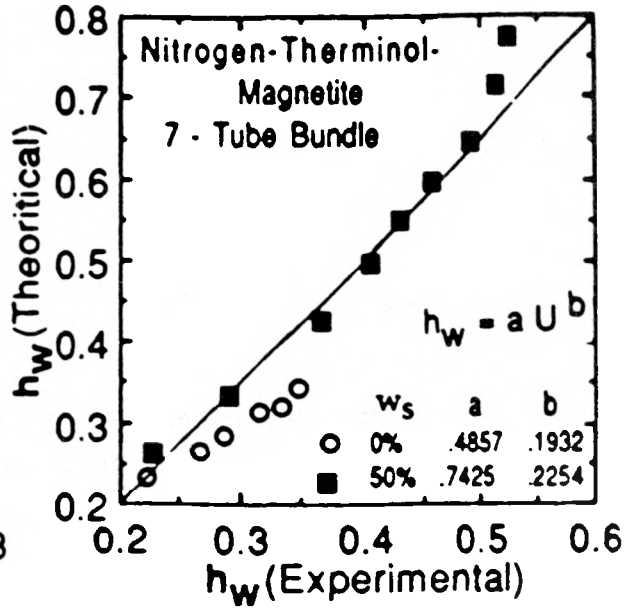

Fig. 6.38. Comparison of experimental h_w values with a semi-theoretical correlation(Eq.6.51).

(6.60). (6.61).

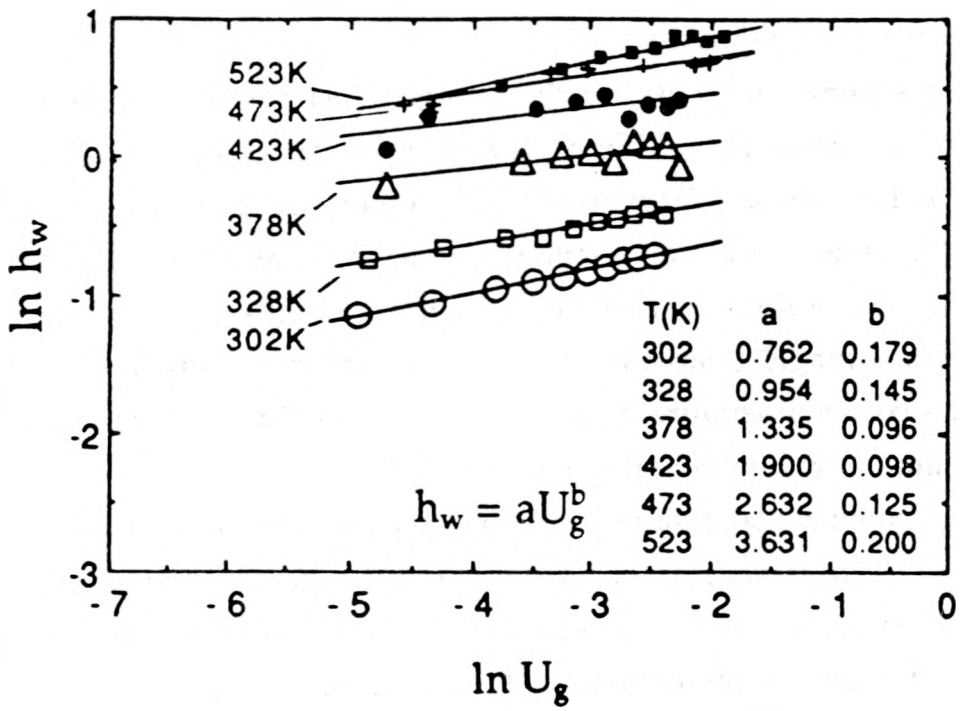

Fig. 6.39. A plot of heat transfer coefficients(probe 1) versus nitrogen velocity shown in logarithmic coordinates at different temperatures. Solids concentration = 40 wt%.

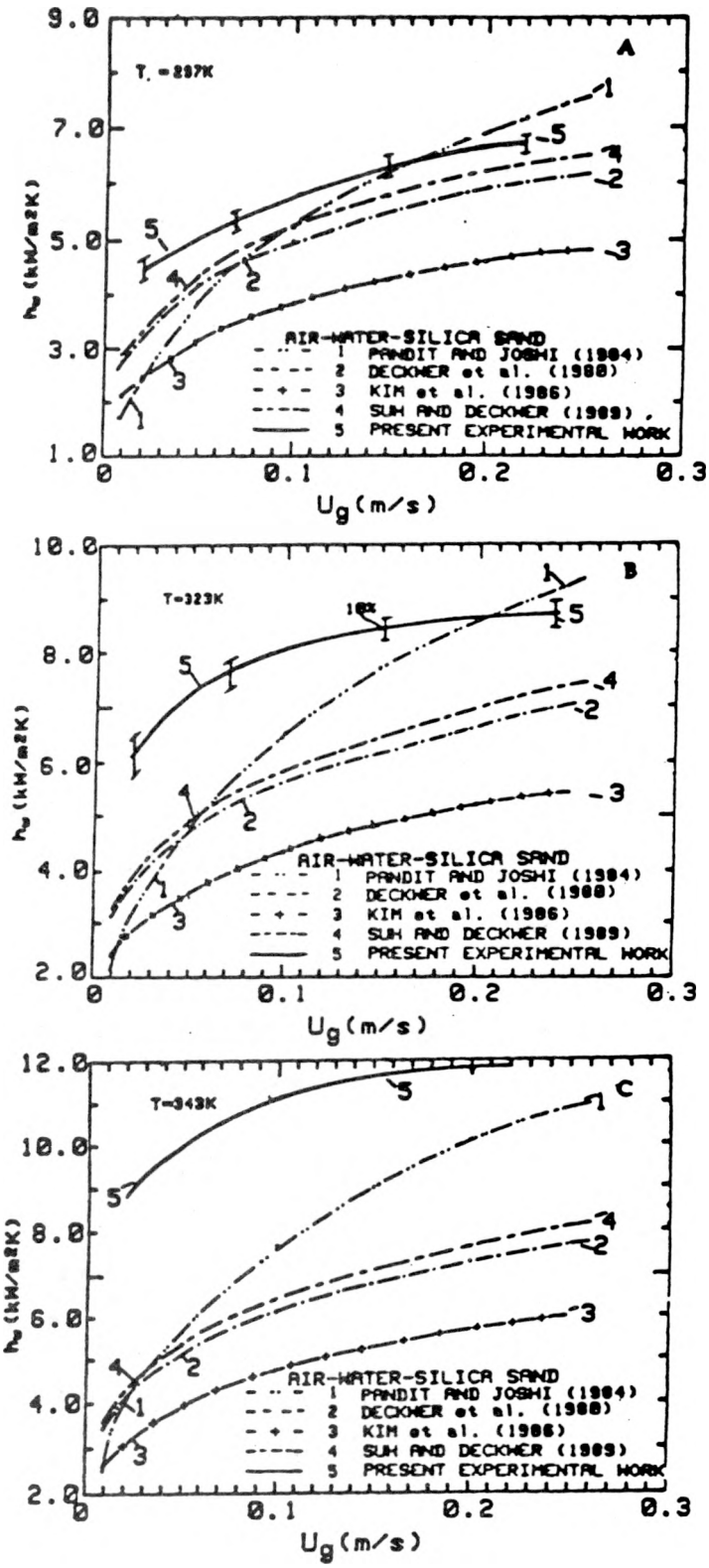

Fig. 6.40. Comparison of the concentration averaged heat transfer coefficient values as a function of air velocity with the predictions of different correlations at temperatures of 297(A), 323(B) and 343K(C).

A semi-empirical approach based on Eq. (6.51) has been tried mainly to understand the nature of dependence of b on the system properties. The values of a and b obtained by regression analysis are given in Table 6.8. It is to be noted that the values of b varies over a range and are significantly different from 0.25. It may also be emphasized that the values of a are dependent on temperature and slurry composition for the system. Comparison of experimental and computed values is shown in Fig. 6.41. According to Deckwer [93], and Deckwer et al. [51] h_w is given by:

$$h_w(kW/m^2K) = 0.0001(k\rho C_p)_{SL}^{0.5} (\rho g/\mu)_{SL}^{0.25} U_g^{0.25} \qquad 6.63$$

$$\equiv a' U_g^{0.25} \qquad 6.64$$

Attempts to correlate the h_w data at each temperature on the basis of Eq. (6.64) yielded results reported in Table 6.8. It is clear that a choice of 0.25 for b is inappropriate as it fails to reproduce the experimental data. Calculations revealed that for the present systems $(k\rho C_p)_{SL}$ varies only within $\pm$ 2 percent. The major changes in h_w creep in through changes $(\rho g/\mu)_{SL}$. Matching experimental data with Eq. (6.63) suggests the following relation for h_w:

$$h_w(kW/m^2K) = 3.5 \times 10^{-6} (k\rho C_p)_{SL}^{0.5} (\rho g/\mu)_{SL}^{0.47} U_g^{0.25} \qquad 6.65$$

Equation (6.65) reproduces the data with an average absolute deviation of 13 percent, the range being 3 - 26. The corresponding numbers for Eq. (6.63) are 29 and 6 - 55 respectively. In summary, the existing theory of Eq. (6.63) is not substantiated by present data both for a or a', and b.

6.5. Conclusions and Recommendations

Our extensive results of heat transfer coefficient measurement from simulated heat transfer surfaces of tubes of different diameters and tube bundles

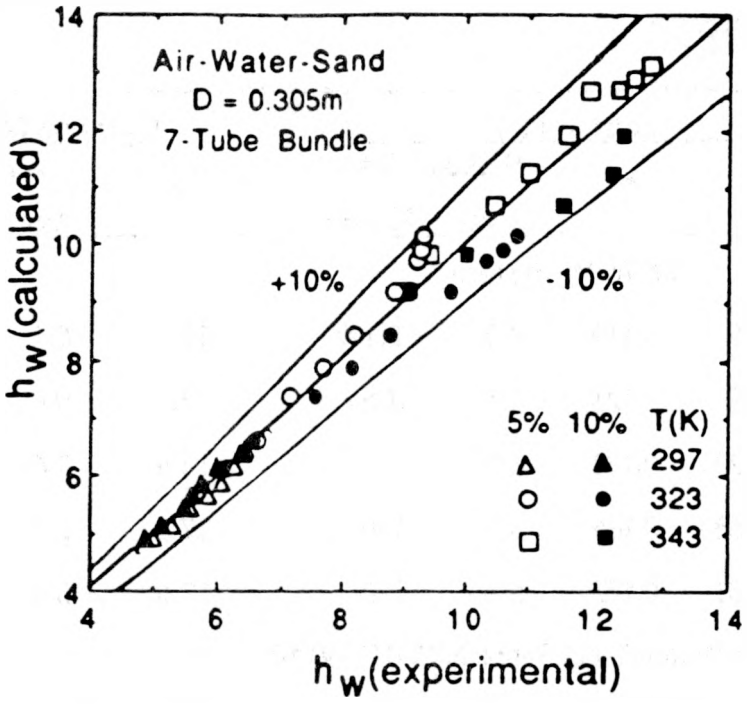

Fig. 6.41. Comparison of experimental and calculated (Eq. 6.51) h_W (kW/m^2K) values for the air-water-silica sand system.

Table 6.8. Values of the constants of Eqs. (6.51) and (6.64) as determined from the experimental h_W values for air-water and air-water-sand systems at several temperatures and measured in 0.305 m bubble column equipped with a seven-tube bundle.

T (K)	Equation (5)				Equation (7)		
	a	b	% Abs. Dev.		a'	% Abs. Dev.	
			Avg.	Range		Avg.	Range
	Air-Water System						
303	7.59	0.119	2.0	0.1-9	11.3	8.4	3-16
313	8.99	0.125	4.1	3-8	12.5	9.8	2-14
323	11.23	0.178	6.1	1-9	14.8	9.6	2-16
333	12.68	0.166	5.7	2-9	17.1	7.9	2-17
343	13.01	0.177	5.1	3-8	19.6	5.8	2-18
	Air-Water-Sand System (5-10 Wt%)						
297	7.85	0.125	2.5	0.8-3	11.4	8.9	1-15
323	13.38	0.199	4.1	2-8	15.6	5.6	2-12
343	17.21	0.160	4.7	1-7	23.7	8.7	2-30

of different configurations and sizes in two bubble columns as a function of gas velocity at different temperatures and involving dispersions of two different liquids (water and Therminol) and solids of different physical properties, sizes and size ranges, have lead to results which may be synthesized in terms of several general conclusions. The scope of this section is to briefly enumerate them and also include the information generated regarding the ability of model expressions and correlations to predict heat transfer coefffcient for design and scaleup purposes. This summary is to precipitate certain concrete recommendations for future research in the area of heat transfer in slurry bubble columns

For all two-phase and three-phase systems, the heat transfer coefficient is found to increase monotonically with air velocity, first rapidly and then slowly and finally approaches to a constant value in the fully developed churn-turbulent flow regime. The heat transfer coefficient is temperature dependent and in general increases with increase in temperature . Similarly, the influence of liquid phase viscosity is pronounced on heat transfer coefficient and it is found to decrease appreciably as the viscosity increases. The difference in h_w for systems involving water and Therminol-66 is more than an order of magnitude. It would be interesting to investigate several liquids of distinctly different viscosity values and at several temperatures. Such data are essential because of the unknown and involved relationship between the viscosity of a liquid and temperature . A good knowledge of the understanding of the viscosity of a liquid on different parameters characterizing its structure and temperature is essential.

The dependence of heat transfer coefficient on the nature of solids present in the three-phase systems is interesting. For fine micron-size range iron oxide powders, it is found that the presence of solids increases the heat transfer coefficient, and increased concentration of solids in the slurry augments the heat transfer coefficient relatively more than in dilute concentrations. It is considered, based on limited data, that the heat transfer rate enhancement occurs through the changes in the rheology of the suspension. For larger particles, the heat transfer coefficient increases but this increase is much more pronounced for slurries involving a liquid of higher viscosity, Therminol-66 versus water. The heat transfer rate augmentation now probably occurs through the direct

participation of the solid phase. Again this is an important feature from a practical stand point. In direct coal liquefaction plants, catalyst particles of a size range are employed and concentrations can be quite high and the temperature of operation is high so that all the three interacting parameters (viscosity, particle size, or size range and slurry viscosity) must be considered to establish the heat transfer rates. At the present time, not enough knowledge exists to resolve these interacting parameters and their influence on heat transfer rates in a unique manner and both theoretical and experimental research is required for the proper understanding.

The influence of internals present in the column on heat transfer rates is also complicated and significant. Experiments have indicated that the presence of tube bundles present in the column increases the heat transfer coefficient by improving the liquid circulation and mixing in the bubble column so that the heat transfer surface is bathed more frequently and more efficiently by the liquid or slurry suspension elements or packets. The same circumstance is created by an increase in the column diameter and hence we have seen an appreciable increase in heat transfer rates of unbaffled columns as the column diameter increases from 0.108 m to 0.305 m. However, the present work also suggests that well baffled bubble columns (columns with tighter tube bundles) will exhibit only feeble dependence of heat transfer coefficient on column diameter. Small diameter bubble columns with single probes can be modelled on the basis of dimensionless hydraulic diameter. The tube-bundle pitch effect could not be established on the basis of present work and to resolve this feature a well planned more elaborate experimental effort will be in order.

The present experimental effort has clearly demonstrated that heat transfer rates increase with increase of solids in the column as long as these can be uniformly suspended, and the presence of heat exchanger surfaces further augments the heat transfer rates by improving the degree of liquid mixing. This is a very useful result and at least qualitative guidance can be drawn from our work for the design of practical slurry bubble column. For quantitative simulation more detailed experimental work will be in order. This is particularly interesting because the available correlations and model-based experssions fail both qualitatively as well as quantitatively to represent the body

of data generated in the present program. We have found an empirical approach to correlate experimental data but to put it on a more fundamental basis further research is needed which is beyond the scope of the present contract.

7. GENERAL CONCLUSIONS AND RECOMMENDATIONS FOR FUTURE WORK

In the earlier sections, a detailed discussion of the heat transfer data generated for individual systems under varying operating conditions and column configurations is presented, and the conclusions derived on the basis of these individual systems are also noted. The inadequacy and paucity of the literature available data are emphasized. The general inability of the theoretical correlations to predict reliable values is universally observed for all the systems. A brief mention of general conclusions emerging from this work is made in the section on executive summary. Here, in the following we list the general conclusions in the context of the need they indicate for future research work both experimental and theoretical. We discuss heat transfer from simulated heat transfer surfaces in the slurry bubble column first and then the gas holdup. This is because the major thrust of the present work is on the former and the latter is considered only to characterize the bubble column operation so that our heat transfer data may be appropriately selected for the design of larger-scale production systems.

A major portion of our effort has concentrated with aqueous systems involving air as the gas-phase. This is primarily due to the operational convenience as we conducted a variety of experiments to disentangle the effect of gas velocity, liquid column height, temperature of operation, solid phase physical properties, solid particle size and size distribution, and slurry concentration. In addition, the column diameter effect and the influence of column internals, size and configuration, are also investigated. These elaborate experimental studies have provided a number of interesting and useful characteristics of significant value in judging the slurry bubble column behavior and these are briefly enumerated in the following.

The heat transfer coefficient increases rapidly as the gas velocity is increased and the column hydrodynamic behavior shifts from discrete bubbling to bubble coalescing regime, and the liquid mixing in the column improves. The rate of heat transfer increase in the churn-turbulent flow regime is much slower and it gets to a constant value as the flow becomes fully developed and liquid mixing is at its optimum state. In this context in an unbaffled column, the heat transfer coefficient is relatively larger for a column of greater diameter than for a narrower column

(less than about 10 cm) as the liquid mixing in the former is much better than in the latter. Certainly, this is dependent on the gas sparger design and our literature analysis has revealed that single nozzle air spargers are inadequate and lead to poor liquid mixing and smaller heat transfer rates. Our above comments and subsequent analysis assumes that the gas is introduced in the column through judiciously spaced nozzles or bubble caps, or through a perforated plate of appropriate pressure drop. This will bring about a well distributed uniform gas flow through the slurry in the bubble column. As a rough guide, a linear gas velocity of about 12 cm/s will bring the heat transfer coefficient at its maximum optimum value. Unfortunately, the existing models and correlations do a poor job in predicting this value and particularly so for nonaqueous systems involving liquids of higher viscosity. A good basic theoretical study oriented towards improving the ability of a design engineer to estimate this maximum heat transfer coefficient in general will be superbly appropriate and is an essential component in the art of understanding the bubble column behavior.

The influence of temperature is pronounced on heat transfer rate. Qualitatively, heat transfer coefficient increases appreciably with increase in temperature at the same air velocity. The increase is enough to influence any design and economic study. Quantitatively, none of the existing theories can even approximately predict these values. We have presented only a semitheoretical approach which has the potential to correlate the data at a given temperature only. The scheme is uncertain for its ability to synthesize data at different temperatures or predict the same. We recommend, that a thorough theoretical effort focused in this direction will be extremely useful and rewarding. The experimental data generated in this effort will be useful in providing guidance for the development of this theory as well as will constitute a basis for testing it.

The influence of internals on heat transfer rates at different temperatures is quite involved. Based on limited data generated in this effort it appears that at room temperature at all U_g values, a loosely packed configuration of internal tubes will not influence the heat transfer rates. A tightly packed column with tube internals on the other hand gave lower heat transfer rates for velocities smaller than those where churn-turbulent regime sets in and higher rates for larger velocities. This can be understood on the basis of liquid mixing. At a higher

temperature (70°C) the behavior is different. Increasing tubes in the column leads to decrease in heat transfer rates. This would suggest relatively less efficient liquid movement at the tube surfaces as the temperature is increased. Holdup data suggest larger number of smaller air bubbles for thirty-seven tube bundle which will impede liquid circulation rate and hence the heat transfer coefficient. More experimental effort will help if it is supplemented with the measurement of bubble diameter also.

Our heat transfer rate measurements conducted in the lower (0 - 0.7m) and upper (1.0 - 1.7 m) sections of the column revealed that the same are independent of the height in the column for the seven-tube bundle while for the thirty-seven tube bundle rates are higher for the upper section than for the lower section. These data are presented in Fig. 7.1 to 7.3 and these also suggest that these variations in heat transfer rates are not dependent on temperature.

The addition of a third solid phase changes the heat transfer rates only in a minor way as compared to the rates for the corresponding two-phase system. This is highlighted in Fig. 7.4. Our work from micron size range particles to as high as 140 μm suggest only a weak dependence of particle size on heat transfer coefficient. The solid phase concentration increase influences the heat transfer only feebly at solids concentration by weight up to thirty percent but the increase thereafter is more pronounced as the weight fraction of solids in the slurry is increased. The physical properties of the solids such as density, specific heat and thermal conductivity have a relatively weak influence on the heat transfer characteristics, Fig. 7.4. More detailed investigations of these aspects do indicate some trends which are only of limited importance to a design engineer. However, the available models and correlations fail to simulate any of these observed features.

The empirical approach to correlate the experimental data by a power function in gas velocity successfully employed in this work need to be further investigated. Attempts will be in order to develop explicit expressions for the constants a and b of the empirical model in terms of the operating parameters and system characteristics in the light of existing theory of Deckwer and coworkers along with Kolmogoroff's theory of isotropic turbulence. A detailed tabulation for these constants generated in this work for different systems and parameters will be particularly useful in this endeavor.

Slurry bubble column dispersion rheology plays a very important role in heat

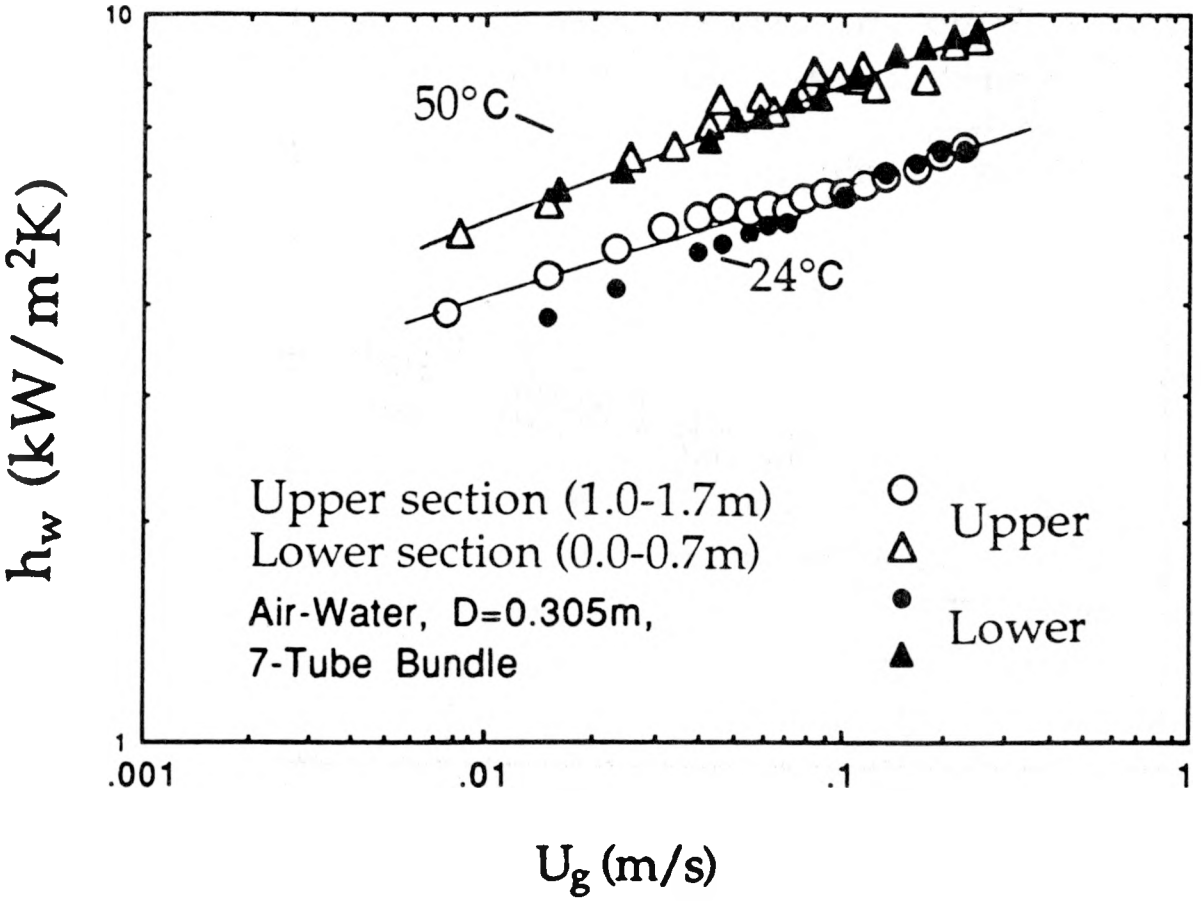

Fig. 7.1. Variation of h_W with air velocity and probe location.

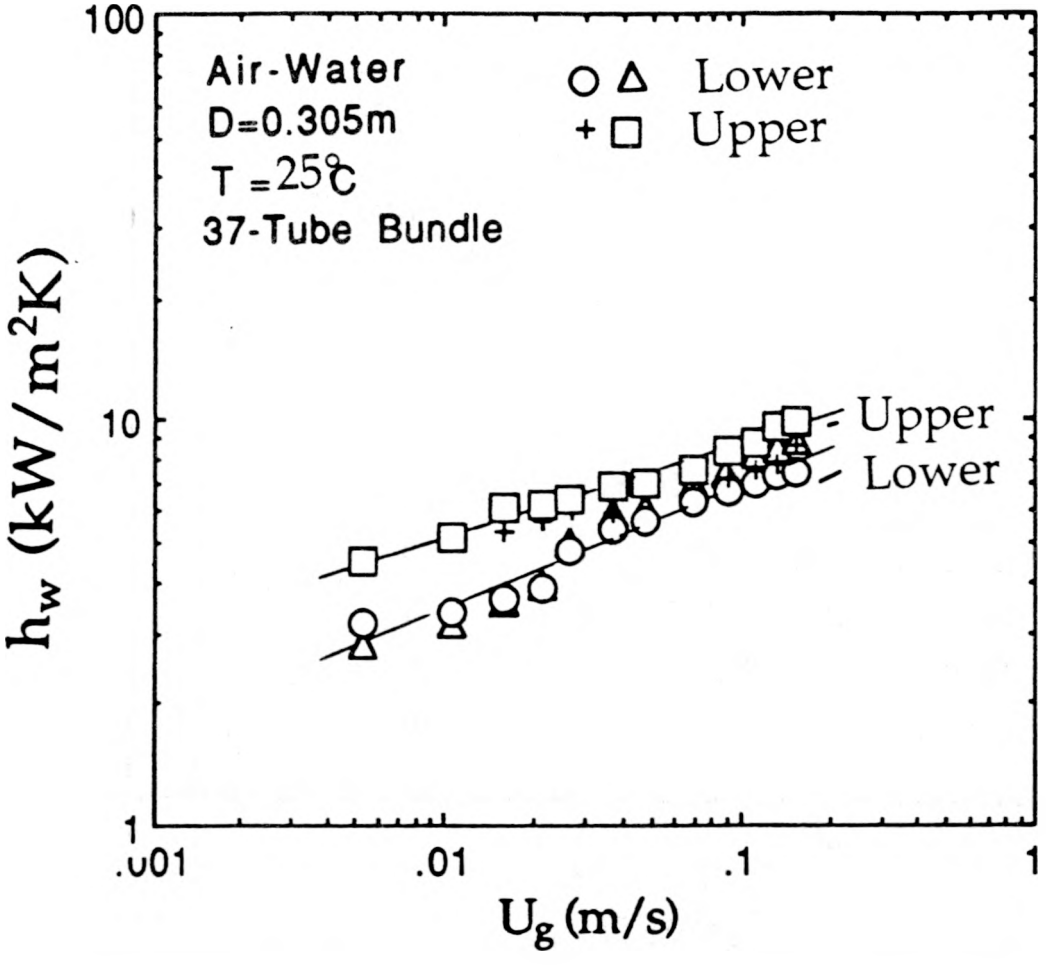

Fig. 7.2. Variation of h_W with air velocity and probe location.

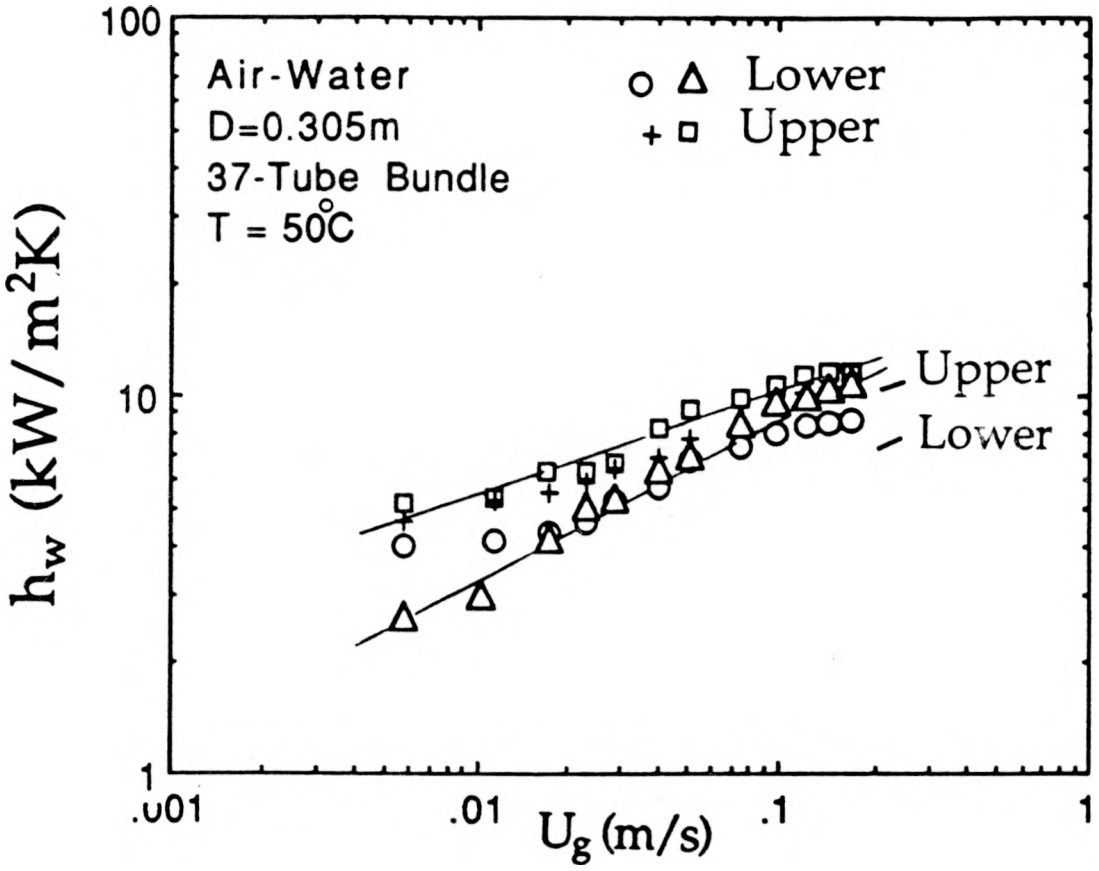

Fig. 7.3. Variation of h_W with air velocity and probe location.

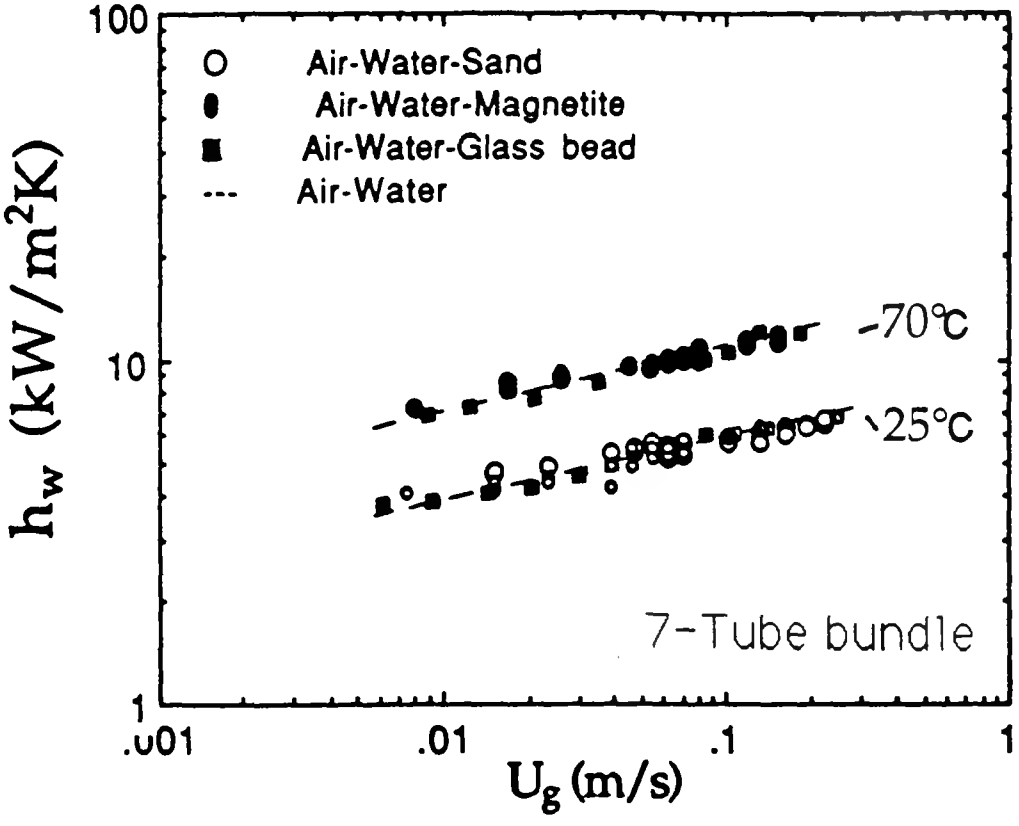

Fig. 7.4. Variation of h_W with air velocity and temperature for different systems.

transfer process through the prevailing hydrodynamics. To establish this explicitly a much more viscous heat transfer fluid, Therminol-66, was investigated. Experiments somewhat analogous to aqueous systems have been performed though on a relatively smaller scale. These experiments on the whole have indicated a qualitative dependence on different parameters which is identical to that observed for aqueous systems. Quantitatively the differences are appreciable and significant. Thus, as displayed in Fig. 7.5, h_W for Therminol-66 systems are more than an order of magnitude smaller than aqueous systems. This brings to light the importance of the liquid phase properties in establishing heat transfer rates in slurry bubble columns.

The dependence of such systems on different parameters is in some cases distinctly different in relative magnitudes than what is observed in aqueous systems. For example, addition of solids enhances the heat transfer rates much more than in an aqueous system, and this enhancement exhibits a systematic increase with increase in solids concentration. In Fig. 4.40, a similar result is displayed for single tubes of different diameters. The temperature increase reduces this enhancement in heat transfer rates with increase in concentration. This will suggest that liquid viscosity plays a very significant role. With increase in temperature, the viscosity decreases and the system tends to behave more like an aqueous system. At 523K the viscosity of Therminol-66 is about the same as that of water at 323K. The thermal conductivity of Therminol-66 is much smaller (by a factor of five) than that of water while it is comparable to that of solids. It would therefore suggest that solids will have more influence in removing heat in Therminol-66 than in water. Similarly, the specific heat of water is more than twice that of Therminol. This will again suggest that water will play a dominant role in removing heat than Therminol in the presence of solids. Solids specific heat is about one-sixth of water and about one-half to one-third that of Therminol. It would be appropriate to undertake some work on heat transfer with liquids of different viscosities to understand and quantify the heat transfer rates in terms of the properties of the system. The single tube internals at room temperature exhibit a bit more pronounced effect than found for aqueous systems. This need to be further investigated.

A similar body of data is generated for the gas holdup. For aqueous systems,

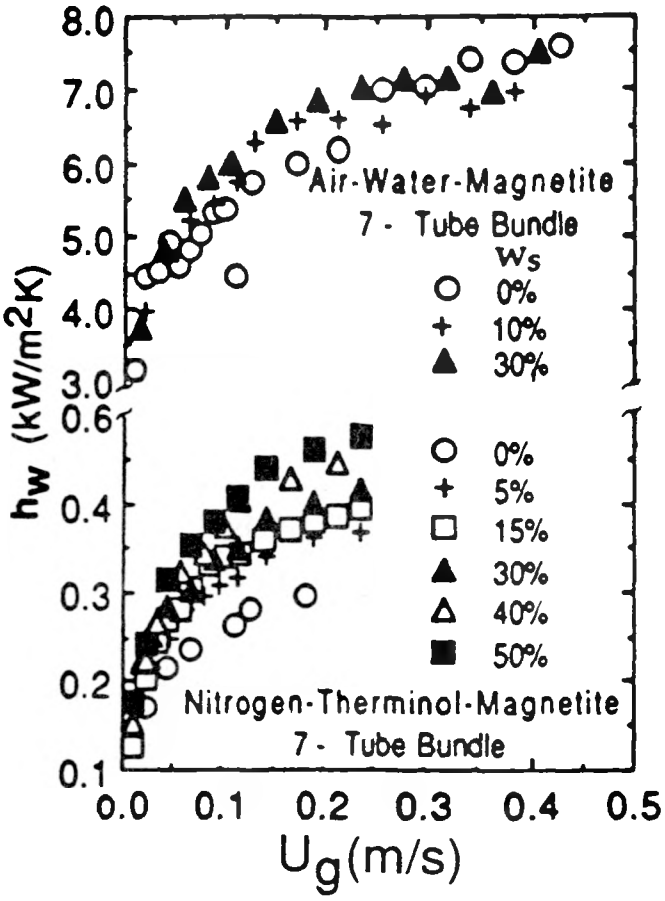

Fig. 7.5. Comparison of h_W data for two systems with widely different viscosities for the liquid phase.

the gas holdup increases rapidly in the discrete bubbling regime, the increase slows down in the bubble coalescence regime, and further slows down in the churn-turbulent regime. The hysteresis effect is encountered whenever foaming is observed and we have taken data with decreasing air velocity. The influence of slow (< 1.0 cm/s) cocurrent liquid flow influences the holdup insignificantly in relation to the values obtained with decreasing air flow velocity in the absence of foam. The existing correlations are found to be inadequate in predicting these experimentally observed air holdup values. A modified drift-flux theory approach has been successful in correlating the data.

The presence of internals (tube bundles) enhances the air holdup and eliminates the hysteresis effect. At room temperature, with either a single tube or a seven-tube bundle, the air holdup is found to be independent of column diameter, 0.108 and 0.305m. The effect of temperature on air holdup is to decrease it with increase in temperature, and above 323K it is almost constant. In Fig. 7.6., it is demonstrated that at room temperature, the air holdup is about the same for a seven and thirty-seven tube bundle, while at a higher temperatures in the range 50 - 70°C, the thirty-seven tube bundle gives a higher value than the seven-tube bundle. This would suggest that bubble diameters be measured in baffled columns as a function of temperature to mechanistically understand this phenomenon.

The addition of solid particles of different physical properties and sizes (1 to 140 μm) always decreases the gas holdup as compared to the corresponding values in the absence of solids. The air holdup increases with increase in air velocity, and decreases with increase in slurry concentration. The hysteresis effects are negligibly small and particle size has a weak dependence. Our detailed work with air-water-magnetite system indicates that with increasing particle size in the powder, the air holdup decreases. The dependence for air-water-glass bead system for air holdup on powder size is not evident. If these differences are realistic, it appears that particle density and wettability play an important role. The air holdup for the magnetite system is smaller as compared to the glass bead system. Further careful work will be essential to resolve these observations. Data obtained at room temperature with internals indicate that holdup increases with internals in the column. This is obviously because of the smaller bubbles. The influence on holdup by the presence of internals seem to decrease as the particle size in the slurry increases.

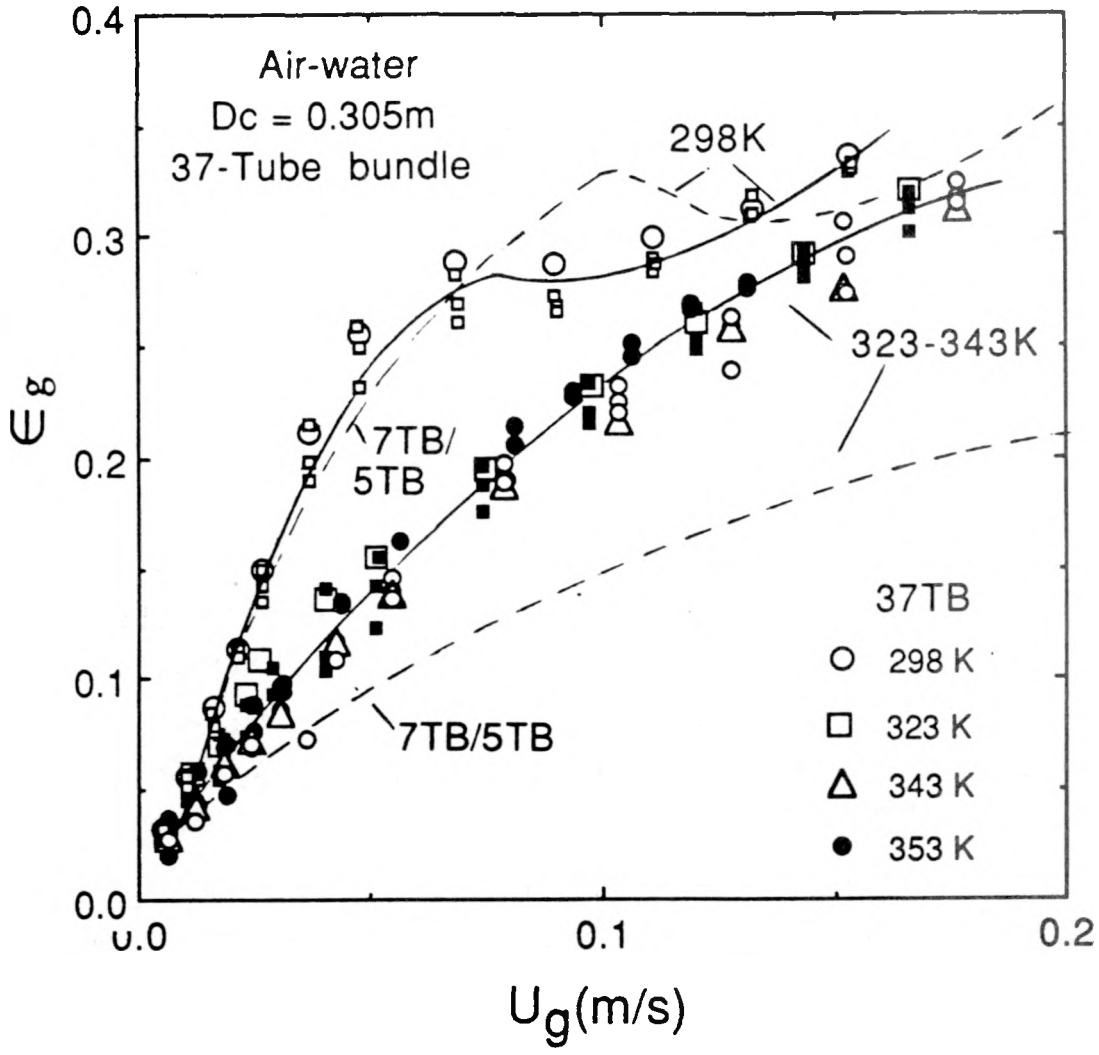

Fig. 7.6. Variation of air holdup for air-water system with air velocity at different temperatures for a column equipped with either a five-tube, a seven-tube or a thirty-tube bundle. D_c = 0.305 m.

The temperature has an appreciable effect on air holdup for three-phase systems as the temperature is raised above the ambient. For aqueuos systems, the air holdup decreases as the temperature increases to about 50^0C and thereafter the decrease is negligibly small as the temperature rises to about 70^0C. At higher temperatures, the influence of slurry concentration on air holdup is not appreciable and this has been confirmed with measurements using internals of varying sizes in the column. The available models have generally not been successful except the correlation uses a slurry viscosity expression and its reliability needs to be established. In this context, it may be pointed out that measurements of slurry viscosity are essential to fully establish the potential of these two correlations. The drift-flux theory in its modified form has been generally successful in at least correlating the data which at best can be regarded as an empirical approach at the present time. More theoretical work is in order in this direction.

The three-phase systems involving more viscous fluids than water have been investigated with a particular system nitrogen-Therminol-magnetite (or red iron oxide). At room temperature with red iron oxide, the nitrogen holdup is influenced to a small extent ($\pm$ 5 percent). The holdup decreases at smaller nitrogen velocities (<0.08 m/s) as the red iron oxide powder is added up to 50 weight percent, but this decrease reduces at the higher nitrogen velocities where the holdup becomes almost identical to that for the two-phase system. The presence of internals (seven-tube) in the small column has decreased the nitrogen holdup in sharp contrast to low viscous slurries where the holdup increased with internals. This would suggest that the influence of internals on gas holdup is viscosity dependent. It implies that bubble dynamics of systems with internals involving relatively more viscous fluids need to be investigated and properly correlated with the geometry of internals. For magnetite powders in the average size range, 27.7 - 45.5 μm, the influence of particle size on gas holdup is negligible. A similar conclusion is reached about the slurry concentration for all the internals investigated. Unlike small red iron oxide particles here the holdup for seven-tube bundle is not much different from the data for these single-tubes. The reason for this may be in the nature of slurry rheology involving fine and large particles.

It is interesting to compare the relative values of gas-phase holdup for less and more viscous fluid systems. In Fig. 7.7 such a comparison is presented. It is

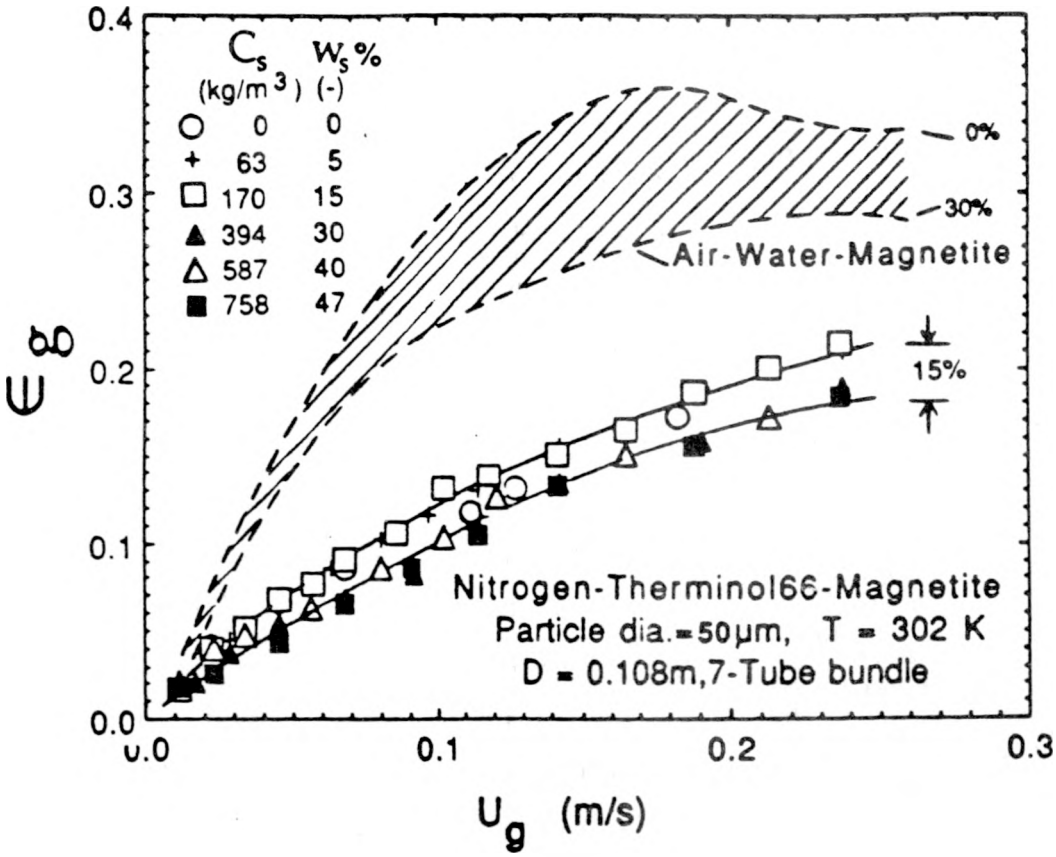

Fig. 7.7. Variation of nitrogen holdup as a function of nitrogen velocity in slurries of different concentrations of 50 μm average diameter powder.

important to note that the holdup for viscous systems is much smaller than for less viscous systems. This result is valid both for two and three-phase systems, and the effect of slurry concentration is more for less viscous systems than for viscous systems.

The influence of temperature on systems involving viscous fluids is investigated in the large column with thirty-seven tube bundle and 36 μm magnetite powder. For nitrogen-Therminol system, the nitrogen holdup increases with nitrogen velocity but the influence of temperature is involved. The holdup slightly decreases as the temperature is raised from 296K to 309K and thereafter it increases with temperature up to 428K. At this temperature and beyond up to 523K, the foam formation is observed and holdup remains constant. For three-phase systems a monotonic increase in gas holdup is observed with increase in temperature in the nonfoaming regime. In the foaming regime the holdup is constant. The addition of solids at room temperature decreases the holdup, while the change is negligible at higher temperatures till the foaming sets in. In the foaming regime (428 - 523K), the influence of solids concentration is negligible up to thirty weight percent but the holdup decreases as the solids concentration is further increased. It would be very useful to launch a careful experimental program of research involving such viscous fluids over a temperature range encompassing both the foaming and nonfoaming regimes.

8. NOMENCLATURE

A	cross-sectional area, m^2
a, b, c, d	numerical constants of Eqs. (6.51) and (6.54)
C_{pL}	liquid heat capacity, J/kg K
$\overline{C}_p$ or $C_{p,SL}$	slurry heat capacity, J/kg K
C_{ps}	solids heat capacity, J/kg K
C_s	solids concentration, kg/m^3
d_b	bubble diameter, m
d_o	particle diameter as defined in Eq. (6.18), m
d_p	particle diameter, m
d_{pi}	mean particle diameter in the range d_{pi-1} to d_{pi}, m
D_c	column diameter, m
D_T	heat transfer probe diameter, m
G	mass flow rate, kg/m^2s
g	acceleration due to gravity, m/s^2
H	section height, m
H_e	expanded dispersion column height, m
H_S	slumped liquid column height, m
H_{Sl}	slumped slurry column height, m
H1, H2, H3, H4	heaters
h	height above the gas distributor plate, m

h_W	heat transfer coefficient, W/ m^2 K
$h_{W, max}$	maximum value of heat transfer coefficient, W/m^2 K
I	current through the heating element, A
k_L	liquid thermal conductivity, W/mK
k_s	solid thermal conductivity, W/mK
$\bar{k}$ or k_{SL}	slurry thermal conductivity, W/mK
l	distance between successive bubbles, m
P	total pressure, Pa
P_v	vapor pressure, Pa
p_v	= g U_g ρ_L , energy dissipation rate per unit volume, kg/ms^3
ΔP	pressure drop across a section, Pa
P1, P2, P3, P4	heat transfer probes
Q	power input to heat transfer probe, W
T_c	column temperature, K
T_s	surface temperature, K
ΔT	temperature difference, K
$U_{b\infty}$	bubble terminal rise velocity, m/s
U_g	superficial gas velocity, m/s
U_o	drift velocity, m/s
U_{SL}	superficial slurry velocity, m/s
V	electrical voltage, V

V_c	liquid circulation velocity, m/s
V_L or U_L	superficial liquid velocity, m/s
v_a	axial component of V_c, m/s
v_F	eddy velocity as defined in Eq. (6.5), m/s
v_L	volume friction of liquid in slurry, dimensionless
v_S	volume friction of solids in slurry, dimensionless
W_L	mass of liquid in slurry, kg
W_s	mass of solids in slurry, kg
w_L	mass fraction of liquid in slurry, dimensionless
w_S	mass fraction of solids in slurry, dimensionless
x_i	mass fraction solids of average size, d_{pi}, dimensionless
1TB, 5TB, 7TB, 37TB	1,5,7, or 37 tube bundle

Dimensionless Numbers

Ar = $d_b^3 (\rho_L - \rho_g) g \rho_L / \mu_L^2$, Archimedes number

Bo = $g D_c^2 \rho_L / \sigma_L$, Bond number

Fr = $U_g^2 / d_b g$, Froude number

Ga = $g D_c^3 \rho_L^2 / \mu_L^2$, Galileo number

Nu = $h_W d_p / k_L$, Nusselt number

Nu' = $h_W d_p \in_L / k_L (1 - \in_L)$, Nusselt number

Pr = $\mu_L C_{p,L} / k_L$ or $\mu_{SL} C_{p,SL} / k_{SL}$, Prandtl number

Re = $U_g d_p \rho_L / \mu_L$ or $U_g d_p \bar{\rho} / \bar{\mu}$, Reynolds number

Re' = $U_L d_p \rho_L / \mu_L (1 - \epsilon_L)$, Reynolds number

St = $h_W / \rho_L C_{pL} U_g$ or $h_W / \rho_{SL} C_{p,SL} U_g$, Stanton number

Greek Symbols

ϵ_g average gas holdup, dimensionless

ϵ'_g local gas holdup, dimensionless

ϵ''_g gas holdup in continuous mode of operation, dimensionless

ϵ_L average liquid-phase holdup, dimensionless

ϵ_s average solid-phase holdup, dimensionless

μ_b apparent effective slurry viscosity, kg/ m s

μ_g gas viscosity, kg/m s

μ_L liquid viscosity, kg/ m s

$\bar{\mu}$ or μ_{SL} slurry viscosity, kg/ m s

$\mu_{SL,W}$ slurry viscosity at surface temperature, kg/ m s

ρ_g gas density, kg/ m^3

ρ_L gas density, kg/ m^3

ρ_m manometer liquid density, kg/ m^3

ρ_s solid density, kg/ m^3

$\overline{\rho}$ or ρ_{SL} slurry density, kg/ m^3

ρ_w water density, kg/ m^3

σ_L liquid surface tension, N/m

σ_w water surface tension, N/m

9. REFERENCES

1. F. Derbyshire and D. Gray, Coal Liquification, Ullman's Encyclopedia of Industrial Chemistry, Vol A7, 197-243, Fifth Edition, 1985.

2. M.B. Sherwin and M.E. Frank, Make Mathanol by Three Phase Reaction, Hydrocarbon Processing, 122-124, November, 1976.

3. J.C.W. Kuo, Two-Stage Slurry Fischer-Tropsch/ZSM-5 Process of Converting Syngas to High Octane Gasoline, Proc. DOE Contractors' Conference on Indirect Liquification, pp.13-1 to 13-28, May 20-21, 1981.

4. J.C.W. Kuo, Two-Stage Slurry Fischer-Tropsch/ZSM-5 Process of Converting Syngas to High Octane Gasoline, Proc. DOE Contractors' Conference on Indirect Liquification, pp. 10-1 to 10-36, September 8-9, 1982.

5. J.C.W. Kuo, Two-Stage Process for Conversion of Synthesis Gas to High Quality Transportation Fuels, Final Report on the DOE Contract No. DE-AC22-83PC60019, October 1985.

6. J. Klosek and R.L. Mednick, Liquid Phase Methanol PDU: Project Status and Plans, A paper presented at the U.S. DOE Contractors' Conference Indirect Liquefaction, Pittsburgh, PA, September 8-9, 1982.

7. D.M. Brown and J. Klosek, Liquid Phase Methanol Update, A paper presented at the U.S. DOE Contractors' Conference Indirect Liquefaction, Pittsburgh, PA, October 12-13, 1983.

8. T.R. Tsao, Results of Laporte Liquid Phase Methanol PDU Operation, A paper presented at the U.S. DOE Contractors' Conference Indirect, Liquefaction, Pittsburgh, PA, October 30-31, 1984.

9. T.R. Tsao and E.C. Heydorn, Liquid Phase Methanol PDU Results, A paper presented at the U.S. DOE Indirect Liquefaction Contractors' Review Meeting, Houston, TX, December 2-5, 1985.

10. J.J. Lewnard, P.R. Stepanoff and P. Rao, Recent Laboratory Activities Towards Developing the Liquid Phase Methanol Process, A paper presented at the U.S. DOE Indirect Liquefaction Contractors' Review Meeting, Pittsburgh, PA, December 2-4, 1986.

11. Liquid Phase Methanol Process Development Unit: Installation, Operation, and Support Studies, Final Report, Prepared for the United States Department of Energy Under Contract No. DE-AC 22-81PC30019 by Air Products and Chemicals, Inc., and Chem Systems Inc., p. 398, August 21, 1987.

12. J.H. Frey, D.W. Studer, J.L. Henderson and R.F. Weimer, Further Process Improvements at the Laporte Liquid Phase Methanol Facility, A paper presented at the U.S. DOE Indirect Liquefaction Contractors' Review Meeting, Pittsburgh, PA, November 15-17, 1988.

13. D.W. Studer, J.L. Henderson, T.H. Hsiung and D.M. Brown, Status Report on the Liquid Phase Methanol Project, A paper presented at the EPRI 14th Annual Conference on Fuel Science and Conversion, Palo Alto, CA, May 18-19, 1989.

14. D.W. Studer, D.M. Brown, J.L. Henderson and T.S. Hsiung, Status of the Development of Methanol Synthesis by the LPMEOH Process, A paper presented at the DOE Indirect Liquefaction Contractors' Review Meeting, Pittsburgh, PA, November 13-15, 1989.

15. H. Schultz, Chemicals, Feedstocks and Fuels from Fischer-Tropsch and Related Synthesis, in L.E. St.-Pierre and G.R. Brown (Editors), Future Sources of Organic Raw Materials, CHEMRAWNI, 167-183, Pergamon Press, New York, 1978.

16. J.B. O'Hara, A. Bela, N.E. Jentz and S.K. Khaderi, Fischer-Tropsch Plant Design Criteria, Chem. Eng. Prog. 72(8), 65-67, 1976.

17. F.C. Thyrion, Indirect Liquefaction, in Synthetic Fuels from Coal, Edited by I. Romey, P.F.M. Paul and G. Imarisio, 5-118, Graham and Trotman LTD., London, 1987.

18. R.B. Anderson, The Fischer-Tropsch Synthesis, Academic Press, New York, 1984.

19. M.E. Dry, The Sasol Fischer-Tropsch Processes, B.E. Leach (Editor), Applied Industrial Catalysis, Volume 2, Chapter 5, 167-213, Academic Press, New York, 1983.

20. D. Frohning, Fischer-Tropsch Synthesis for Fuel Production from Coal, in G.E. Beghi (Editor), Synthetic Fuels, 113-134, D. Reidel Publishing Company, Boston, 1985.

21. J.H. Field, H.E. Benson and R.B. Anderson, Synthetic Liquid Fuels by Fischer-Tropsch Process, Chem. Eng. Prog., 56 (4), 44-48, 1960.

22. H. Kolbel and M. Ralek, The Fischer-Tropsch Synthesis in the Liquid Phase, Catal. Rev. Sci. Eng. 21 (2), 225-274, 1980.

23. M.J. Baird, R.R. Schehl and W.P. Haynes, Fischer-Tropsch Processes Investigated at the Pittsburgh Energy Technology Center Since 1944, Ind.

Eng. Chem. Prod. Res. Dev. 19, 175-191, 1980.

24. P.C. Keith, Gasoline from Natural Gas, The Oil and Gas Journal, 45, 102-112, 1946.

25. M.L. Kastens, L.L. Hirst and R.G. Dressler, An American Fischer-Tropsch Plan, Ind. Eng. Chem. 44 (3), 450-466, 1952.

26. UOP Inc., Comparison of FT Reactor Systems - Phase I, Final Report, DOE Contract DEA CO10-78ET 10159, 1981.

27. W.D. Deckwer, FT Process Alternatives Hold Promise, The Oil and Gas Journal, 78, No. 45 198-213, Nov. 10, 1990.

28. M.L. Reikena, A.G. Vickers, E.C. Haun and R.C. Koltz, A Comparison of Fischer-Tropsch Reactors, Chem. Eng. Prog. 78(4), 86-90, 1982.

29. C.N. Satterfield, G.A. Huff, H.G. Stenger, J.L. Carter and R.J. Madon, Ind. Eng. Chem. Fundam. 24, 450-454, 1985.

30. J.B. O'Hara, A. Bela, N.E. Jentz, S.K. Khaderi, H.W. Klumpe, B.I. Loran, D.G. Reynolds and R.V. Teeple, Fischer-Tropsch Complex Conceptual Design/Economic Analysis, ERDA R and D Report No. 114 - Interim Report No. 3, ERDA Contract No. E (49-18) - 1775, January 1977; as quoted in references 28 and 22.

31. A.J. Forney, D. Bienstock and R.J. Demski, Use of a Large Diameter Reactor in Synthesizing Pipeline Gas and Gasoline by the Hot-Gas Recycle Process, U.S. Bureau of Mines, ROI 6126, 1962, as quoted in reference 28.

32. G.J. Thompson, A.G. Vickers and P.R. Pujado, Mathematically Modeled Comparison of Fischer-Tropsch Reaction System, 90th National AIChE Meeting, Houston, Texas, April 1981, as quoted in reference 28.

33. W. Faragher and J. Foucher, FIAT Final Report, 1267, PB 97, 368, Vol. I, Part C, p. 123, 1947, as quoted in reference 22.

34. H.H. Storch, N. Golumbric and R.B. Anderson, The Fischer-Tropsch and Related Synthesis, Wiley, New York, 1951.

35. J.H. Crowell, H.E. Benson, J.H. Field and H.H. Storch, Fischer-Tropsch Oil Circulation Processes, Ind. Eng. Chem. 42, 2376-2384, 1950.

36. H.E. Benson, J.H. Field, D. Beinstock and H.H. Storch, Oil Circulation Process for Fischer-Tropsch Synthesis, Ind. Eng. Chem. 46, 2278-2285, 1954.

37. M.E. Dry, In Catalysis Science and Technology, J.R. Anderson and M. Boudart (Editors), Vol. I, 159-255, Springer-Verlag, Berlin, 1981.

38. A. Zaidi, Y. Louisi, M. Ralek and W.D. Deckwer, Mass Transfer in the Liquid Phase Fishcher-Tropsch Synthesis, Ger. Chem. Eng. 2, 94-120, 1979.

39. W.D. Deckwer, Y. Serpmen, M. Ralek and B. Schmidt, Fischer-Tropsch Synthesis in the Slurry Phase on Mn/Fe Catalysts, Ind. Eng. Chem. Process Des. Dev. 21, 222-231, 1982.

40. M.D. Schlesinger, J.H. Crowell, M. Leva and H.H. Storch, Fischer-Tropsch Synthesis in Slurry Phase, Ind. Eng. Chem. 43 (6), 1474-1479, 1951.

41. M.D. Schlesinger, H.E. Benson, E.M. Murphy and H.H. Storch, Chemicals from the Fischer-Tropsch Synthesis, Ind. Eng. Chem. 46 (6), 1322-1326, 1954.

42. C.C. Hall and A.H. Taylor, Design and Operation of a Fluid Catalyst Pilot Plant for Fischer-Tropsch Synthesis, J. Inst. Petrol. 41, 101-124, 1955.

43. R. Farley and D.J. Ray, The Design and Operation of a Pilot-Scale Plant for Hydrocarbon Synthesis in the Slurry Phase, J. Inst. Petrol. 50, No. 482, 27-48, 1964.

44. P.H. Calderbank, F. Evans, R. Farley, G. Jepson and A. Poll, Rate Processes in the Catalyst-Slurry Fischer-Tropsch Reaction, Catalysis in Practice (Instn, Chem. Engrs.) 66-74, 1964.

45. A.K. Mitra and A.N. Roy, Performance of Slurry Reactor for Fischer-Tropsch and Related Synthesis, Indian Chemical Engineer, 127-132, 1963.

46. T. Sakai and T. Kunugi, Liquid Phase (Slurry) Method-Fischer-Tropsch Synthesis, Sekiyu Gakkai Shi. 17, 863-868, 1974.

47. S.C. Saxena, Indirect Liquefaction of Coal: Fischer-Tropsch Synthesis and Transport Processes in Slurry Bubble Column Reactors, Advances in Transport Processes, to be published.

48. J. Zahradnik and F. Kastanek, Gas Holdup in Uniformly Aerated Bubble Column Reactors, Chem. Eng. Commun. 3, 413-429, 1979.

49. Y.S. Touloukian, R.W. Powell, C.Y. Ho and P.G. Klemens, Thermophysical Properties of Matter, Volume 2, Thermal Conductivity-Nonmetallic Solids, 1970, IFI/Plenum, New York.

50. Y.S. Touloukian and E.H. Buyco, Thermophysical Properties of Matter, Volume 5, Specific Heat-Nonmetallic Solids, 1970, IFI/Plenum, New York.

51. As given in W.D. Deckwer, Y. Louisi, A. Zaidi and M. Ralek, Hydrodynamic Properties of the Fischer-Tropsch Slurry Process, Ind. Eng. Chem. Process Des. Dev. 19, 699-708, 1980.

52. V. Vand, Viscosity of Solutions and Suspensions, J. Phys. Chem. 52, 277-321, 1948.

53. K. Akita and F. Yoshida, Gas Holdup and Volumetric Mass Transfer Coefficient in Bubble Columns, Ind. Eng. Chem. Process Des. Dev., 12, 76-80, 1973.

54. G.A. Hughmark, Holdup and Mass Transfer in Bubble Columns, Ind. Eng. Chem. Process Des. Dev., 6, 218-220, 1967.

55. H. Hikita, S. Asai, K. Tanigawa, K. Segawa and M. Kitao, Gas Holdup in Bubble Columns, Chem. Eng. J., 20, 59-67, 1980.

56. I.G. Reilly, D.S. Scott, T. DeBruijn, A. Jain and J. Piskorz, A Correlation for Gas Holdup in Turbulent Coalescing Bubble Columns, Canadian J. Chem. Eng., 64, 705-717, 1986.

57. D.N. Smith, W. Fuchs, R.J. Lynn, D.M. Smith and M. Hess, Bubble Behavior in a Slurry Bubble Column Reactor Model, ACS Symp. Series 237, Chemical and Catalytic Reactor Modeling, Editors: M.P. Dudukovic and P.L. Pills, pp. 125-147, 1984.

58. E. Barnea and J. Mizrahi, A General Approach to the Fluid Dynamics of Particulate Systems. Part I. General Correlation for Fluidization and Sedimentation, Chem. Eng. J., 5, 171-189, 1973.

59. A Kumar, T.E. Dugaleesan, G.S. Ladda and H.E. Hoelscher, Bubble Swarm Characteristics in Bubble Columns, Canadian J. Chem. Eng., 54, 503-508, 1976.

60. E. Sada, S. Katoh, H. Yoshil, T. Yamanishi and A. Nakanishi, Performance of the Gas Bubble Column in Molten Salt Systems, Ind. Eng. Chem. Process Des. Dev. 23, 151-154, 1984.

61. J.H. Hills, The Operation of a Bubble Column at High Throughputs I. Gas Holdup Measurements, Chem. Eng. J., 12, 89-99, 1976.

62. G.S. Grover, C.V. Rode and R.V. Chaudhari, Effect of Temperature on Flow Regimes and Gas Holdup in a Bubble Column, Can. J. Chem. Eng. 64, 501-504, 1986.

63. R. Zou, X. Jiang, B. Li, Y. Zu and L. Zhang, Studies on Gas Holdup in a Bubble Column Operated at Elevated Temperatures, Ind. Eng. Chem. Res. 27, 1910-1916, 1988.

64. N.K. Roy, D.K. Guha and M.N. Rao, Fractional Gas Holdup in Two-Phase and Three-Phase Batch-Fluidized Bubble-Bed and Foam-Systems, Indian Chem. Eng., Trans. 27-Trans. 31, April 1963.

65. D.H. Ying, E.N. Givens and R.F. Weimer, Gas Holdup in Gas-Liquid and Gas-Liquid-Solid Flow Reactors, Ind. Eng. Chem. Process Des. Dev., 19, 635-638, 1980.

66. D.N. Smith and J.A. Ruether, Dispersed Solid Dynamics in a Slurry Bubble Column, Chem. Eng. Sci. 40, 741-754, 1985.

67. S.C. Saxena, Heat Transfer From a Cylindrical Probe Immersed in a Bubble Column, Chem. Eng. J., 41, 25-39, 1989.

68. S.C. Saxena, R. Vadivel and A.K. Verma, Heat Transfer and Hydrodynamics of Bubble Columns with Internals, Proc. Third Congreso Latinoamericano De Transferencia De Calor Y Materia, Guanajuato, GTO, Mexico, pp. 131-140, July 4-7, 1988.

69. S.C. Saxena and A.K. Verma, Transport Phenomena in Multiphase Reactors, Proc. Int. Conf. on Advances in Chem. Eng., 371-380, D.N. Saraf and D. Kunzru (Editors), Tata McGraw-Hill Publishing Company Limited, New Delhi, India, 1989.

70. T. Maruyama, S. Yoshida and T. Mizushina, The Flow Transition in a Bubble Column, J. Chem. Eng. Japan, 14, 352-357, 1981.

71. D.B. Bukur and J.G. Daly, Gas Holdup in Bubble Columns for Fischer-Topsch Synthesis, Chem. Eng. Sci., 42, 2967-2969, 1987.

72. D.B. Bukur, D. Petrovic and J.G. Daly, Flow Regime Transitions in a Bubble Column with a Paraffin Wax as the Liquid Medium, Ind. Eng. Chem. Res., 26, 1087-1092, 1987.

73. S.C. Saxena and R. Vadivel, Heat Transfer From a Tube Bundle in a Bubble Column, Int. Commun. Heat Mass Transfer, 15, 657-667, 1988.

74. D.J. Nicklin, Two-Phase Bubble Flow, Chem. Eng. Sci. 17, 693-702, 1962.

75. G.B. Wallis, One-Dimensional Two-Phase Flow, McGraw-Hill Book Company, 1969.

76. W. O'Dowd, D.N. Smith, J.A. Ruether and S.C. Saxena, Gas and Solids Behavior in a Baffled and Unbaffled Slurry Bubble Column, A.I.Ch.E. J. 33, 1959-1970, 1987.

77. A.C. Saxena, N.S. Rao and S.C. Saxena, Bubble Size Distribution in Bubble Columns, Can. J. Chem. Eng. 68, 159-161, 1990.

78. S.C. Saxena, D. Patel, D.N. Smith and J.A. Ruether, An Assessment of Experimental Techniques for the Measurement of Bubble Size in a Bubble Slurry Reactor as Applied to Indirect Coal Liquefaction, Chem. Eng. Comm. 63, 87-127, 1988.

79. S.A. Patel, J.G. Daly and D.B. Bukur, Holdup and Interfacial Area Measurements Using Dynamic Gas Disengagement, A.I.Ch.E. J. 35, 931-942, 1989.

80. S.C. Saxena and B.B Patel, Heat Transfer and Hydrodynamic Investigations in a Baffled Bubble Column: Air-Water-Glass Bead System, Chem. Eng. Comm., to be published.

81. N. Zuber and J.A. Findlay, Average Volumetric Concentration in Two-Phase Flow Systems, Trans. ASME: J. Heat Transfer 87, Series C, 453-468, 1965.

82. S.C. Saxena, N.S. Rao and M.Y. Kagzi, Hydrodynamic and Heat Transfer Investigations Conducted in a Bubble Column With Fine Powders and a Viscous Liquid, Powder Technology, to be published.

83. S.C. Saxena and N.S. Rao, Heat Transfer and Gas Holdup in a Two-Phase Bubble Column: Air-Water System-Review and New Data, Exptl. Thermal and Fluid Science, in press.

84. H. Kolbel, W. Seimes and R. Muller, Wärmeubergang in Blasensäulen, Chem. Ing. Tech. 30, 400-404, 1958.

85. J.R. Fair, A.J. Lambright and J.W. Anderson, Heat Transfer and Gas Holdup in a Sparged Contactor, Ind. Eng. Chem. Process Des. Dev. 1, 33-36, 1962.

86. W. Burkel, Der Wuärmeubergang an Heizund Kiihlflachen in Begasten Flüssigkeiten, Chem. Ing. Tech. 44, 265-268, 1972.

87. H. Hakita, S. Asai, H. Kikukawa, T. Zalke and M. Ohue, Heat Transfer Coefficient in Bubble Columns, Ind. Eng. Process Des. Dev. 20, 540-545, 1981.

88. W.F. Hart, Heat Transfer in Bubble-Agitated Systems. A General Correlation, Ind. Eng. Chem Process Des. Dev. 15, 109-114, 1976.

89. A. Steiff and P.M. Weinspach, Heat Transfer in Stirred and Non-Stirred Gas-Liquid Reactors, Ger. Chem. Eng. 1, 150-161, 1978.

90. W. Kast, Analyse Des Wärmeubergangs in Blasensäulen, Int. J. Heat Mass Transfer, 5, 329-336, 1962.

91. A. Mersmann, Heat Transfer in Bubble Columns, Int. Chem. Engng. 17, 385-388, 1977.

92. P. Zehner, Momentum, Mass and Heat Transfer in Bubble Columns Part 2. Axial Blending and Heat Transfer, Int. Chem. Engng. 26, 29-35, 1986.

93. W.D. Deckwer, On the Mechanism of Heat Transfer in Bubble Column Reactors, Chem. Eng. Sci. 35, 1341-1346, 1980.

94. H. Kolbel and H. Langemann, Erdoel-Zeitschv. 80, 405, 1964, as quoted in reference 38.

95. A.G. Shaykhutdinov, N.U. Bakirov and A.G. Usmanov, Determination and Mathematical Correlation of Heat Transfer Coefficient Under Conditions of Bubble Flow, Cellular and Turbulent Foam, Int. Chem. Engng. 11, 641-645, 1975.

96. M. Nishikawa, H. Kato and K. Hashimoto, Heat Transfer in Aerated Tower Filled with Non-Newtonian Liquid, Ind. Eng. Chem. Process Des. Dev. 16, 133-144, 1977.

97. J.B. Joshi and M.M. Sharma, Liquid Phase Backmixing in Sparged Contactors, Can. J. Eng. 56, 116-119, 1978.

98. J.B. Joshi, M.M. Sharma, Y.T. Shah, C.P.P. Singh, M. Ally and G.E. Klinzing, Heat Transfer in Multiphase Contactors, Chem. Eng. Commun. 6, 257-271, 1980.

99. D.N. Smith, G.J. Stiegel and J.A. Ruether, Modeling Three-Phase Reactor Systems, in Encyclopedia of Fluid Mechanics, Vol. 6, Chapter 15, pp. 535-682, Gulf Publishing Co., Houston, 1986.

100. H. Kolbel, E. Borchers and J. Martins, Wärmeubergang in Blasensäulen III, Messungen an Gasdurchströmten Suspensionen, Chemie-Ing.-Techn. 32, 84-88, 1960.

101. H. Kolbel, W. Siemes and K. Müller, Wärmeubergang an Blasensäulen, Chemie-Ing.-Techn. 30, 400-404, 1958.

102. H. Kolbel, E. Borchers and K. Müller, Wärmeubergang in Blasensäulen II. Messungen an Viscosen Suspersionen, Chemie-Ing.-Techn. 30, 729-734, 1958.

103. A. Mersmann, H. Noth, D. Ringer and R. Wunder, Maximum Heat Transfer in Equipment with Dispersed Two-Phase Systems, Int. Chem. Eng. 22, 16-29, 1982.

104. S.C. Saxena, M. Rosen, D.N. Smith and J.A. Ruether, Mathematical Modeling of Fischer-Tropsch Slurry Bubble Column Reactors, Chem. Eng. Comm. 40, 97-151, 1986.

105. S.C. Saxena, N.S. Rao and A.C. Saxena, Heat Transfer from a Cylindrical Probe Immersed in a Three-Phase Slurry Bubble Column, Chem. Eng. J. 44, 141-156, 1990.

106. A.B. Pandit and J.B. Joshi, Three-Phase Sparged Reactors-Some Design Aspects, Revs. Chem. Eng. 2, 1-84, 1984.

107. S.D. Kim, Y. Kang and H.K. Kwon, Heat Transfer Characteristics in Two- and Three-Phase Slurry-Fluidized Beds, A.I.Ch.E. J. 32, 1397-1400, 1986.

108. I.S. Suh, G.T. Jin and S.D. Kim, Heat Transfer Coefficients in Three-Phase Fluidized Beds, Int. J. Multiphase Flow 11, 255-259, 1985.

109. I.S. Suh and W.D. Deckwer, Unified Correlation of Heat Transfer Coefficients in Three-Phase Fluidized Beds, Chem. Eng. Sci. 44, 1455-1458, 1989.

110. Y. Kato, K. Uchida, T. Kago and S. Morooka, Liquid Holdup and Heat Transfer Coefficient Between Bed and Wall in Liquid-Solid and Gas-Liquid-Solid Fluidized Beds, Powder Tech. 28, 173-179, 1981.

111. S.C. Saxena, N.S. Rao and A.C. Saxena, Heat Transrer and Gas Holdup Studies in a Bubble Column: Air-Water-Glass Bead System, Chem. Eng. Comm., in press.

112. S.C. Saxena, P.R. Thimmapuram and N.S. Rao, Gas Holdup and Heat Transfer in a Baffled Slurry Bubble Column, A.I.Ch.E. Annual Meeting, Los Angeles, CA, 1991.

113. S.C. Saxena, N.S. Rao and A.C. Saxena, Heat Transfer and Holdup Studies in a Three-Phase Slurry Buble Column with Internals, A.I.Ch.E. Sym. Series (Editor: A.W. Weimer), in press.

114. S.C. Saxena, N.S. Rao and M. Yousuf, Heat Transfer and Hydrodynamic Investigations Conducted in a Bubble Column with Powders of Small Particles and a Viscous Liquid, Chem. Eng. J., to be published.

115. S.C. Saxena, N.S. Rao and P.R. Thimmapuram, Transport Studies in a Baffled Bubble Column with Slurries Involving Viscous Fluids, Indian

Chem. Eng. Congress-1990, held at Varanasi, India, 1991.

116. S.C. Saxena, R. Vadivel and A.C. Saxena, Gas Holdup and Heat Transfer from Immersed Surfaces in Two- and Three-Phase Systems in Bubble Columns, Chem. Eng. Comm. 85, 63-83, 1989.

117. J.B. Joshi and M.M. Sharma, A Circulation Cell Model for Bubble Columns, Trans. Instn. Chem. Engrs. 57, 244-251, 1979.

118. R.A. Mashelkar, Bubble Columns, Br. Chem. Eng. 15, 1297-1304, 1976.

119. P. Zehner, Momentum, Mass and Heat Transfer in Bubble Columns, Part I. Flow Model of the Bubble Column and Liquid Velocities, Int. Chem. Eng. 26, 22-28, 1986.

120. S.C. Saxena, N.S. Rao and A.C. Saxena, Estimation of Heat Transfer Coefficient for Immersed Surfaces in Bubble Columns Involving Fine Powders, Powder Technology 63(2), 197-202, 1991.

121. S.C. Saxena N.S. Rao and I.A. Khan, Heat Transfer from an Immersed Tube Bundle in a Three-Phase Slurry Bubble Column, 4th Int. Symp. on Transport Phenomena in Heat and Mass Transfer, July 14-18, 1991, Kensington, Australia.

122. S.C. Saxena, R. Vadivel and A.C. Saxena, Hydrodynamics and Heat Transfer Characteristics of Bubble Columns Involving Fine Powders, Powder Technology 59, 25-35, 1989.

123. R.F. Probstein and M.Z. Sengun, Dense Slurry Rheology with Application to Coal Slurries, Physico-Chemical Hydrodynamics 9, 299-313, 1987.

124. R. Botton, D. Cosserat and J.C. Charpentier, Influence of Column Diameter and High Gas Throughputs on the Operation of a Bubble Column, Chem. Eng. J. 16, 107-115, 1978.

125. S.C. Saxena, A.C. Saxena and N.S, Rao, Prediction of Heat Transfer Coefficient from an Immersed Surface in a Slurry Bubble Column, Int. Comm. Heat Mass Transfer 17, 247-258, 1990.

126. S.C. Saxena and B.B. Patel, Heat Transfer Investigations in a Bubble Column with Immersed Probes of Different Diameters, Chem. Eng. Comm., to be published.

127. S.C. Saxena, A.K. Verma, R. Vadivel and A.C. Saxena, Heat Transfer from a Cylindrical Probe in a Slurry Bubble Column, Int. Comm. Heat Mass Transfer 16, 267-281, 1989.

128. S.C. Saxena, N.S. Rao and A.C. Saxena, Investigation of Heat Transfer Phenomenon in Three-Phase Slurry Bubble Columns: Simulation of Indirect Coal Liquefaction Process, Proc. 1989 Int. Conf. on Coal Science, Volume II, 679-682, 1989, Tokyo, Japan.

129. S.C. Saxena, N.S. Rao and B.B. Patel, Heat Transfer and Hydrodynamic Investigations in Two- and Three-Phase Systems in a Baffled Bubble Column, Proc. Ninth Int. Heat Transfer Conf., Jerusalem, Israel, Ed. G. Hetsroni, 3, 407-412, 1990.

130. S.C. Saxena and B.B. Patel, Heat Transfer from a Tube Bundle in a Slurry Bubble Column Involving Fine Powders, Powder Technology 61, 207-610, 1990.

10. LIST OF FIGURES

Fig. 3. 10. Schematic of the D. C. power supply system for the heater probes.

Fig. 3.11. Detailed schematic of the temperature measuring system.

Fig. 3.12. Schematic of the 0.305 m diameter slurry bubble column along with air supply loop, temperature and pressure measuring circuits. (1) air compressor, (2) refrigerator drier, (3) oilscer filter, (4) pressure regulator valve, (5) rotameters, (6) pressure gauge, (7) gate valves, (8) one-way valve, (9) liquid drain, (10) conical section, (11) bubble-cap distributor plate, (12) perforated plate distributor, (13) stainless steel wire cloth, (14) metal inserts, (15) glass column, (16) diverger section, (17) trap bottles, (18) purgemeters, (19) manometers, (20) pressure sensor, (21) pressure monitor, (22) on-off valve, (23) data acquisition system, (24) computer, (25) key-board, (26) disc drive, (27) monitor, (28) printer, and (29) plotter.

Fig. 3.13A. Design details of the bottom end assembly of the 0.305 m diameter slurry bubble column. (1) gas inlet pipe, (2) Teflon coated nut, (3) liquid drain adapter, (4) liquid drain, (5) gaskets, (6) flanges., (7) soft inserts, (8) conical glass section, (9) bubble cap distributor plate, (10) cylindrical holder, (11) perforated plate distributor, (12) stainless steel wire cloth, (13) spacer studs, (14) locating pins, and (15) metal insert. All dimensions are in mm.

Fig. 3.13B. Arrangement of the bubble-caps on the distributor plate. All dimensions are in mm.

Fig. 3.13C. Design details of the perforated gas distributor plate for the 0.305 m diameter slurry bubble column. (1) perforated distributor, (2) stainless steel wire cloth, (3) bottom conical section, (4) flange, (5) gasket, (6) metal insert., (7) soft inserts, and (8) glass column. All dimensions are in mm.

Fig. 3.13D. Design details of the diverger section at the top end of the 0. 305 m diameter slurry bubble column. (1) stainless steel perforated plate, (2) diverger section, (3) gaskets, (4) flange, and (5) glass column. All dimensions are in mm.

Fig. 3.14. (A) Three-arm locating clamp, (B) single heat transfer probe, (C) orientation of thermocouples for the 0.305 m diameter bubble column. All dimensions are in mm. (A): (1) ring clamp, (2) screw, (3) radial arms, (4) Teflon rounded cap, (5) column surface, (6) telescopic arms (7) spring, (8) locking pin, and (9) front end of the telescopic arm.

Fig. 3.15. Design details of the radial thermocouple probe. (1) copper-constantan thermocouples, (2) thermocouple well, (3) Silicone rubber, (4)
ceramic tube, (5) column wall, and (6) swagelock connector. All dimensions are in mm.

Fig. 3.16. Design details of the radial thermocouple probe. (1) copper-constantan thermocouples, (2) thermocouple well, (3) Silicone rubber, (4) stainless steel, (5)

column wall, and (6) swagelok connector. All dimensions are in mm.

Fig. 3.17. Orientation of heater and heat transfer probes in tube bundles. Single heat transfer probe (A), four heater and single heat transfer probe (B), three heater and four heat transfer probes (C), location of heater section in the single heat transfer probe (D), and location of four heater sections in the four heat transfer probe bundle (E).

Fig. 3.18A. Design details of the heated section of the heat transfer probes and thermocouple locations used in the thirty-seven tube bundle.

Fig. 3.18B. A sectional view of the tube bundle through plane aa in the figure, not to scale. All dimensions are in mm.

Fig. 3.18C. The plan view of the thirty-seven tube bundle.

Fig. 3.18C. A photographic view of the thirty-seven tube bundle.

Fig. 3.19A. Design details of the radial thermocouple probe. (1) copper-costantan thermocouples, (2) thermocouple well, (3) copper cement,, (4) ceramic tube, (5) column wall, and (6) Swagelok connector. All dimensions are in mm.

Fig. 3.19B. Design details of the radial thermocouple probe. (1) copper-constantan thermocouples, (2) thermocouple well, (3) copper cement, (4) ceramic tube, (5) column wall, and (6) Swagelok connector. All dimensions are in mm.

Fig. 3.19C. Design details of the radial thermocouple probe. (1) copper-constantan thermocouples, (2) thermocouple well, (3) copper cement, (4) ceramic tube, (5) column wall, and (6) Swagelok connector. All dimensions are in mm.

Fig. 3.19D. Design details of the radial thermocouple probe. (1) copper-constantan thermocouples, (2) thermocouple well, (3) copper-cement, (4) ceramic tube, (5) column wall, and (6) Swagelok connector. All dimensions are in mm.

Fig. 3.20. Block diagram of the heater controllers including switches and thermocouple connections.

Fig. 3.21. Block assembly representation of the data acquisition and analysis system.

Fig. 3.22. Schematic of gas supply system to the two slurry bubble columns.

Fig. 4.1. Variation of gas holdup with increasing and decreasing air velocity for different slumped water column height: (A) average, (B) local.

Fig. 4.2. Variation of air holdup with air velocity and slumped water column height: (A) average, (B) local.

Fig. 4.3. Variation of average air holdup with air and liquid velocities.

Fig. 4.4. Dependence of average air holdup on air velocity and tube bundle size.

Fig. 4.3. Variation of ϵ_g with increasing and decreasing U at various V.

Fig. 4.5. Variation of average air holdup for increasig and decreasing nitrogen velocity and diferent slumped liquid column height..

Fig. 4.6. Dependence of nitrogen holdup on decreasig nitrogen velocity for heat transfer probes of different diameters and seven-tube bundle.

Fig. 4.7. Variation of average red iron oxide, water and air holdups as a function of decreasing air velocity in the column at 295K with a coaxial heat transfer probe (A) d_p = 1.02 μm; and (B) d_p = 2.38 μm.

Fig. 4.8. Variation of average solids, liquid and gas holdup as a function of decreasing air velicty and solids concentration for glass beads of (A) 50.0 μm, (B) 117.6 μm, and (C) 143.3 μm.

Fig. 4.9. The effect of slurry concentration on air holdup for the 7TB arrangement: (A) 50 μm, (B) 119 μm, and (C) 143 μm.

Fig. 4.10. Dependence of air holdup on air velocity and slurries of different particle sizes and concentrations. Data are also compared with the predictions of three models.

Fig. 4.11. Dependence of air holdup on particle diameter in the slurry as a function of air velocity.

Fig. 4.12. Dependence of air holdup on air velocity, particle diameter and concentration in the slurry.

Fig. 4.13. Dependence of nitrogen holdup on nitrogen velocity and slurry concentration as determined in a bubble column equipped with heat transfer probes of different diameters and a seven-tube bundle.

Fig. 4.14. Variation of holdup for nitrogen-Therminol-red iron oxide system for different internals and nitrogen velocity.

Fig. 4.15. Influence of nitrogen velocity and solids concentration on nitrogen holdup for the nitrogen-Therminol-magnetite (36.6 μm) system for the three probes. - - - 0, —— 50, weight percent smooth plots.

Fig. 4.16. Effect of particle diameter on nitrogen holdup for the 31.8 mm probe internal at solids concentration in weight percent of (A): 15, (B): 30, and (C): 50.

Fig. 4.17. Effect of probe diameter on nitrogen holdup at different solids concentrations in weight percent of (A): 0, (B): 15, (C): 30, and (D): 50.

Fig. 4.18. Variation of column temperature as a function of radial distance from the probe surface at various air velocities.

Fig. 4.19. Variation of heat transfer coefficient with time at different air velocities at two different locations in the column: (A) 0.57m, and (B) 1.18m above the distributor plate.

Fig. 4.20. Variation of the heat transfer coefficient with time at different air velocity for the water flow rate of 6.8 mm/s (A), and 11.9 mm/s (B).

Fig. 4.21. Variation of the heat transfer coefficient and average air holdup as a function of air velocity for three heater locations in the column.

Fig. 4.22. Dependence of heat transfer coefficient for the central tube in the bundle on air velocity.

Fig. 4.23. Dependence of heat transfer coefficient on heater location in the bundle and air velocity.

Fig. 4.24. Variation of the heat transfer coefficient at 307K with air velocity at different water flow velocities.

Fig. 4.25. Dependence of heat transfer coefficient on the nature of internals in the column.

Fig. 4.26. Variation of heat transfer coefficient with air velocity at three concentrations of slurry of 1.02 μm mean iron oxide particles in water at 313K.

Fig. 4.27. Variation of heat transfer coefficient with air velocity at three concentrations of slurry of 2.38 μm mean iron oxide particles in water at 313K.

Fig. 4.28. Dependence of heat transfer coefficient on air velocity and solids concentration for particles of diameter (A) 1.02 μm, and (B) 2.38 μm, in the slurry.

Fig. 4.29. Heat transfer coefficient dependence on (A) particle size and solids concentration in the slurry, and (B) nature of internals in the column.

Fig. 4.30. Variation of heat transfer coefficient with superficial air velocity for slurries of different solids concentrations and particle size.

Fig. 4.31. Variation of heat transfer coefficient with superficial air velocity for slurries of different particle sizes at the solid concentration of 104 kg/m^3.

Fig. 4.32. Influence of slurry concentration on heat transfer coefficient for particles of mean diameter (A) 50 μm, (B) 119 μm, and (C) 143 μm.

Fig. 4.33. Dependence of heat transfer coefficient on air velocity and particle diameter in the slurry.

Fig. 4.34. Dependence of heat transfer coefficient on air velocity and slurry concentration for particles of different sizes.

Fig. 4.35. Dependence of heat transfer coefficient on particle diameter in the slurry as a function of air velocity.

Fig. 4.36. Dependence of heat transfer coefficient on air velocity and particle diameter for slurries of (A) 10 weight percent, and (B) 30 weight percent.

Fig. 4.37. Dependence of heat transfer coefficient on air velocity, particle diameter and slurry concentration.

Fig. 4.38. Dependence of heat transfer coefficient for nitrogen-Therminol-red iron oxide on nitrogen velocity and slurry concentration as determined in a bubble column equipped with heat transfer probes of different diameters and a seven-tube bundle.

Fig. 4.39. Dependence of h_W on the nature of internals.

Fig. 4.40. Influence of nitrogen velocity and solids concentration on heat transfer coefficient for the nitrogen-Therminol-magnetite (36.6 μm) system for three probes.

Fig. 4.41. Effect of particle diameter on heat transfer coefficient for the 31.8 mm probe at solids concentrations in weight percent of (A): 15, (B): 30, and (C): 50.

Fig. 4.42. Effect of probe diameter on heat transfer coefficient at different solids concentrations in weight percent of (A): 0, (B): 15, (C): 30, and (D): 50.

Fig. 4.43. Variation of average air holdup with air velocity and initial water column height.

Fig. 4.44. Variation of air holdup in different sections of the larger column with air velocity.

Fig. 4.45. Influence of configuration of internals on air holdup as a function of air velocity and temperature.

Fig. 4.46. Influence of bubble column diameter and internals on air holdup at 297K as a function of air velocity.

Fig. 4.47. Variation of air holdup with decreasing superficial air velocity for the air-water system at four temperatures. □ SET 1, ■ SET 2, ○ SET 3, ● SET 4.

Fig. 4.48. Dependence of air holdup on air velocity and temperature for the column with thirty-seven tube bundle and air-water system.

Fig. 4.49. Variation of nitrogen holdup with increasing (○ , □ , △) and decreasing (● , ■ , ▲) velocity at different temperatures and solids concentration.

Fig. 4.50. Dependence of air holdup on air velocity, temperature and slurry concentration.

Fig. 4.51. Dependence of air holdup as a function of air velocity and temperature on solids concentration, and its comparison with the predictions of different correlations. The concentrations of glass beads (d_p = 14.3 μm) in the slurry is (A) five (52 kg/m^3), (B) ten (110 kg/m^3), and (C) twenty (249K kg/m^3) weight percent.

Fig. 4.52. Dependence of air holdup on air velocity and temperature for (A) 90 μm, (B) 50 μm, and (C) 50-90 μm, average size powders. Experimental data are also compared with the predictions of different correlations.

Fig. 4.53. Variation of air holdup for the air-water-glass bead system with decreasing superficial air velocity and temperature for slurries of 125 μm particles at two concentrations.

Fig. 4.54. Variation of air holdup for the air-water-glass bead system with decreasing superficial air velocity and temperature for slurries of 212 μm particles at two concentrations.

Fig. 4.55. Variation of air holdup for the air-water-glass bead system with decreasing superficial air velocity and temperature for the large column with thirty-seven tube bundle.

Fig. 4.56. Effect of particle diameter on air holdup at different temperatures for two slurry concentrations.

Fig. 4.57. Effect of slurry concentration on air holdup at different temperatures and slurry particle sizes.

Fig. 4.58. Dependence of air holdup on air velocity, temperature, particles size and slurry concentration.

Fig. 4.59. Effect of temperature on nitrogen holdup at different solids concentrations in the slurry. 0 = 298K, □ = 328K, △ = 378K, ● =428K, + = 473K, ■ = 523K.

Fig. 4.60. Radial temperature profile at various air velocities.

Fig. 4.61. Variation of heat transfer coefficient with time at different air velocities for lower (A), middle (B) and upper (C) regions of the column.

Fig. 4.62. Variation of heat transfer coefficient with air velocity for different regions of the column at 297K.

Fig. 4.63. Dependence of heat transfer coefficient with temperature, air velocity and tube bundle configuration.

Fig. 4.64. Variation of heat transfer coefficient with decreasing air velocity for air-water system at four locations in the column and at four temperatures.
□ Probe 1, ■ Probe 2, ○ Probe 3, ● Probe 4.

Fig. 4.65. Dependence of heat transfer coefficient on thermal flux as a function of gas velocity and column temperature: (A) probe-1 and (B) probe-3.

Fig. 4.66. Axial and radial variation of h_W with U_g at different temperatures. Solids concentration = 0 wt%.

Fig. 4.67. Variation of heat transfer coefficient with gas velocity and temperature for (A) probe-1, and (B) probe-3.

Fig. 4.68. Variation of heat transfer coefficient with air velocity, temperature and slurry concentration.

Fig. 4.69. Dependence of heat transfer coefficient on air velocity, temperature and slurry concentration for powders of mean diameter (A) 143.3μm, (B) 90 μm, (C) 50μm, and (D) 50-143 μm.

Fig. 4.70. Variation of heat transfer coefficient for the air-water-glass bead system with superficial air velocity and temperature for heat transfer probes 1 and 3 and slurries of 125 μm particles at two concentrations.

Fig. 4.71. Variation of heat transfer coefficient for air-water-glass bead system with superficial air velocity and temperature for heat transfer probes 1 and 3 and slurries of 212 μm particles at two concentrations.

Fig. 4.72. Variation of heat transfer coefficient for (A) air-water and (B) air-water-glass bead systems with superficial air velocity and temperature for heat transfer probes 1 and 3.

Fig. 4.73. Effect of particle diameter on heat transfer coefficient at different temperatures for two slurry concentrations and heat transfer probe 3.

Fig. 4.74. Effect of slurry concentrations on heat transfer coefficient at different temperatures and slurry particle sizes for heat transfer probe 3.

Fig. 4.75. Dependence of heat transfer coefficient on air velocity, temperature, particle size and slurry concentration. (A) 50 μm and 3 wt %; (B) 90 μm, 5 and 10 wt %.

Fig. 4.76. Axial and radial variation of h_W with U_g at different temperatures. Solids concentration = 15 wt %.

Fig. 4.77. Axial and radial variation of h_W with U_g at different temperatures. Solids concentration = 30 wt %.

Fig. 4.78. Axial and radial variation of heat transfer coefficient with nitrogen velocity at different temperatures. Solids conc. = 40 weight percent. ○ = probe 1, □ = probe 2, △ = probe 3, + = probe 4.

Fig. 4.79. Variation of heat transfer coefficient (probe 1) with nitrogen velocity and solids concentration at different temperatures. ○ = 0 wt%, □ = 15 wt%, △ =30 wt%, ● = 40 wt%.

Fig. 4.80. Effect of temperature on heat transfer coefficient at different solids concentrations in the slurry. ○ = 298K, □ = 328K, △ = 378K, + = 428K, ● = 473K, ■ = 523K.

Fig. 5.1. Comparison of experimental and computed air holdup values for the air-water system as a function of superficial air velocity at 309K.

Fig. 5.2. Parity plot for gas holdup.

Fig. 5.3. Bubble size frequency distribution in the 10.8 cm diameter bubble column for the air-water system. Air velocity = 3.2 cm/s.

Fig. 5.4. Histogram of bubble-size distribution in the 10.8 cm diameter bubble column for the air-water system. Air velocity = 3.2 cm/s.

Fig. 5.5. Histogram of the bubble-size distribution in the 30.5 cm diameter bubble column for the air-water system. Air velocity = 3.2 cm/s.

Fig. 5.6. Bubble size frequency distribution in the 30.5 cm diameter bubble column for the air-water system. Air-velocity = 3.6 cm/s.

Fig. 5.7. Bubble size frequency distribution in the 30.5 cm diameter bubble column for the air-water system. Air velocity = 5.8 cm/s.

Fig. 5.8. Bubble size frequency distribution in the 30.5 cm diameter bubble column for the air-water system. Air velocity = 9.2 cm/s.

Fig. 5.9. Comparison of experimental and calculated gas holdup values.

Fig. 5.10. Comparison of experimental air holdup values as a function of air velocity at different temperatures with the predictions based on different correlations.

Fig. 5.11. Parity plot for the air-water system gas holdup data. Calculated ϵ_g values are according to Eq. (5.21).

Fig. 5.12. Comparison of the four sets experimental data of air holdup of air - water system with the predictions of different models at four temperatures (1- Experiment, 2 - Grover et al., 3 - Zou et al., 4 - Reilly et al., 5 - Smith et al., 6 - Roy et al.).

Fig. 5.13. Comparison of experimental air holdup data with the predictions of modified Nicklin's model for air-water and air-water-glass bead systems.

Fig. 5.14. Comparison of 19 mm probe internal nitrogen holdup data with the predictions of correlations for nitrogen-Therminol system: (A) without and (B) with solids.

Fig. 5.15. Comparison of experimental nitrogen holdup data for 19 mm probe internal with the predictions based on the drift-flux theory.

Fig. 5.16. Comparison of the averaged air holdup values for a range of particle sizes, slurry concentrations and temperatures as a function of air velocity with the predictions of different correlations.

Fig. 5.17. Comparison of experimental air holdup data with the modified drift-flux theory approach.

Fig. 5.18. Comparison of experimental air holdup data with the predictions of different models for the air-water-glass bead system (1 - Experimental, 2 - Reilly et al.[56], 3 - Roy et al.[64], 4 - Smith et al.[57].)

Fig. 5.19. Parity plot for gas holdup. ϵ_g (calculated) are according to the relation of Eq. (5.21).

Fig. 5.20. Comparison of averaged experimental air holdup values with the calculated values.

Fig. 5.21. Comparison of experimental and calculated air holdup values on Nicklin's approach.

Fig. 5.22. Comparison of air holdup values for air-water-silica sand system over a range of slurry concentrations and temperatures as a function of air velocity with the predictions of different correlations.

Fig. 5.23. Parity plot for the air-water-silica sand system gas holdup data. Calculated values are based on Eq. (5.21).

Fig. 5.24. Comparison of experimental data (0%, O 50%) for the 19.0 mm probe with the predictions of correlations.

Fig. 5.25. Comparison of experimental and calculated nitrogen holdup values based on drift-flux theory.

Fig. 5.26. Comparison of ϵ_g with model predictions. A - [64], B - [56], C - [57], and P- Present data.

Fig. 5.27. Comparison of experiment and theory [76] for ϵ_g.

Fig. 6.1. Comparison of the present experimental heat transfer coefficient values with the measurements of other workers for the air-water system as a function of superficial air velocity and temperatures in the range 300-344 K.

Fig. 6.2. Comparison of experimental heat transfer coefficient with various computed sets for air-water system as a function of superficial air velocity at 309 K.

Fig. 6.3. Parity plot of h_W (kW/m^2K) for air-water system: (A) power function and (B) logarithmic function.

Fig. 6.4. Comparison of the variation of heat transfer coefficient as observed in the larger column for the air-water system at 297K with the predictions of the available correlations and models as a function of air velocity.

Fig. 6.5. Dependence of heat transfer coefficient for the air-water system on air velocity and temperature. Comparison of experimental data with the predictions of different correlations.

Fig. 6.6. Comparison of h_W for a bubble column equipped with tube bundles of different sizes.

Fig. 6.7. Comparison of experimental heat transfer coefficient data (probe 3) of air-water system with the predictions of different models at four temperatures. (1-Experimental, 2-Deckwer, 3-Suh and Deckwer, 4-Kim et al., 5- Pandit and Joshi).

Fig. 6.8. Comparison of experimental heat transfer coefficient data for probe 3

with the predictions of the proposed semi-empirical correlation.

Fig. 6.9. Comparison of experimental h_W data for the 19 mm probe internal with the predictions of different correlations.

Fig. 6.10. Comparison of experimental h_W data for 19 mm probe internal with the predictions based on Eq. (6.51).

Fig. 6.11. Comparison of h_W for 19mm probe internal with those based on Eq. (6.52).

Fig. 6.12. A plot of heat transfer coefficient (probe 1) versus nitrogen velocity shown in logarithmic coordinates at different temperatures. Solids concentration = 0 wt%.

Fig. 6.13. Comparison of experimental h_W values as a function of U_g with the predictions of four theoretical models for slurries of two different average size particles at concentrations of (A) 107 and 108, (B) 231 and 238, and (C) 383 and 404 kg/m^3.

Fig. 6.14. Parity plot of h_W (kW/m^2K) for air-water-red iron oxide based on Eq. (6.51), power function, with the values of the constants listed in Table 6.1.

Fig. 6.15. Parity plot of h_W (kW/m^2K) for air-water-iron-oxide based on Eq. (6.54), logarithmic function, with the values of the constants listed in Table 6.1.

Fig. 6.16. Parity plot of h_W (kW/m^2K) for air-water-iron-oxide system with global constants: (A) power function, and (B) logarithmic function.

Fig. 6.17. Parity plot of h_W (kW/m^2K) for air-water-iron oxide system based on Eq. (6.56).

Fig. 6.18. Comparison of h_W data for air-water-glass bead system with different models.

Fig. 6.19. Parity plot of h_W (kW/m^2K) for air-water-glass bead system: (A) power function, and (B) logarithmic function.

Fig. 6.20. Comparison of experimental and calculated heat transfer coefficient values with global constants for power function, Eq. (6.57).

Fig. 6.21. Comparison of experimental and calculated heat transfer coefficient values with global constants for semi-logarithmic function, Eq. (6.58).

Fig. 6.22. Comparison of experimental and calculated values of heat transfer

coefficient on the basis of the proposed correlation.

Fig. 6.23. Comparison of averaged heat transfer coefficient values as a function of air velocity with the predictions of different correlations at (A) 297, (B) 323, and (C) 343K.

Fig. 6.24. Comparison of experimental heat transfer coefficients with the predictions of different models for the air-water-glass bead system, (1-Experimental, 2-Deckwer, 3-Suh and Deckwer, 4-Kim et al., 5-Pandit and Joshi).

Fig. 6.25. Comparison of heat transfer data with the predictions of different models.

Fig. 6.26. Parity plot for heat transfer coefficient (kW/m^2K). Calculated values are based on Eq. (6.51).

Fig. 6.27. Parity plot for heat transfer coefficient (kW/m^2K). Calculated values are based on Eq. (6.54).

Fig. 6.28. Comparison of experimental and calculated heat transfer coefficient (kW/m^2K) based on Eq. (6).

Fig. 6.29. Comparison of experimental and calculated heat transfer coefficient (kW/m^2K) based on Eq. (7).

Fig. 6.30. Comparison of experimental h_W values with the predictions of four theoretical models for slurries of 46.6 μm average size magnetite particles at concentrations of (A) 107, (B) 167, and (C) 258 kg/m^3.

Fig. 6.31. Parity plot of h_W (kW/m^2K) for air-water-magnetite system: (A) power function, and (B) logarithmic function.

Fig. 6.32. Comparison of averaged experimental heat transfer coefficient with the predictions of different correlations at (A) 297, (B) 323, and (C) 343K.

Fig. 6.33. Correlation of heat transfer data on Eq. (6.51) for (A) air-water, and (B) air-water-magnetite systems.

Fig. 6.34. Comparison of experimental data (□-0%, O-50%) for 19.0 mm probe with the theoretical predictions. A: Deckwer et al. [51], B: Suh and Deckwer [109], C: Kim et al. [107], and D: Pandit and Joshi [106].

Fig. 6.35. Comparison of experimental and computed h_W values according to Eq. (6.51).

Fig. 6.36. Comparison of experimental and computed h_W values according to Eq. (6.62).

Fig. 6.37. Comparison of h_W with model predictions. A - [51], B - [109], C - [107], D - [106] and P - Present data.

Fig. 6.38. Comparison of experimental data with a semi-theoretical correlation (Eq. 6.51).

Fig. 6.39. A plot of heat transfer coefficients (probe 1) versus nitrogen velocity shown in logarithmic coordinates at different temperatures. Solids concentration = 40 wt%.

Fig. 6.40. Comparison of the concentration averaged heat transfer coefficient values as a function of air velocity with the predictions of different correlations at temperatures of 297(A), 323(B) and 343K(C).

Fig. 6.41. Comparison of experimental and calculated (Eq. 6.51) h_W (kW/m^2K) values for the air-water-silica sand system.

Fig. 7.1. Variation of h_W with air velocity and probe location.

Fig. 7.2. Variation of h_W with air velocity and probe location.

Fig. 7.3. Variation of h_W with air velocity and probe location.

Fig. 7.4. Variation of h_W with air velocity and temperature for different systems.

Fig. 7.5. Comparison of h_W data for two systems with widely different viscosities for the liquid phase.

Fig. 7.6. Variation of air holdup for air-water system with air velocity at different temperatures for a column equipped with either a five-tube, a seven-tube or a thity-tube bundle. D_c = 0.305m.

Fig. 7.7. Variation of nitrogen holdup as a function of nitrogen velocity in slurries of different concentrations of 50 μm average diameter powder.

11. LIST OF TABLES

Table 4.9. Smoothed heat transfer coefficient and air holdup values for air-water-magnetite system at 308K. Column diameter: 0, 108 m, Internal: 19 mm Single tube, Particle diameters: 35.7, 49, 58, 69, 90.5, 115.5 and 137.5, Solids concentration: 0, 10, 15, 20 and 30 wt%.

Table 4.10. Experimental air holdup values for air-water-magnetite system at 309K. Column diameter: 0.105 m, Internal: Seven-tube bundle, Particle diameters: 35.7, 90.5 and 137.5 μm, Solids concentrations: 10 and 30 wt%.

Table 4.11. Smoothed nitrogen holdup values for nitrogen-Therminol-red iron oxide system at 301-309K. Column diameter: 0.108 m, Internal: 19, 31.8, 50.8 mm single tubes and seven-tube bundle. Particle diameter: 1.7 μm, Solids concentrations: 0, 15, 30 and 50 wt%.

Table 4.12. Experimental values of h_W (kW/m^2K) for different electrical power inputs to the heater at a fixed column temperature T_c. Column diameter: 0.108m, Internal: 19 mm single tube. System: Air-water.

Table 4.13. Experimental h_W (kW/m^2K) and air holdup values for air-water system in the continuous mode operation at 307 ± 1K. Column diameter: 0.108 m, Internal: 19 mm single tube.

Table 4.14. Experimental h_W (kW/m^2K) and air holdup values at different heater locations for air-water system at 315 ± 1 K. Column diameter: 0.108 m, Internal: Seven-tube bundle.

Table 4.15. Experimental (A) and smoothed (B) h_W (kW/m^2K) values for air-water system at 309K. Column diameter: 0.108 m, Internal: 19 mm single tube.

Table 4.16. Experimental h_W (kW/m^2K) values for air-water system at 309K. Column diameter: 0.108 m, Internal: Seven-tube bundle.

Table 4.17. Experimental h_W (kW/m^2K) values for air-water-red iron oxide and air-water-magnetite systems at 313K. Column diameter: 0.108 m, Internal: 19 mm single tube.

Table 4.18. Experimental h_W (kW/m^2K) values for air-water-glass bead values at 315K. Column diameter: 0.109 m, Internal: 19 mm single tube.

Table 4.19. Smoothed h_W (kW/m^2K) values for air-water-glass bead system at 309K. Column diameter: 0.108 m, Internals: 19 mm single tube and seven-tube bundle.

Table 4.20. Smoothed h_W (kW/m^2K) values for air-water-magnetite system at 309K. Column diameter: 0.108 m, Internal: Seven-tube bundle, Particle diameters: 37.5, 90.5 and 137.5 μm, solids concentrationds: 10 and 30 wt%.

Table 4.21. Smoothed h_W (kW/m^2K) values for nitrogen-Therminol-red iron oxide system at 301-309K. Column diameter: 0.108 m, Internals: 19.0, 31.8, 50.8 mm single tubes and seven-tube bundle.

Table 4.22. Smothed h_W (kW/m^2K) values for nitrogen-Therminol-magnetite system at 306K. Column diameter: 0.108 m, Internal: 19.0, 31.8 and 51.8 mm single tubes, Particle diameters: 26.6, 37.7 and 45.5 μm.

Table 4.23. Air holdup values smoothed over-concentration range for air-water and air-water-glass bead systems for different particle diameters and at different temperature levels. Column diameter: 0.305 m, Internal: Seven-tube bundle.

Table 4.24. Smoothed air holdup values for air-water system at different temperature levels. Column diameter: 0.305 m, Internal: Thirty-seven bundle.

Table 4.25. Nitrogen gas holdup values smoothed over the solids concentration range for nitrogen-Therminol-magnetite system at different temperature levels. Column diameter: 0.305 m, Internal: Thirty-seven tube bundle, Particle diameter: 36.0 μm, solids conc. : 0, 15, 30 and 40 wt%.

Table 4.26. Smoothed air holdup and h_W (kW/m^2K) values for air-water-silica sand system at different temperature levels. Column diameter: 0.305m, Internal: Seven-tube bundle.

Table 4..27. Smoothed air holdup values for air-water-glass bead system at different temperature levels. Column diameter: 0.305 m, Internal: Thirty-seven tube bundle.

Table 4.28. Air holdup values smoothed over particle size and the solids concentration range for air-water-magnetite system at different temperature levels. Column diameter: 0.305 m, Internal: Seven-tube bundle. Particle diameters: 50 and 90 μm, Solids concentrations: 3, 5 and 10 wt%.

Table 4.29. Experimental h_W (kW/m^2K) values as a function of power input to the probe at U_g = 0.376 m/s. Column diameter: 0.305 m, Internal: 19 mm single tube, System: Air-water.

Table 4.30. Experimental h_W (kW/m^2K) values in different regions of the 0.305 m bubble column for air-water system at 297 $\pm$ 3K. Internal: 19 mm single tube.

Table 4.31. Smoothed h_W (kW/m^2K) values for air-water system at different temperature levels. Column diameter: 0.305 m, Internal: Seven-tube bundle.

Table 4.32. Smoothed h_W (kW/m^2K) values for air-water system at different temperature levels in different regions of the tube bundle. Column diameter: 0.305m, Internal: Thirty-seven tube bundle.

Table 4.33. Smoothed h_W (kW/m^2K) values for nitrogen-Therminol-magnetite system at different temperature levels. Column diameter: 0.305 m, Internal: Thirty-seven tube bundle. Particle diameter: 36.6 μm, Solids concentrations: 0, 15, 30 and 40 wt%.

Table 4.34. Smoothed h_W (kW/m^2K) values for air-water and air-water-silica sand systems at different temperature levels. Column diameter: 0.305 m, Internal: Seven-tube bundle, Particle diameter: 65.0 μm.

Table 4.35. Smoothed h_W (kW/m^2K) values for air-water and air-water-glass bead systems at different temperature levels. Column diameter: 0.305 m, Internal: Seven-tube bundle, Particle diameters: 50, 90 and 143.3 μm.

Table 4.36. Smoothed h_W (kW/m^2K) values for air-water-glass bead system at different temperature levels. Column diameter: 0.305 m, Internal: Thirty-seven tube bundle, Particle diameters: 125, 168 and 212 μm.

Table 4.37. Smoothed h_W (kW/m^2K) values for air-water and air-water-magnetite systems at different temperature levels. Column diameter: 0.305 m, Internal: Seven-tube bundle. Particle diameters: 50 and 90 μm. Solids concentrations: 3, 5 and 10 wt%.

Table 5.1. Values of $U_{b\infty}$ based on Eq. (5.21) and determined from experimental gas holdup data for air-water and air-water-glass bead systems at 309K in 0.108m bubble column.

Table 5.2. Values of $U_{b\infty}$ based on Eq. (5.21) and determined from experimental gas holdup data for nitrogen-Therminol and nitrogen-Therminol-red iron oxide systems in 0.108 m bubble column at ambient temperature.

Table 5.3. Values of $U_{b\infty}$ based on Eq. (5.21) and determined from experimental gas holdup data for air-water magnetite system in 0.108 m in bubble column equipped with a 19 m tube. The data was measured at 308K for particles in the size range 35.7 - 137.5 μm and slurry concentrations in the range 10 - 30 wt%.

Table 5.4. Values of $U_{b\infty}$ based on Eq.(5.21) and determined from experimental gas holdup data for nitrogen-Therminol-magnetite system for different internals in 0.108 m bubble column at ambient temperature.

Table 6.1. Constants of Eqs. (6.51) and (6.54) as determined from the experimental h_W values for air-water-red iron oxide system at 313K and measured in 0.108 m bubble column equipped with 19 mm heat transfer probe.

Table 6.2. Values of the constants of Eqs. (6.51) and (6.54) as determined from the experiemntal h_W values for three different systems in the temperature range 308 - 316K and measured in 0.108 m bubble column equipped with 19 mm heat transfer probe.

Table 6.3. Global constants of Eqs. (6.51) and (6.52) as determined from the experimental h_W values for air-water-magnetite and air-water-glass bead systmes in the temperature range 308 - 316K and measured in 0.108 m bubble column equipped with 19 mm heat transfer probe.

Table 6.4. Values of the constants of Eqs. (6.51) and (6.54) as determined from the experimental h_W values for air-water and air-water-glass bead systems at 393K and measured in 0.108 m bubble column equipped with a 19 mm single tube and a seven-tube bundle.

Table 6.5. Values of the constants of Eqs. (6.51) and (6.54) as determined from the experimental h_W values for air-water-magnetite system at 308K and measured in 0.108m bubble column equipped with a 19 mm single heat transfer probe.

Table 6.6. Values of the constants of Eq. (6.51) as determined from the experimental h_W values for air water and air-water-magnetite systems and measured in 0.305m bubble column equipped with a seven-tube bundle.

Table 6.7. Values of the constants of Eq. (6.51) as determined from the experimental h_W values for nitrogen-therminol-magnetite system at 306-312K and measured in 0.108m bubble column equipped with three single heat transfer probes.

Table 6.8. Values of the constants of Eqs. (6.51) and (6.64) as determined from the experimental h_W values for air-water and air-water-sand systems at several temperatures and measured in 0.305m bubble column equipped with a seven-tube bundle.

12. ACKNOWLEDGEMENTS

We are grateful to the Department of Energy, Pittsburgh Energy Technology Center, for sponsoring and partly supporting this work; and to the University of Illinois at Chicago for supplementing the DOE financial support which only enabled to bring this comprehensive effort to completion. The valuable assistance rendered by the department workshop in fabricating and erecting the experimental facility is heartily appreciated. This team consisted of Messrs. W. Schindler, A. Sawczuk, G. Scott and J. Sitasz. The meticulous effort of Mr. R. Roszak in typing and organizing this report brought it to its present final form. Mr. George Cinquegrane of Pittsburgh Energy Technology Center very willingly offered his cooperation in timely sorting out all the technical and administrative matters relating to this contract and it is a pleasure to record our appreciation for this much needed assistance.

★U.S. GOVERNMENT PRINTING OFFICE: 1991 -548 -138/40053